An examination of the late Miocene C_4 grass expansion through sedimentary charcoal morphometrics and morphotypes

by

Sarah R. Barney

A thesis submitted to the Graduate Faculty of
Auburn University
in partial fulfillment of the
requirements for the Degree of
Master of Science

Auburn, Alabama
May 2, 2026

Sedimentary Charcoal, Paleofire, Paleoecology, Charcoal Morphometrics, C_4 grass expansion

Approved by

Richard S. Vachula, Advisor, Assistant Professor, Department of Geosciences, College of Science and Mathematics
Anson H. Cheung, Postdoctoral Research Associate, Department of Atmospheric and Environmental Sciences, University at Albany, SUNY
Thomas M. Cullen, Assistant Professor, Department of Geosciences, College of Science and Mathematics
Stephanie Rogers, Associate Professor, Department of Geosciences, College of Science and Mathematics

Abstract

The C_4 Fire Hypothesis posits that an increase in fire was the catalyst for the late Miocene C_4 grass expansion by clearing forest canopies to create and maintain open landscapes preferred by C_4 grasses, creating a positive feedback loop. However, to date, few analyses have directly resolved whether the fire feedback is supported, though several studies have identified support for components of the Fire Hypothesis. We reconstructed the fuel type of the late Miocene fire regime by analyzing the morphological and morphometric characteristics of charcoal found in Ocean Drilling Program Leg 184 Site 1146 (South China Sea; l19°27.40′N, 116°16.37′E) legacy cores and compared it to previously published paleoclimate data to critically examine the Fire Hypothesis and understand the extent of the role of fire in the C_4 grass expansion. The sedimentary charcoal interpretations reflect fire activity primarily from the Pearl River Basin and Southeast China. From 8 to 5 Ma, the fuel type per morphology type shifted from woody to grassy fuel, the opposite of what would be expected in the Fire Hypothesis. Charcoal accumulation rates show an increase of fire around the time of the expansion (7.3–6.9 Ma). Influence diagnostics, leave-one-out refitting, jackknife and bootstrap resampling, and robust regression all show that the 7.3–6.9 Ma increase in CHAR is stable and not driven by individual data points. However, fuel-indicative characteristics of the charcoal (morphology and L:W ratio) show no discernable transition in fuel type during the period of increased fire activity, suggesting neither C_4 nor C_3 vegetation were preferentially burnt at this time. The observed increase in fire activity aligns with regional climatic changes including a decrease in monsoon intensity and increase aridification starting around 7 Ma. Our findings partially support the Fire Hypothesis in that we see evidence for an increase in fire activity, but not preferential burning recorded in the South China Sea as initially argued.

Artificial Intelligence (AI) Use Disclosure Statement

In the preparation of this thesis, the following Artificial Intelligence (AI) tool was used: ChatGPT. This tool was used to search for additional methods of statistical analysis and coding assistance in Chapters 1 and 2. The author acknowledges full responsibility for the intellectual content of this work and has ensured that AI-assisted sections have been reviewed and revised for accuracy and appropriate academic style. All AI-generated content was reviewed and validated for relevance, appropriateness, and accuracy before incorporation into the final document to maintain scholarly integrity of this research.

Acknowledgments

I would first like to thank my advisor, Dr. Richard Vachula, for accepting me into his lab and guiding me throughout my graduate career so that I can confidently call myself a scientist. I would also like to thank my committee Dr. Anson Cheung, Dr. Thomas Cullen, and Dr. Stephanie Rogers for offering different perspectives and asking interesting questions. Finally, I would like to extend special gratitude Alexandra Tsalickis for support and mentorship throughout this project.

Table of Contents

Abstract 2

AI Use Disclosure Statement 3

Acknowledgments 4

List of Tables 7

List of Figures 8

List of Abbreviations 9

Chapter 1 (Assessing fuel type changes in the late Miocene C_4 grass expansion through sedimentary charcoal analysis of the South China Sea Ocean Drilling Program Site 1146) 10

Introduction 11

Methods 14

Results 20

Discussion 23

Conclusion 33

References 34

Appendix 1 (A multi-site examination of fuel type and fire activity in the late Miocene C_4 grass expansion through sedimentary charcoal from IODP cores) 51

Abstract 52

Introduction 53

Methods 57

Results 66

Discussion 69

References 85

Appendix 2 101

Appendix 3 104

List of Tables

Table 1 101

Table 2 104

List of Figures

Figure 1 16

Figure 2 22

Figure 3 23

Figure 4 31

Figure 5 58

Figure 6 69

Figure 7 72

Figure 8 75

Figure 9 78

Figure 10 80

Figure 11 102

Figure 12 103

Figure 13 103

List of Abbreviations

CHAR	Charcoal accumulation rate
EASM	East Asian Summer Monsoon
EAWM	East Asian Winter Monsoon
IODP	International Ocean Discovery Program
L:W	Length to width ratio
Ma	Megaannum
ODP	Ocean Drilling Program

Chapter 1

Assessing fuel type changes in the late Miocene C_4 grass expansion through sedimentary charcoal analysis of the South China Sea Ocean Drilling Program Site 1146

This chapter is currently under review after major revisions in *Paleoceanography and Paleoclimatology*.

Barney, S.R., Cheung, A.H., Welch, J.C., and Vachula, R.S. (2026). Assessing fuel type changes in the late Miocene C4 grass expansion through sedimentary charcoal analysis of the South China Sea Ocean Drilling Program Site 116. *Paleoceanography and Paleoclimatology* [under review].

Introduction

Grasslands and savannas dominate the tropics and subtropics. They cover about 30% of the Earth's land area, and are largely comprised of C_4 grasses (Vendraminei et al., 2023). Despite the initial evolution of the C_4 photosynthetic pathway around 30 megaannum (Ma), the domination of C_4 grasses only occurred relatively recently and globally asynchronously between late Miocene and Pliocene (ca. 8 to 3 Ma) (Cerling et al., 1993; Edwards, et al., 2010). C_3 and C_4 plants are differentiated by their photosynthetic pathway and subsequent water use efficiency, with C_4 plants being able to retain more water and thereby being better adapted for hot, dry environments (Ehleringer and Cerling, 2002). The C_3 photosynthetic pathway evolved 2.8 billion years ago. However, a global depletion of CO_2, higher temperatures, and aridification around 30 million years ago reduced the efficiency of C_3 photosynthesis and triggered the evolution of the C_4 pathway (Edwards et al., 2010; Sage, 2004). C_4 pathways became prevalent in the Miocene and was associated with a global decline in CO_2 resulting in aridification and cooling (Edwards et al., 2010; Herbert et al., 2016; Pagani et al., 1999). Due to the C_4 superior photosynthetic efficiency in dry and low-CO_2 climates, the decline in CO_2 has been credited as the catalyst for the rapid C_4 expansion (Cerling et al., 1993).

However, global climate conditions in the late Miocene were not unique in the context of Earth's climatic history (e.g., CO_2 decline, aridification, cooling) (Herbert et al., 2016), suggesting other factors could have influenced the C_4 grass expansion (Edwards, et al., 2010; Herbert et al., 2016). Keeley and Rundel (2005) observed evidence for elevated fire activity during C_4 proliferation in marine sediment records and introduced the Fire Hypothesis. This hypothesis suggests that fire catalyzed the C_4 expansion by clearing C_3 forest canopies providing dry, sunny, and open environments preferable to C_4 grasses. These C_4 grasses are more

flammable and resprout faster than C_3 plants, thus provided more fuel that increased the number of fires, creating a positive feedback loop (Keeley & Rundel, 2005; Ripley et al. 2015).

Following the proposition of the hypothesis by Keeley and Rundel (2005), several independent studies have found support for it based on reconstructions from various locations. Feakins et al. (2020) used a multi-proxy analysis of $\delta^{13}C$ of bulk organic carbon, plant wax n-alkanes and n-alkanoic acids, lignin phenols, charcoal, and pollen to identify that the C_4 transition started around 8 Ma with an increase in fire activity in the Indus Fan (IODP site U1457), supporting the Fire Hypothesis. Off the Namibian Coast (ODP site 1081), Hoetzel et al. (2013, 2015) showed the C_4 grass expansion began around 8.3 Ma from pollen records and with the charcoal record indicating that fire activity increased between 7.1 and 5.8 Ma, also supporting the Fire Hypothesis. Further, Karp et al. (2021) used stable carbon and hydrogen isotopes in plant wax and polycyclic aromatic hydrocarbons in marine sediments retrieved from the Bengal Fan (ODP Sites 717 and 718) to refine and revise the hypothesis to include seasonal drought as a factor in the positive feedback loop. Seasonal drought reduced fuel moisture, increased flammability, and further inhibited the reestablishment of C_3 forest cover (Keeley & Rundel, 2005). Although studies have shown an increase in fire activity and regional climatic change when the C_4 grass expansion began, there has been very few direct assessments of the potential preferential burning of C_3 plants due to the lack of a fuel type proxy (Feakins et al., 2020; Hoetzel et al., 2013; 2015; Karp et al., 2021; Zhou et al., 2017). Therefore, whether the Fire Hypothesis can be fully supported by proxy evidence remains unclear.

Recent advances relating the morphometry and morphology of charcoal particulates in sediments to fuel types offer an opportunity to resolve fuel changes during the late Miocene C_4 grass expansion. Charcoal is the product of the incomplete combustion of organic matter that

retains characteristics of the original fuel type burned. Charcoal can be a variety of sizes from microscopic scales (10–50 μm) to macroscopic sizes (>125 μm; Umbanhowar & Mcgrath, 1998; Vachula, 2019; Whitlock & Larsen, 2001). These charcoal particulates can be moved by water or air from the area burned to bodies of water to be deposited, where they can be preserved for millions of years and used to reconstruct fire activity (Daniau et al., 2019; Genet et al., 2021; Haliuc et al., 2023; Patterson et al., 1987; Whitlock & Larsen, 2001). The particulates retain distinguishable morphometric and morphological data that can be used to characterize the fuel type (Crawford & Belcher, 2014; Enache & Cumming, 2006; Vachula et al., 2021). The morphological types are distinguished by their shape and presence or absence of plant structure; more elongated particulates suggest branches or grasses, and more compact particulates suggest leaves or woody material (Crawford & Belcher, 2014; Enache & Cumming, 2006). Morphometric data is tied to the type of vegetation burnt and taphonomy (Crawford & Belcher, 2014; Pereboom et al., 2020; Vachula et al., 2021). For example, length-to-width ratio greater than or equal to 3.5 suggest grass and non-woody material whereas less than 3.5 suggest woody material (Crawford & Belcher, 2014; Li et al., 2019; Ogura, 2007; Zhang and Lu, 2005). Similarly, recent work exploring other morphometrics (e.g., circularity, rectangularity) has shown promise in further distinguishing fuel types burned (Galinger et al., 2025).

In this study, we reconstruct aspects of the late Miocene fire regime (fire activity and fuel type) recorded by marine sediment samples from Ocean Drilling Program (ODP) Site 1146 in the South China Sea. Here we aim to critically test the Fire Hypothesis and to understand the extent of the role of fire in the late Miocene C_4 grass expansion in Southeast China. To support the Fire Hypothesis at this site, three key lines of evidence are needed: (1) an increase in fire activity concurrent with C_4 proliferation, (2) preferential burning of woody vegetation, and (3) a

changing climate that may have facilitated the shift in fire activity and C_4 expansion (Karp et al., 2021; Keeley & Rundel, 2005). Using microcharcoal found in the ocean core samples, we reconstruct fire activity from charcoal accumulation rates and fuel type from charcoal morphological and morphometric data. We compare our data to previously published vegetation data ($\delta^{13}C_{alk}$; Zhou et al., 2017) to understand the vegetation land cover and the vegetation burning. Further, we examine previously published paleoclimate data ($\delta^{18}O$, $\delta^{13}C$, and Mg/Ca ratios; (Holbourn et al., 2021; Steinke et al., 2010) to understand the possible influence of regional climate change on the C_4 grass expansion.

2. Methods

2.1 Study Site

We focus on ODP Site 1146, drilled in 1999 and located ~200 km south of Hong Kong in the South China Sea (19°27.40′N, 116°16.37′E; Wang et al., 2000). Fifty samples (2 cm resolution) were obtained from holes 1146A and 1146C via an IODP repository request. The sediment is carbonate and clay rich, and was primarily transported from the Pearl River Delta and by westerly winds (Wang et al., 2000; Clift et al., 2014; Jia et al., 2003). Currently, the Pearl River covers 4.4 x 10^5 km^2 in southern China and has an average discharge of 9631 m^3/s (Zhang et al., 2024). The age range of our samples is from the late Miocene (8.0 Ma) to late Pliocene (5.0 Ma; Wang et al., 2000).

In the late Miocene, the regional climate, as recorded in the South China Sea, shows fluctuations in the East Asian monsoons. Between ~7 and 5.5 Ma, The East Asian Summer Monsoon (EASM) weakened, which reduced the moisture brought to the region, and the East Asian Winter Monsoon (EAWM) strengthened, which brought dry air from inland (Figure 1;

Holbourn et al., 2021: Holbourn et al., 2018; Li et al., 2004; Steinke et al., 2010). The uplift of the Tibetan Plateau enhanced the thermal gradient between the land and ocean, preventing moisture from arriving into the continental interior and further intensify aridification (Zhisheng et al., 2001). C_4 vegetation has been present in East Asia over the last ~19 Ma (Zhou et al., 2017), and the transition from a C_3 to a C_4 dominated landscape occurred in a stepwise fashion around 20 Ma, 15 Ma, and a gradual expansion from 7 to 4 Ma (Li et al., 2023). At each step, C_4 plant abundance became progressively more abundant at 10–20%, 20–30% and >30% relative to C_3 plants, respectively (Li et al., 2023). Zhou et al., 2017 recorded two additional steps at 1 Ma and 0.4 Ma (Zhou et al., 2017).

While our samples (8–5 Ma) do not encompass the entire timespan of the rise in C_4 abundance in East Asia, they are contemporaneous with the gradual expansion from 7 to 4 Ma. Additionally, other studies examining the C_4 grass expansion in Asia from other locations primarily recorded between 7 and 4 Ma (Passey et al., 2009; Shen et al., 2018; Chinese Loess Plateau region and IODP Site 1430 in the Japan Sea, respectively). While Zhou et al., 2017 identified a major expansion at 1 Ma and 0.4 Ma, this could be a reflection of a more complete sedimentary record in more recent times (Sadler, 1981; Wilkinson & Vachula, 2023). Therefore, our results are best understood within this gradual expansion of the stepwise ecological change.

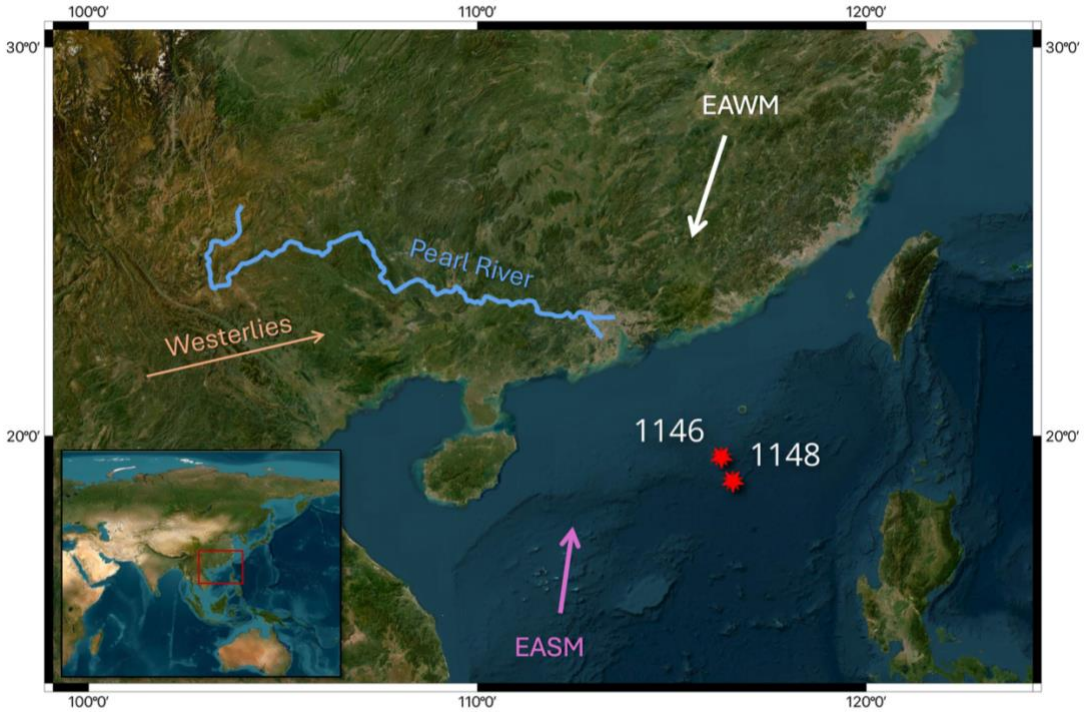

Figure 1: Map of present day ODP Site 1146 and Site 1148 in the South China Sea. The Pearl River and westerlies are the primary transportation mechanisms for sediment that is deposited at both sites. The monsoon directions are denoted by the arrow direction. Base map is from ESRI, river data is from HydroRIVERS Technical Documentation v1.0, and the projection is World Geodetic System 1984.

2.2 Age-depth model determination

The splice and chronology used in this study were from Holbourn et al. (2021). The splice was based on stratigraphic correlation from magnetic susceptibility, gamma-ray attenuation bulk density, and natural gamma radiation data (Wang et al., 2000) but was modified by removing duplications and inserting a 1.45 m segment to close a gap between 372.90 meters composite depth (mcd) and 374.35 mcd (Holbourn et al., 2021). The chronology of the Miocene

sequence for Site 1146 was based on benthic foraminiferal isotopic records (Wang et al., 2000; Holbourn et al., 2021) and computed obliquity and eccentricity solutions (Laskar et al., 2004).

2.3 Sedimentary charcoal analysis

All samples were processed using an adapted methodology from Vachula et al. (2018). Hydrochloric acid was incrementally added to each sample (~150 mg) until effervescence ceased to eliminate carbonates. Six mL each of NaClO (2.25%) and $(NaPO_3)_6$ (6%) were added to bleach organic matter and disaggregate the sediment, respectively. After digesting for 24 hours, the samples were sieved (45 μm) to isolate charcoal particles, of which images were taken using a Nikon SMZ745T microscope equipped with a DSFi3 camera.

Charcoal particle abundances were tallied, normalized by sample weight, and charcoal accumulation rates were calculated by the following equation:

$$CHAR = \left(\frac{charcoal\ count}{sample\ weight\ (mg)}\right) \times \frac{(bottom\ composite\ depth - top\ composite\ depth)}{(bottom\ age - top\ age)}$$

CHAR in marine sediments is used as a proxy for fire activity, reflecting overall amount of biomass burned (Genet et al., 2021; Haliuc et al., 2023).

Morphometric characteristics of each particle were collected using CharTool (Snitker, 2020). In this study, we focus on the morphometric parameters of L:W $(\text{major axis} \div \text{minor axis of the best fitting ellipse})$, roundness $(4 \times \text{area} \div (\pi \times \text{major axis}^2))$, circularity $(4\pi \times \text{area} \div \text{perimeter}^2)$, solidity $(\text{area} \div \text{convex area})$, rectangularity $(\text{perimeter} \div ((\text{width} + \text{height}) \times 2))$, and feret diameter (longest distance between any two points along the selection boundary).

A morphological flow chart adapted from Enache and Cumming (2006) was utilized to characterize the morphologies of charcoal particles in each sediment sample. In this study, the

groups of the morphology types we quantified were elongated (no ramifications; type F; from Enache and Cumming (2006)), elongated (ramifications; type D), geometric (types S/B and C), and irregular (types M and P). Extensive research has linked morphology type and L:W to fuel type (Crawford & Belcher, 2014; Enache & Cumming, 2006; Feurdean, 2021; Frank-DePue et al., 2023), and with feret diameter differentiating between herbaceous and woody fuel (Galinger et al., 2025). The other morphometrics have little research connecting them to specific aspects of a fire regime but give us insight into the subtle shape differences and tendencies of the charcoal particulates. Exploring the variety of morphometric measurements may illuminate their significant ability to characterize shape shifts of charcoal in sediment.

2.4 Previously published paleoclimate data

For the comparison of paleoclimate data to the sedimentary charcoal data, we utilized $\delta^{18}O$ from benthic foraminifera (*C. wuellerstorfi/C. mundulus*) and $\Delta\delta^{13}C$ from planktic (*T. sacculifer*) and benthic foraminifera (*C. wuellerstorfi/C. mundulus*) from Holbourn et al., 2021. Additionally, for inferred SST estimates we utilized *G. sacculifer-quadrilobatus* Magnesium/Calcium ratio from Steinke et al., 2010, and we used the age model from Holbourn et al., 2021 on this data. We utilized $\delta^{13}C_{alk}$ from leaf wax for vegetation changes (Zhou et al., 2017). For fire signal to compare to CHAR, we utilized pyrogenic carbon (PyC) percentage, and for fuel type resolution comparison, we utilized $\delta^{13}C_{pyC}$ (Zhou et al., 2017)**.** All these data are from Site 1146.

For additional fire signal, we utilized black carbon (BC) percentage from ODP Site 1148 (Figure 1; Jia et al., 2003).

There are no other vegetation proxies from the same core to support interpretations about fuel type and C_3/C_4 vegetation. As a result, interpretations of C_3/C_4 composition of vegetation are solely based on $\delta^{13}C_{alk}$ from Zhou et al., 2017.

2.5 Statistical analysis

All statistical analyses were conducted in R version 4.4.3 using tidyverse to import, clean, and manipulate data and ggplot2 for figures (Wickham et al., 2019, 2025). We quantified the relationships between morphometric characteristics and morphological type abundances using Pearson correlation (*r*). We used a null hypothesis probability level of 5% (p-value < 0.05) to determine statistical significance.

We used constrained incremental sum of squares cluster analysis (CONISS; Grimm, 1987) to quantitatively assess stratigraphical clustering of charcoal abundance data and identify the timing in morphology type. CONISS is computed from a distance matrix, where Euclidean distance is used to quantify dissimilarity among samples. It is considered a hierarchical agglomerative technique because it progressively merges individual samples into larger clusters until all observations are combined into a single grouping. The boundaries of the zones are determined by inspection of the stratigraphic diagrams. The analysis was conducted with package rioja (Juggins, 2024).

To evaluate if the changes and variability in PyC% and BC% are larger than analytical error, we used simple linear regression models with age as the predictor variable. Model fit was assessed using R^2, and statistical significance was evaluated using t-tests on regression coefficients. To determine whether increased CHAR was robust to sampling variability and not driven by individual data points, we used influence diagnostics and sensitivity analyses. First, an

ordinary least squares (OLS) regression was used of CHAR against age. From this, Cook's distance, leverage, and DFbetas was calculated to identify points with disproportionate influence on the model. A leave-one-out (LOO) analysis was used where the regression was refit after sequentially removing each observation. To further quantify sensitivity to sampling variation, jackknife estimate of the regression slope was calculated and a nonparametric bootstrap (2,000 resamples) was conducted to obtain a bootstrap distribution of slope estimates. For the bootstrap analysis, we used the package boot (Canty et al., 2025). Finally, a robust regression model was fit using M-estimation to evaluate whether the CHAR–age relationship remained when downweighing potential outliers. The package MASS was used to conduct this analysis (Ripley et al., 2025). Together, these analyses assessed CHAR increase remained consistent across multiple resampling and influence-resistant approaches.

3. Results

The 1146A samples we analyzed resolved an average of 0.66 ka each (standard deviation (σ) = 0.11 ka), and the 1146C samples averaged 26.68 ka (σ = 2.45 ka). Charcoal accumulation rates varied (average (μ) = 1.4 (#·cm)/(mg·Ma), σ = 1.0 (#·cm)/(mg·Ma)) and were generally low (μ = 1.3 (#·cm)/(mg·Ma), σ = 0.8 (#·cm)/(mg·Ma)) from 8.0 Ma to 7.3 Ma and 6.9 Ma to 5.1 Ma (μ = 1.2 (#·cm)/(mg·Ma), σ = 0.6 (#·cm)/(mg·Ma)), with the greatest values (maximum = 5.5 (#·cm)/(mg·Ma)) occurring between 7.3 Ma and 6.9 Ma (Figure 2).

The OLS regression of CHAR against age showed a weak, non-significant positive trend (slope = 0.0012, p = 0.26, R^2 = 0.03). Influence diagnostics indicated that several observations had moderate influence (Cook's distance up to 0.27). However, all leverage values are low (< 0.1), meaning no point is extremely far from the rest in terms of age, or strongly altered the

regression coefficients (all DFbetas < 0.6). Leave-one-out refitting demonstrated that the slope remained positive in all cases (0.00094–0.00134), indicating that the CHAR increase was not driven by a single data point. The jackknife estimate of the slope (0.0012) was almost the same to the full-model estimate, and bootstrap resampling (2,000 iterations) produced a similar mean slope (0.0012 ± 0.0010 SE). Robust regression also resulted in a positive slope (0.0006). Collectively, these analyses show that the 7.3–6.9 Ma increase in CHAR is stable across influence diagnostics, resampling, and robust modeling approaches.

Circularity ($\mu = 0.33$, $\sigma = 0.17$), feret diameter ($\mu = 173.71\mu m$, $\sigma = 110.20\ \mu m$), roundness ($\mu = 0.42$, $\sigma = 0.17$), solidity ($\mu = 0.55$, $\sigma = 0.17$), rectangularity ($\mu = 0.94$, $\sigma = 0.08$), and L:W ($\mu = 4.62$, $\sigma = 2.44$) all varied throughout time, but there were few notable temporal trends in these morphometric data (Figure 2). One notable aspect of the morphometric data are their significant relationships among one another, along with irregular and elongated (no ramifications) morphotypes (Table 1).

Elongated (no ramifications) and irregular were the two most common morphotypes identified (both with 45.12%), with both fluctuating through time (Figure 2). Geometric (8.94%) and elongated (ramifications) (0.91%) had much smaller charcoal assemblages. Irregular morphotypes dominated from 6.2 to 5.1 Ma, whereas before 6.2 Ma elongated (no ramifications) was more prevalent. CONISS revealed two prominent morphological zones separating ~6.2 Ma (Figure 3).Linear regression analyses showed weak but statistically significant relationships between age and both PyC% and BC%. For PyC%, age was a negative predictor ($\beta = -0.0012 \pm 0.00035$ SE, $t = -3.42$, $p < 0.001$), explaining 7.6% of the variance ($R^2 = 0.076$; $N = 143$). For BC%, age was a positive predictor ($\beta = 0.0098 \pm 0.0022$ SE, $t = 4.50$, $p < 0.001$), explaining 7.7% of the variance ($R^2 = 0.077$; $N = 244$).

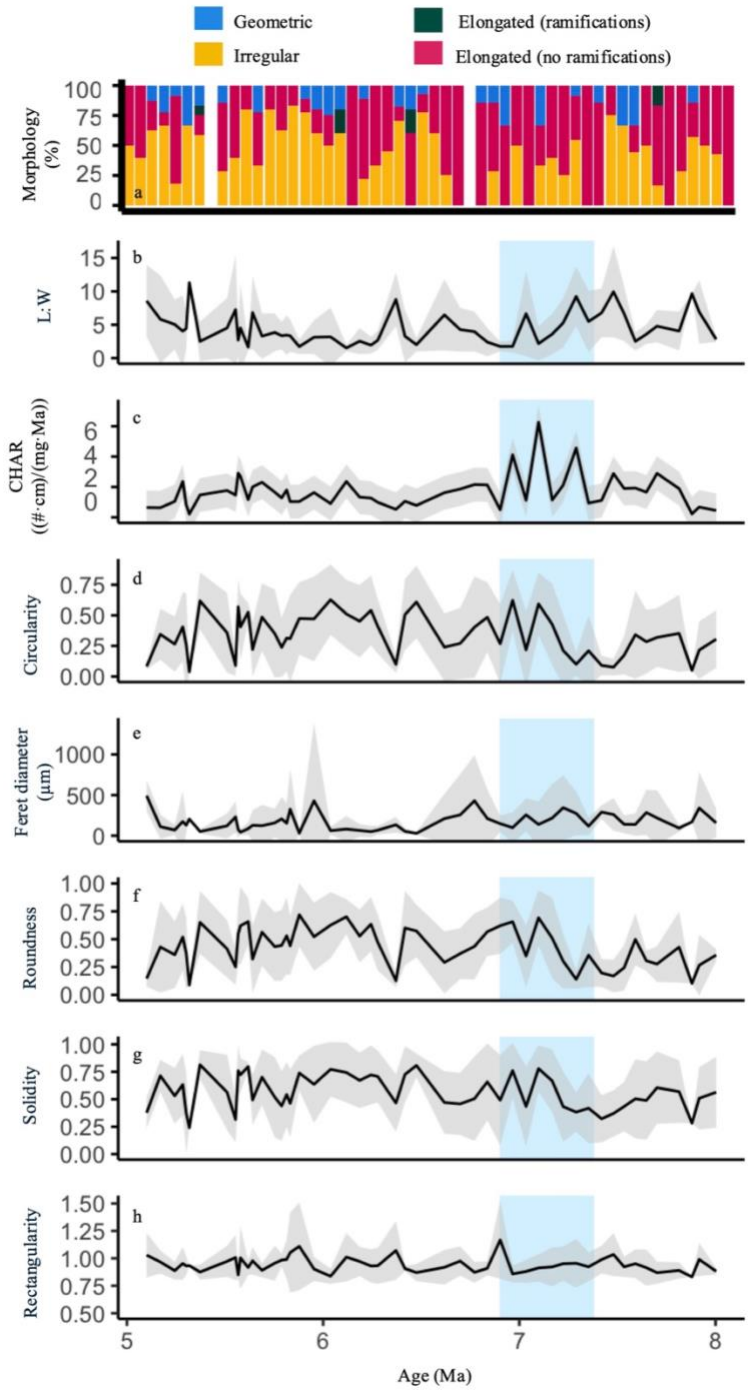

Figure 2: Morphologies, charcoal accumulation rates (CHAR), and average morphometric measurements of charcoal in marine sediments from ODP Site 1146 in the South China Sea. (a) Morphology percentage, (b) L:W, (c) CHAR, (d) circularity, (e) feret diameter, (f) roundness, (g)

solidity, and (h) rectangularity. Grey ribbon represents the standard deviation of the mean. Blue rectangle highlights the interval with increased CHAR (7.3–6.9 Ma).

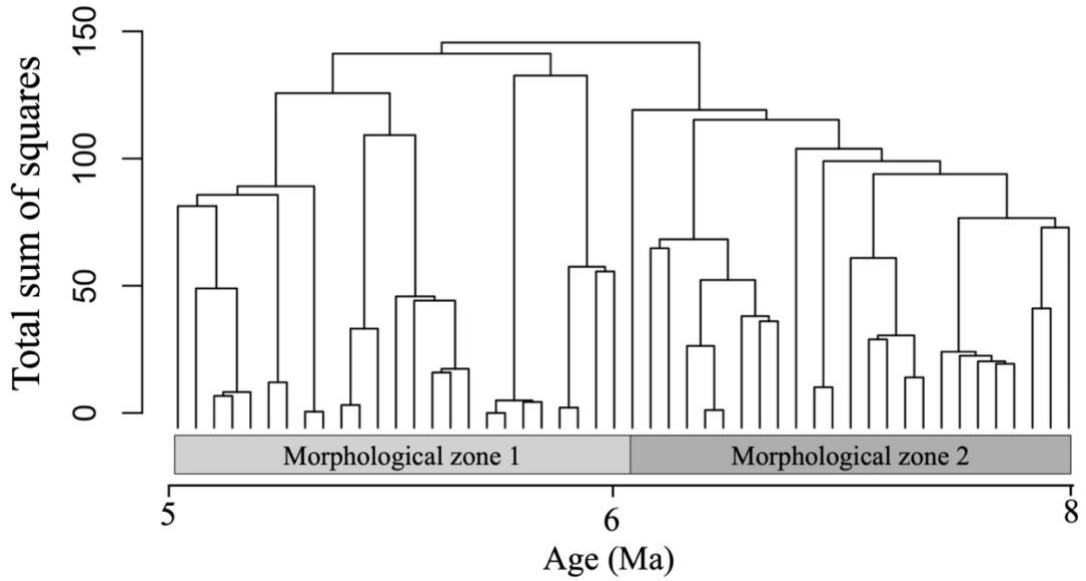

Figure 3: Two morphological zones identified based on CONISS.

4. Discussion

4,1 Provenance of sedimentary charcoal

Sedimentary charcoal preserved in ODP Site 1146 was primarily reflective of fire on the adjacent SouthChina margin. The main source of sediment to the South China Sea is the Pearl River Basin since the early Miocene (~30 Ma), whereas aeolian dust only accounts for small portion of sediment input (Du et al., 2020; Jin et al., 2022). Other studies from the Iberian margin and Southern Africa demonstrated that marine microcharcoal is dominated by transport from nearby river systems, with atmospheric inputs forming only a small background signal (Genet et al., 2021; Haliuc et al., 2023). Therefore, the Pearl River system represented the most likely source regions for charcoal delivered to the South China Sea. Particle size also plays a critical

role in determining charcoal provenance (Whitlock & Larsen, 2001). Fine particles (<100 μm) can be lofted high into the atmosphere and transported over long distances (Clark & Patterson, 1997). Around 30% of the charcoal particles found in our samples were <100 μm (μ = 66.3 μm). This suggests the sedimentary charcoal record predominantly captures integrated regional and local fire signals, rather than site-specific burning. Together, this indicates that the sedimentary charcoal from Site 1146 is best interpreted as a regional fire proxy for South China, shaped by fluvial transportation from the Pearl River system.

4.2 Fire activity and vegetation change across the gradual C_4 expansion

Between 7.3–6.9 Ma, there was an interval of increased CHAR values in our data, suggesting an increase in fire activity. The sensitivity analyses showed that the positive trend between 7.3 and 6.9 Ma in CHAR remained even when influential points are removed, and the trend was not driven by a few influential data points. Even though the trend was not statistically significant in a simple regression, it was robust to sampling variability.

The increased CHAR coincided with a small increase in both the pyrogenic carbon (0.02–0.09%; Zhou et al., 2017) and black carbon percentage (0.017–0.027%; Jia et al., 2003; Figure 4). The discrepancies in the overall fire activity trends reflected in PyC and BC percentages, and CHAR likely stemmed from differing source areas. PyC is formed at high temperatures during fire and biomass burning and is emitted into the atmosphere before deposition (Bird et al., 2015). Therefore, the source area for PyC from Site 1146 was likely from higher latitudes and altitudes of continental East Asia (Zhou et al., 2017). BC was primarily transported by winds before deposition at Site 1148, meaning the fire signal from the BC is large-scale across East Asia (Jia et al., 2003). Therefore, PyC and BC are likely capturing a

broader, East Asian signal, whereas CHAR is more likely to be originating from the Pearl River Basin and South China(Patterson et al., 1987; Preston & Schmidt, 2006). Natural variability is high in PyC% ($R^2 = 0.076$) and BC% ($R^2 = 0.077$), indicating that most variation reflects background noise rather than age-related trends. Together, the increase in the three proxies from 7.3–6.9 Ma demonstrates a fire activity signal, supported by the drastic increase in CHAR (Figure 2).

During the period of increased fire activity in CHAR (7.3– 6.9 Ma), average L:W ratio has a negative shift (5.5–1.8). This is the opposite of what would be expected according to the Fire Hypothesis, as it suggests there was a transition from grassy to woody fuel (Crawford & Belcher, 2014; Li et al., 2019; Ogura, 2007; Umbanhowar & Mcgrath, 1998; Zhang and Lu, 2005). Additionally, the charcoal morphology types do not demonstrate a transition in fuel type during the increased fire activity (Figure 2). Over the full resolution of our data (8.0–5.0 Ma), we found there is a transition from primarily elongated (no ramifications) to irregular morphology type at ~6.2 Ma, implying a gradual shift from grassy to woody fuel type (Figure 2; Figure 3; Crawford & Belcher, 2014; Feurdean et al., 2021; Vachula et al., 2021). This is also opposite of the expectations of the Fire Hypothesis. Given that L:W ratios are well studied proxies for fuel source characterization (Crawford & Belcher, 2014; Feurdean et al., 2023; Vachula et al., 2021), the absence of detectable changes across the C_3/C_4 transition implies there was no change in fuel type.

Differences between charcoal morphology and L:W ratios likely reflect the distinct ways in which these metrics characterize charcoal assemblages. While morphology captures the full diversity of particle shapes within a sample (Enache & Cumming, 2006), L:W represents an average of all charcoal particles within a sample (Crawford & Belcher, 2014). As a result,

samples containing a mixture of elongated and irregular particles may show intermediate L:W values despite clear morphological heterogeneity. Thus, these proxies are complementary, with morphology reflecting assemblage composition and L:W indicating the dominant shape of the particles (Enache & Cumming, 2006; Vachula et al., 2021; Crawford & Belcher, 2016; Pereboom et al., 2020).

Fuel type recorded by the charcoal particles is supported by the $\delta^{13}C_{pyC}$ data, where the range of values for C_3 plants is between −32‰ and −20‰, and the range for C_4 plants is between −15‰ and −9‰ with +1‰ enrichment (Zhou et al., 2017). In the time spans of both increased CHAR (7.3–6.9 Ma) and the full resolution of this study (8.0–5.0 Ma) the $\delta^{13}C_{pyC}$ primarily reflects C_3 vegetation (−25.00‰–−18.03‰; Figure 4; Zhou et al., 2017). Therefore, we infer that the C_4 grass expansion occurred independently of any significant, megaannum-scale alteration in fuel type.

Our findings only partially support the Fire Hypothesis as it applies to Southeast China. The original Fire Hypothesis posits a mechanism of preferential burning, where C_3 forests burned to create space for C_4 grasses (Keeley & Rundel, 2005). While our data demonstrate an increase in fire activity from 7.3 to 6.9 Ma, there is no accompanying evidence for a shift in fuel type or preferential burning of woody vegetation during the increase in fire activity (Figure 2). The shift from predominantly grassy to woody fuel type via morphology type assemblages throughout the scope of our data (8.0–5.0 Ma) is contradictory to the Fire Hypothesis, which would see the opposite shift. Our findings contrast other published perspectives that inferred preferential burning from other proxies such as pollen, plant and fire biomarkers, and stable carbon isotopes (Feakins et al., 2020; Hoetzel et al., 2013; Karp et al., 2021). The absence of fuel type changes through average L:W in our data suggests that although fire activity increased,

other factors must have had a greater influence on the C_4 expansion. Consequently, while an increase in fire activity may have played a role in shaping the late Miocene ecosystems, our results do not wholly support the Fire Hypothesis in that our data show that woody plants did not preferentially burn prior to the C_4 grass expansion.

4.3 Marine charcoal preservation limitations

As the charcoal particulates in our samples are allochthonous and traveling long distances to the deposition sites, the assemblage may be biased and not fully representative of the vegetation on the adjacent landmass (Genet et al., 2021; Haliuc et al., 2023). However, we believe our conclusions based on these measurements are robust as we do not see clear evidence for taphonomic bias, which we explore below. Further, we assert that charcoal morphology and morphometrics are one of the only proxies that encompasses both fuel type and fire activity, thus making the characteristics a reasonable tool for examining fuel type in the late Miocene.

Despite the potential of sedimentation and transportation changing the morphometrics, there is no evidence of this in our data. We found that circularity increases as feret diameter decreases ($r = –0.47$, $p < 0.01$), meaning as the charcoal particles become smaller, they become more circular. While this could be a sign of erosion from longer transportation (Crawford & Belcher, 2014), we do not believe this to be the case. Throughout the time of our study (8.0–5.0 Ma), the EASM weakened and the EAWM strengthened (Holbourn et al., 2018), and, in turn, SST increased and upwelling weakened, which would cause decreased erosion of the charcoal particulates once they are deposited. The weak negative correlation between circularity, and feret diameter with the climate proxies suggests that neither transportation nor sedimentation affected our morphometric data. Our overall morphology type, morphometrics, and subsequent fuel type

assignments will not change with increased transportation time as the relative shape of the charcoal particulates remains unchanged.

Although size-dependent waterlogging could affect charcoal preservation and our interpretations, we do not see clear evidence for this as a bias in our data. Charcoal particulates initially float in water, and larger particles sink first once they become waterlogged (Nichols et al., 2000). In marine sediments, charcoal particulates are likely smaller because they remain afloat longer and are able to be transported further to then be deposited in marine sediment (Genet et al., 2021; Haliuc et al., 2023; Higuera et al., 2007; Nichols et al., 2000). We also observed small charcoal particulates in our samples based on the feret diameter (μ = 173.71 μm, σ = 110.20 μm) that range from 28.61 μm to 492.44 μm. The feret diameter is skewed towards higher values, suggesting we may have lost smaller particles due to the 45 μm sieve. Further, the quality of preservation decreases with increased transport, especially fluvial transport, and some charcoal particulates may be lost altogether because of fragmentation or dispersal from the initial burn site, which could explain the relatively small feret diameters (Nicholas, 2000). Overall, the observed size range suggests that transport and waterlogging did not significantly bias our charcoal record.

4.4 Regional climatic controls on the C_4 expansion

The increase in CHAR aligns with changes in regional climate proxies (7.3–6.9 Ma; Figure 4; Steinke et al., 2010; Holbourn et al., 2021), suggesting that regional climate changes drove C_4 expansion as opposed to fire alone. From 7.3–6.9 Ma, there was a downward shift of $\Delta\delta^{13}C$, reflective of a weakened biological pump and reduced productivity due to less runoff and nutrient input, suggesting the EASM weakened (Figure 4; Holbourn et al., 2021). Concurrently,

there was a slight positive shift in benthic $\delta^{18}O$, indicating cooler temperatures and an increase in global ice volume (Figure 4; Holbourn et al., 2021). Similarly, warmer sea surface temperatures in the South China Sea, inferred from foraminifera Mg/Ca measurements indicate less wind-driven upwelling and therefore a weaker EASM (Figure 4; Steinke et al., 2010). Regionally, these proxy data support a climate shift towards: (1) weakening of the EASM; (2) strengthening of the EAWM; (3) increased aridity and; (4) reduced freshwater runoff to the South China Sea. These shifts coincide with our evidence for elevated fire activity in our data and by minimal fuel type changes (Figure 4). This juxtaposition suggests that top-down climatic controls spurred elevated fire activity rather than bottom-up fuel type changes.

Altogether, our paleofire data and comparison to regional paleoclimate data suggest that changes in regional climate were likely the driver of the C_4 proliferation and increased fire activity (Tipple & Pagani, 2007). Indeed, C_4 plants were likely present in vegetation since 30 Ma (Edwards et al., 2010); their proliferation only occurred during the transitioning into a weakening EASM system because as it set up the ideal arid environment for C_4 grasses. At the time of our observed increase in CHAR, the C_3 plant population was already declining. However, C_4 plants are more resilient to changing precipitation patterns and are more successful in arid environments (Tipple & Pagani, 2007), further enabling their establishment (Weiguo et al., 2005). Increased fire activity and the unchanged fuel types, evident in our data, could also be attributed to aridification and the weakening of EASM as reducing available moisture would have increased flammability of both C_3 woody vegetation and C_4 plants, creating space for fire-resilient C_4 grasses (Hui et al., 2021; Karp et al., 2018; Pausas & Paula, 2020). C_4 grasses accumulate high biomass, storing most of it underground, which allows them to be resilient under high stress disturbances like monsoons and fire (Bond, 2008; Liu et al., 2005; Shen et al.,

2018). The combination of intensifying aridification and fire, as well as weakening monsoon seasons likely all contributed to fostering an environment best suited for C_4 grasses, allowing their spread and domination of southeast Asia.

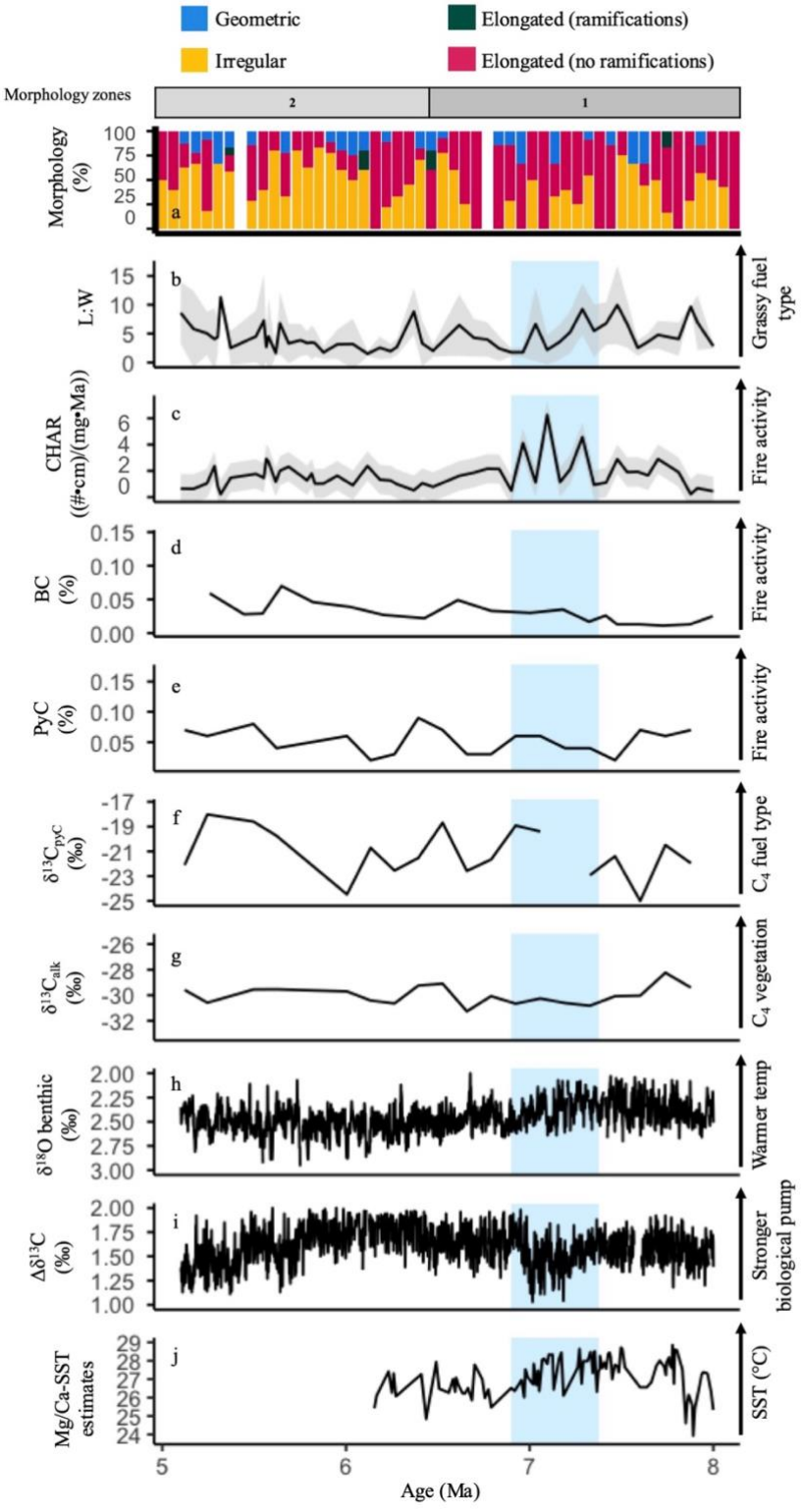
Geometric
Irregular
Elongated (ramifications)
Elongated (no ramifications)
Morphology zones
2
1
Morphology (%)
100
75
50
25
0
a
L:W
15
10
5
0
b
Grassy fuel type
CHAR ((#•cm)/(mg•Ma))
6
4
2
0
c
Fire activity
BC (%)
0.15
0.10
0.05
0.00
d
Fire activity
PyC (%)
0.15
0.10
0.05
e
Fire activity
$\delta^{13}C_{pyC}$ (‰)
-17
-19
-21
-23
-25
f
C_4 fuel type
$\delta^{13}C_{alk}$ (‰)
-26
-28
-30
-32
g
C_4 vegetation
$\delta^{18}O$ benthic (‰)
2.00
2.25
2.50
2.75
3.00
h
Warmer temp
$\Delta\delta^{13}C$ (‰)
2.00
1.75
1.50
1.25
1.00
i
Stronger biological pump
Mg/Ca-SST estimates
29
28
27
26
25
24
j
SST (°C)
5
6
7
8
Age (Ma)

Figure 4: Comparison of charcoal data from ODP Site 1146 with previously published records from ODP Sites 1146 and 1148. (a) Morphology type (this study), (b) average L:W (this study), (c) Charcoal Accumulation Rate (CHAR; this study), (d) black carbon (BC) percentage from ODP site 1148 (Jia et al., 2003), (e) PyC (%) (Zhou et al.,2017), (f) $\delta^{13}C_{pyC}$ (Zhou et al., 2017), (g) $\delta^{13}C_{alk}$ (Zhou et al., 2017), (h) δ18O from benthic foraminifera (*C. wuellerstorfi/C. mundulus*; Holbourn et al., 2021), (i) $\Delta\delta^{13}C$ from planktic (*T. sacculifer*) and benthic foraminifera (*C. wuellerstorfi/C. mundulus*; Holbourn et al., 2021), and (j) *G. sacculifer-quadrilobatus* Magnesium/Calcium ratio inferred SST estimates (used age model from Holbourn et al., 2021; Steinke et al., 2010). Blue rectangle highlights the interval with increased CHAR (7.3–6.9 Ma). Gray rectangles show the morphological zones based on CONISS.

4.5 Relationships between the different morphometrics and morphotypes

Our study further offers an opportunity to quantify the relationships between the morphometrics and morphotypes that are used to understand charcoal fuel types beyond the late Miocene C_4 grass expansion and the Fire Hypothesis. Morphology type is a well-established qualitative fuel type proxy. However, as with any qualitative proxy, a degree of human influence and bias can affect morphology type assignments to fuel types (Frank-DePue et al., 2023). On the other hand, morphometrics offer a quantitative approach to assigning fuel type to the charcoal particulates and previous research primarily focuses on average L:W (aspect ratio) to differentiate woody versus grass/non-woody fuel (Crawford & Belcher, 2014; Feurdean et al., 2023; Vachula et al., 2021). A few studies have connected increased circularity to increased transportation time, but not fuel type (Crawford & Belcher, 2014; Nichols et al., 2000). Further, although other morphometrics have been linked to fuel types (Galinger et al., 2025), little work

has examined the interrelationships between different morphometrics. Our data show that roundness, circularity, and solidity all have strong positive correlations to each other suggesting that they are recording the same general shape variation (Table 1). Irregular morphotype is strongly correlated with circularity and roundness, and elongated (no ramifications) morphotype was strongly correlated with L:W ratio (Table 1). These correlations suggest that the morphometrics we measured are supporting and quantifying what we already saw when assigning the morphology types. Therefore, we conclude that morphometrics alone are insufficient to assign fuel type to charcoal particulates due to the influences of sedimentation, deposition, and weathering (Frank-DePue et al. 2023).

5. Conclusions

Our study found that regional climate change was the primary driver of C_4 proliferation and the associated increase in fire activity observed from sedimentary charcoal primarily from the Pearl River. This is in contrast with the Fire Hypothesis that proposes that only fire activity initiated the C_4 expansion. We observe increased fire activity between 7.3–6.9 Ma. Across all influence and sensitivity analyses, the 7.3–6.9 Ma rise in CHAR remains consistently positive, demonstrating that the observed increase is robust to sampling variability. However, during this interval, our data show no evidence that woody vegetation was preferentially burned, based on charcoal average L:W ratios and composite morphology types. Across the broader time span of 8.0–5.0 Ma, charcoal morphometric traits show no significant shifts that would indicate a transition from woody to grassy fuel type, and the morphology abundances show a transition from grassy to woody fuel types. Instead, the increase in charcoal abundance corresponds with regional climate proxy changes, supporting regional climate change as the key factor in C_4

expansion and only partially supporting the Fire Hypothesis in Southeast China. Additionally, our results provide new insight into the use of charcoal morphometrics. Some morphometric measures overlap in their ability to characterize sedimentary charcoal particles. For future paleoecological and paleofire research, we recommend using morphometrics in combination with morphology types to identify fuel sources, rather than relying on morphometrics alone.

References Cited

Barney, S. R., Cheung, A. H., Welch, J. C., & Vachula, R. S. (2025). Sedimentary charcoal morphometrics and morphologies of Ocean Drilling Program Site 1146 [dataset]. *Auburn University Scholarly Repository*. https://doi.org/10.35099/2xac-vh03.

Alam, M., Muguli, T., Gurumurthy, G. P., Arif, M., Sohrin, Y., Singh, A. D., Radhakrishna, T., Pandey, D. K., & Verma, K. (2023). Hydroclimatic conditions and sediment provenance in the northeastern Arabian Sea since the late Miocene: Insights from geochemical and environmental magnetic records at IODP Site U1457 of the Laxmi Basin. *Geological Magazine*, *160*(4), 813–829. https://doi.org/10.1017/S0016756822001273

Berger, W. H., Lange, C. B., & Pérez, M. E. (2002). The early Matuyama Diatom Maximum off SW Africa: A conceptual model. *Marine Geology*, *180*(1), 105–116. https://doi.org/10.1016/S0025-3227(01)00208-0

Bird, M. I., Wynn, J. G., Saiz, G., Wurster, C. M., & McBeath, A. (2015). The Pyrogenic Carbon Cycle. *Annual Review of Earth and Planetary Sciences*, *43*(Volume 43, 2015), 273–298. https://doi.org/10.1146/annurev-earth-060614-105038

Bond, W. J. (2008). What Limits Trees in C4 Grasslands and Savannas? *Annual Review of Ecology, Evolution, and Systematics*, *39*(1), 641–659. https://doi.org/10.1146/annurev.ecolsys.39.110707.173411

Bond, W. J., & Keeley, J. E. (2005). Fire as a global 'herbivore': The ecology and evolution of flammable ecosystems. *Trends in Ecology & Evolution*, *20*(7), 387–394. https://doi.org/10.1016/j.tree.2005.04.025

Cerling, T. E., Wang, Y., & Quade, J. (1993). Expansion of C4 ecosystems as an indicator of global ecological change in the late Miocene. *Nature*, *361*(6410), 344–345. https://doi.org/10.1038/361344a0

Chauhan, M. M., Ali, S., Khan, A. M., Kumar, P., Murari, M. K., Samal, P., Singh, B. P., Adlakha, V., Saikia, L., Phartiyal, B., & Sharma, A. (2025). Tracing South Asian monsoon variability through a late miocene record from the himalayan foreland basin. *Npj Climate and Atmospheric Science*, *9*(1), 21. https://doi.org/10.1038/s41612-025-01293-5

Clark, J. S., & Patterson, W. A. (1997). Background and Local Charcoal in Sediments: Scales of Fire Evidence in the Paleorecord. In J. S. Clark, H. Cachier, J. G. Goldammer, & B. Stocks (Eds.), *Sediment Records of Biomass Burning and Global Change* (pp. 23–48). Springer. https://doi.org/10.1007/978-3-642-59171-6_3

Clift, P. D., Kulhanek, D. K., Zhou, P., Bowen, M. G., Vincent, S. M., Lyle, M., & Hahn, A. (2020). Chemical weathering and erosion responses to changing monsoon climate in the Late Miocene of Southwest Asia. *Geological Magazine*, *157*(6), 939–955. https://doi.org/10.1017/S0016756819000608

Clift, P. D., Wan, S., & Blusztajn, J. (2014). Reconstructing chemical weathering, physical erosion and monsoon intensity since 25 Ma in the northern South China Sea: A review of competing proxies. *Earth-Science Reviews*, *130*, 86–102. https://doi.org/10.1016/j.earscirev.2014.01.002

Crawford, A. J., & Belcher, C. M. (2014). Charcoal morphometry for paleoecological analysis: The effects of fuel type and transportation on morphological parameters. *Applications in Plant Sciences*, *2*(8), 1400004. https://doi.org/10.3732/apps.1400004

Daniau, A.-L., Desprat, S., Aleman, J. C., Bremond, L., Davis, B., Fletcher, W., Marlon, J. R., Marquer, L., Montade, V., Morales-Molino, C., Naughton, F., Rius, D., & Urrego, D. H. (2019). Terrestrial plant microfossils in palaeoenvironmental studies, pollen, microcharcoal and phytolith. Towards a comprehensive understanding of vegetation, fire and climate changes over the past one million years. *Revue de Micropaléontologie*, *63*, 1–35. https://doi.org/10.1016/j.revmic.2019.02.001

Diester-Haass, L., Meyers, P. A., & Rothe, P. (1990). Miocene history of the Benguela Current and Antarctic ice volumes: Evidence from rhythmic sedimentation and current growth across the Walvis Ridge (Deep Sea Drilling Project Sites 362 and 532). *Paleoceanography*, *5*(5), 685–707. https://doi.org/10.1029/PA005i005p00685

Dinerstein, E., Olson, D., Joshi, A., Vynne, C., Burgess, N. D., Wikramanayake, E., Hahn, N., Palminteri, S., Hedao, P., Noss, R., Hansen, M., Locke, H., Ellis, E. C., Jones, B., Barber, C. V., Hayes, R., Kormos, C., Martin, V., Crist, E., … Saleem, M. (2017). An Ecoregion-Based Approach to Protecting Half the Terrestrial Realm. *BioScience*, *67*(6), 534–545. https://doi.org/10.1093/biosci/bix014

Du, S., Xiang, R., Liu, J., Liu, J. P., Islam, G. M. A., & Chen, M. (2020). The present-day atmospheric dust deposition process in the South China Sea. *Atmospheric Environment*, *223*, 117261. https://doi.org/10.1016/j.atmosenv.2020.117261

Dupont, L. M., Donner, B., Vidal, L., Pérez, E. M., & Wefer, G. (2005). Linking desert evolution and coastal upwelling: Pliocene climate change in Namibia. *Geology*, *33*(6), 461–464. https://doi.org/10.1130/G21401.1

Dupont, L. M., Rommerskirchen, F., Mollenhauer, G., & Schefuß, E. (2013). Miocene to Pliocene changes in South African hydrology and vegetation in relation to the expansion of C4 plants. *Earth and Planetary Science Letters*, *375*, 408–417. https://doi.org/10.1016/j.epsl.2013.06.005

Dupont, L. M., & Wyputta, U. (2003). Reconstructing pathways of aeolian pollen transport to the marine sediments along the coastline of SW Africa. *Quaternary Science Reviews*, *22*(2), 157–174. https://doi.org/10.1016/S0277-3791(02)00032-X

Edwards, E. J., Osborne, C. P., Strömberg, C. A. E., Smith, S. A., C Grasses Consortium, Bond, W. J., Christin, P.-A., Cousins, A. B., Duvall, M. R., Fox, D. L., Freckleton, R. P., Ghannoum, O., Hartwell, J., Huang, Y., Janis, C. M., Keeley, J. E., Kellogg, E. A., Knapp, A. K., Leakey, A. D. B., … Tipple, B. (2010). The Origins of C $_4$ Grasslands: Integrating Evolutionary and Ecosystem Science. *Science*, *328*(5978), 587–591. https://doi.org/10.1126/science.1177216

Edwards, E. J., Osborne, C. P., Strömberg, C. A. E., Smith, S. A., C4 Grasses Consortium, Bond, W. J., Christin, P.-A., Cousins, A. B., Duvall, M. R., Fox, D. L., Freckleton, R. P., Ghannoum, O., Hartwell, J., Huang, Y., Janis, C. M., Keeley, J. E., Kellogg, E. A., Knapp, A. K., Leakey, A. D. B., … Tipple, B. (2010). The Origins of C4 Grasslands:

Integrating Evolutionary and Ecosystem Science. *Science*, *328*(5978), 587–591. https://doi.org/10.1126/science.1177216

Enache, M. D., & Cumming, B. F. (2006). Tracking recorded fires using charcoal morphology from the sedimentary sequence of Prosser Lake, British Columbia (Canada). *Quaternary Research*, *65*(02), 282–292. https://doi.org/10.1016/j.yqres.2005.09.003

Feakins, S. J., Liddy, H. M., Tauxe, L., Galy, V., Feng, X., Tierney, J. E., Miao, Y., & Warny, S. (2020). Miocene C4 Grassland Expansion as Recorded by the Indus Fan. *Paleoceanography and Paleoclimatology*, *35*(6), e2020PA003856. https://doi.org/10.1029/2020PA003856

Feurdean, A. (2021). Experimental production of charcoal morphologies to discriminate fuel source and fire type: An example from Siberian taiga. *Biogeosciences*, *18*(12), 3805–3821. https://doi.org/10.5194/bg-18-3805-2021

Feurdean, A., Vachula, R. S., Hanganu, D., Stobbe, A., & Gumnior, M. (2023). Charcoal morphologies and morphometrics of a Eurasian grass-dominated system for robust interpretation of past fuel and fire type. *Biogeosciences*, *20*(24), 5069–5085. https://doi.org/10.5194/bg-20-5069-2023

Frank-DePue, L., Vachula, R. S., Balascio, N. L., Cahoon, K., & Kaste, J. M. (2023). Trends in sedimentary charcoal shapes correspond with broad-scale land-use changes: Insights gained from a 300-year lake sediment record from eastern Virginia, USA. *Journal of Paleolimnology*, *69*(1), 21–36. https://doi.org/10.1007/s10933-022-00260-x

Galinger, M. R., Vachula, R. S., Goertzen, L. R., Hansen, C. J., & Cullen, T. M. (2025). A new approach to experimental charcoal analyses: Implications for the Cretaceous and other

greenhouse climate intervals. *Global and Planetary Change*, *255*, 105079. https://doi.org/10.1016/j.gloplacha.2025.105079

Genet, M., Daniau, A.-L., Mouillot, F., Hanquiez, V., Schmidt, S., David, V., Georget, M., Abrantes, F., Anschutz, P., Bassinot, F., Bonnin, J., Dennielou, B., Eynaud, F., Hodell, D. A., Mulder, T., Naughton, F., Rossignol, L., Tzedakis, P., & Sánchez-Goñi, M. F. (2021a). Modern relationships between microscopic charcoal in marine sediments and fire regimes on adjacent landmasses to refine the interpretation of marine paleofire records: An Iberian case study. *Quaternary Science Reviews*, *270*, 107148. https://doi.org/10.1016/j.quascirev.2021.107148

Genet, M., Daniau, A.-L., Mouillot, F., Hanquiez, V., Schmidt, S., David, V., Georget, M., Abrantes, F., Anschutz, P., Bassinot, F., Bonnin, J., Dennielou, B., Eynaud, F., Hodell, D. A., Mulder, T., Naughton, F., Rossignol, L., Tzedakis, P., & Sánchez-Goñi, M. F. (2021b). Modern relationships between microscopic charcoal in marine sediments and fire regimes on adjacent landmasses to refine the interpretation of marine paleofire records: An Iberian case study. *Quaternary Science Reviews*, *270*, 107148. https://doi.org/10.1016/j.quascirev.2021.107148

Gibson, D. J. (2009). *Grasses and Grassland Ecology*. Oxford University Press.

Grimm, E. C. (1987). CONISS: A FORTRAN 77 program for stratigraphically constrained cluster analysis by the method of incremental sum of squares. *Computers & Geosciences*, *13*(1), 13–35. https://doi.org/10.1016/0098-3004(87)90022-7

Haliuc, A., Daniau, A.-L., Mouillot, F., Chen, W., Leys, B., David, V., Hanquiez, V., Dennielou, B., Schefuß, E., Bayon, G., & Crosta, X. (2023). Microscopic charcoals in ocean

sediments off Africa track past fire intensity from the continent. *Communications Earth & Environment*, *4*(1), 1–11. https://doi.org/10.1038/s43247-023-00800-x

Herbert, T. D., Lawrence, K. T., Tzanova, A., Peterson, L. C., Caballero-Gill, R., & Kelly, C. S. (2016). Late Miocene global cooling and the rise of modern ecosystems. *Nature Geoscience*, *9*(11), 843–847. https://doi.org/10.1038/ngeo2813

Higuera, P. E., Peters, M. E., Brubaker, L. B., & Gavin, D. G. (2007). Understanding the origin and analysis of sediment-charcoal records with a simulation model. *Quaternary Science Reviews*, *26*(13), 1790–1809. https://doi.org/10.1016/j.quascirev.2007.03.010

Hoetzel, S., Dupont, L. M., & Wefer, G. (2015). Miocene–Pliocene vegetation change in south-western Africa (ODP Site 1081, offshore Namibia). *Palaeogeography, Palaeoclimatology, Palaeoecology*, *423*, 102–108. https://doi.org/10.1016/j.palaeo.2015.02.002

Hoetzel, S., Dupont, L., Schefuß, E., Rommerskirchen, F., & Wefer, G. (2013). The role of fire in Miocene to Pliocene C4 grassland and ecosystem evolution. *Nature Geoscience*, *6*(12), 1027–1030. https://doi.org/10.1038/ngeo1984

Holbourn, A. E., Kuhnt, W., Clemens, S. C., Kochhann, K. G. D., Jöhnck, J., Lübbers, J., & Andersen, N. (2018). Late Miocene climate cooling and intensification of southeast Asian winter monsoon. *Nature Communications*, *9*(1), 1584. https://doi.org/10.1038/s41467-018-03950-1

Holbourn, A., Kuhnt, W., Clemens, S. C., & Heslop, D. (2021). A ∼12 Myr Miocene Record of East Asian Monsoon Variability From the South China Sea. *Paleoceanography and Paleoclimatology*, *36*(7), e2021PA004267. https://doi.org/10.1029/2021PA004267

Huang, Y., Clemens, S. C., Liu, W., Wang, Y., & Prell, W. L. (2007). Large-scale hydrological change drove the late Miocene C4 plant expansion in the Himalayan foreland and Arabian Peninsula. *Geology*, *35*(6), 531–534. https://doi.org/10.1130/G23666A.1

Hui, Z., Gowan, E. J., Hou, Z., Zhou, X., Ma, Y., Guo, Z., & Zhang, J. (2021). Intensified fire activity induced by aridification facilitated Late Miocene C4 plant expansion in the northeastern Tibetan Plateau, China. *Palaeogeography, Palaeoclimatology, Palaeoecology*, *573*, 110437. https://doi.org/10.1016/j.palaeo.2021.110437

Inoue, J., & Usuki, T. (2025). Effects of particle size and pretreatment methods on the morphometry of grass charcoal particles: Implications for morphometric analysis of microcharcoal particles. *The Holocene*, *35*(4), 471–476. https://doi.org/10.1177/09596836241307296

Jia, G., Peng, P., Zhao, Q., & Jian, Z. (2003). Changes in terrestrial ecosystem since 30 Ma in East Asia: Stable isotope evidence from black carbon in the South China Sea. *Geology*, *31*(12), 1093–1096. https://doi.org/10.1130/G19992.1

Jin, H., Wan, S., Clift, P. D., Liu, C., Huang, J., Jiang, S., Li, M., Qin, L., Shi, X., & Li, A. (2022). Birth of the Pearl River at 30 Ma: Evidence from sedimentary records in the northern South China Sea. *Earth and Planetary Science Letters*, *600*, 117872. https://doi.org/10.1016/j.epsl.2022.117872

Karp, A. T., Behrensmeyer, A. K., & Freeman, K. H. (2018). Grassland fire ecology has roots in the late Miocene. *Proceedings of the National Academy of Sciences of the United States of America*, *115*(48), 12130–12135. https://doi.org/10.1073/pnas.1809758115

Karp, A. T., Uno, K. T., Polissar, P. J., & Freeman, K. H. (2021). Late Miocene C4 Grassland Fire Feedbacks on the Indian Subcontinent. *Paleoceanography and Paleoclimatology*, *36*(4), e2020PA004106. https://doi.org/10.1029/2020PA004106

Keeley, J. E., & Rundel, P. W. (2005). Fire and the Miocene expansion of C4 grasslands. *Ecology Letters*, *8*(7), 683–690. https://doi.org/10.1111/j.1461-0248.2005.00767.x

Laskar, J., Correia, A. C. M., Gastineau, M., Joutel, F., Levrard, B., & Robutel, P. (2004). Long term evolution and chaotic diffusion of the insolation quantities of Mars. *Icarus*, *170*(2), 343–364. https://doi.org/10.1016/j.icarus.2004.04.005

Lehmann, C. E. R., Anderson, T. M., Sankaran, M., Higgins, S. I., Archibald, S., Hoffmann, W. A., Hanan, N. P., Williams, R. J., Fensham, R. J., Felfili, J., Hutley, L. B., Ratnam, J., San Jose, J., Montes, R., Franklin, D., Russell-Smith, J., Ryan, C. M., Durigan, G., Hiernaux, P., … Bond, W. J. (2014). Savanna Vegetation-Fire-Climate Relationships Differ Among Continents. *Science*, *343*(6170), 548–552. https://doi.org/10.1126/science.1247355

Li, B., Wang, J., Huang, B., Li, Q., Jian, Z., Zhao, Q., Su, X., & Wang, P. (2004). South China Sea surface water evolution over the last 12 Myr: A south-north comparison from Ocean Drilling Program Sites 1143 and 1146. *Paleoceanography*, *19*(1). https://doi.org/10.1029/2003PA000906

Li, M., Wan, S., Colin, C., Jin, H., Zhao, D., Pei, W., Jiao, W., Tang, Y., Tan, Y., Shi, X., & Li, A. (2023). Expansion of C4 plants in South China and evolution of East Asian monsoon since 35 Ma: Black carbon records in the northern South China Sea. *Global and Planetary Change*, *223*, 104079. https://doi.org/10.1016/j.gloplacha.2023.104079

Liu, W., Huang, Y., An, Z., Clemens, S. C., Li, L., Prell, W. L., & Ning, Y. (2005). Summer monsoon intensity controls C4/C3 plant abundance during the last 35 ka in the Chinese

Loess Plateau: Carbon isotope evidence from bulk organic matter and individual leaf waxes. *Palaeogeography, Palaeoclimatology, Palaeoecology*, *220*(3), 243–254. https://doi.org/10.1016/j.palaeo.2005.01.001

Miao, Y., Song, Y., Li, Y., Yang, S., Li, Y., Zhao, Y., & Zeng, M. (2020). Late Pleistocene fire in the Ili Basin, Central Asia, and its potential links to paleoclimate change and human activities. *Palaeogeography, Palaeoclimatology, Palaeoecology*, *547*, 109700. https://doi.org/10.1016/j.palaeo.2020.109700

Miao, Y., Wu, F., Warny, S., Fang, X., Lu, H., Fu, B., Song, C., Yan, X., Escarguel, G., Yang, Y., Meng, Q., & Shi, P. (2019). Miocene fire intensification linked to continuous aridification on the Tibetan Plateau. *Geology*, *47*(4), 303–307. https://doi.org/10.1130/G45720.1

Mohanty, R. N., Gupta, A. K., & Clemens, S. (2025). Benguela upwelling system triggered and intensified southern African aridification in the Late Miocene. *Communications Earth & Environment*, *6*(1), 989. https://doi.org/10.1038/s43247-025-02948-0

Mouillot, F., & Field, C. B. (2005). *Fire history and the global carbon budget: A 1°× 1° fire history reconstruction for the 20th century*. *11*(3), 398–420. https://doi.org/10.1111/j.1365-2486.2005.00920

Nichols, G. J., Cripps, J. A., Collinson, M. E., & Scott, A. C. (2000). Experiments in waterlogging and sedimentology of charcoal: Results and implications. *Palaeogeography, Palaeoclimatology, Palaeoecology, Fire and the Palaeoenvironment*, *164*(1), 43–56. https://doi.org/10.1016/S0031-0182(00)00174-7

Pagani, M., Freeman, K. H., & Arthur, M. A. (1999). Late Miocene Atmospheric CO $_2$ Concentrations and the Expansion of C $_4$ Grasses. *Science*, *285*(5429), 876–879. https://doi.org/10.1126/science.285.5429.876

Pagani, M., Zachos, J. C., Freeman, K. H., Tipple, B., & Bohaty, S. (2005). Marked Decline in Atmospheric Carbon Dioxide Concentrations During the Paleogene. *Science*, *309*(5734), 600–603. https://doi.org/10.1126/science.1110063

Passey, B. H., Ayliffe, L. K., Kaakinen, A., Zhang, Z., Eronen, J. T., Zhu, Y., Zhou, L., Cerling, T. E., & Fortelius, M. (2009). Strengthened East Asian summer monsoons during a period of high-latitude warmth? Isotopic evidence from Mio-Pliocene fossil mammals and soil carbonates from northern China. *Earth and Planetary Science Letters*, *277*(3), 443–452. https://doi.org/10.1016/j.epsl.2008.11.008

Patterson, W. A., Edwards, K. J., & Maguire, D. J. (1987). Microscopic charcoal as a fossil indicator of fire. *Quaternary Science Reviews*, *6*(1), 3–23. https://doi.org/10.1016/0277-3791(87)90012-6

Pausas, J. G., & Paula, S. (2020). Grasses and fire: The importance of hiding buds. *The New Phytologist*, *226*(4), 957–959.

Pereboom, E. M., Vachula, R. S., Huang, Y., & Russell, J. (2020). The morphology of experimentally produced charcoal distinguishes fuel types in the Arctic tundra. *The Holocene*, *30*(7), 1091–1096. https://doi.org/10.1177/0959683620908629

Polissar, P. J., Uno, K. T., Phelps, S. R., Karp, A. T., Freeman, K. H., & Pensky, J. L. (2021). Hydrologic Changes Drove the Late Miocene Expansion of C4 Grasslands on the Northern Indian Subcontinent. *Paleoceanography and Paleoclimatology*, *36*(4), e2020PA004108. https://doi.org/10.1029/2020PA004108

Preston, C. M., & Schmidt, M. W. I. (2006). Black (pyrogenic) carbon: A synthesis of current knowledge and uncertainties with special consideration of boreal regions. *Biogeosciences*, *3*(4), 397–420. https://doi.org/10.5194/bg-3-397-2006

Quade, J., Cerling, T. E., & Bowman, J. R. (1989). Development of Asian monsoon revealed by marked ecological shift during the latest Miocene in northern Pakistan. *Nature*, *342*(6246), 163–166. https://doi.org/10.1038/342163a0

Ripley, B., Venables, B., Bates, D. M., ca 1998), K. H. (partial port, ca 1998), A. G. (partial port, & polr), D. F. (support functions for. (2025). *MASS: Support Functions and Datasets for Venables and Ripley's MASS* (Version 7.3-65) [Computer software]. https://cran.r-project.org/web/packages/MASS/index.html

Rommerskirchen, F., Condon, T., Mollenhauer, G., Dupont, L., & Schefuss, E. (2011). Miocene to Pliocene development of surface and subsurface temperatures in the Benguela Current system. *Paleoceanography*, *26*(3). https://doi.org/10.1029/2010PA002074

Rubbelke, C. B., Bhattacharya, T., Feng, R., Burls, N. J., Knapp, S., & McClymont, E. L. (2023). Plio-Pleistocene Southwest African Hydroclimate Modulated by Benguela and Indian Ocean Temperatures. *Geophysical Research Letters*, *50*(19), e2023GL103003. https://doi.org/10.1029/2023GL103003

S), A. C. (author of original code for, R, B. R. (conversion to, maintainer 1999--2022, support), author of parallel, & fixes), A. R. B. (minor bug. (2025). *boot: Bootstrap Functions* (Version 1.3-32) [Computer software]. https://cran.r-project.org/web/packages/boot/index.html

Sadler, P. M. (1981). Sediment Accumulation Rates and the Completeness of Stratigraphic Sections. *The Journal of Geology*, *89*(5), 569–584. https://doi.org/10.1086/628623

Sage, R. F. (2004). The evolution of C4 photosynthesis. *New Phytologist*, *161*(2), 341–370. https://doi.org/10.1111/j.1469-8137.2004.00974.x

Schefuß, E., & Dupont, L. M. (2020). Multiple drivers of Miocene C4 ecosystem expansions. *Nature Geoscience*, *13*(7), 463–464. https://doi.org/10.1038/s41561-020-0590-5

Scheiter, S., Higgins, S. I., Osborne, C. P., Bradshaw, C., Lunt, D., Ripley, B. S., Taylor, L. L., & Beerling, D. J. (2012). Fire and fire-adapted vegetation promoted C4 expansion in the late Miocene. *New Phytologist*, *195*(3), 653–666. https://doi.org/10.1111/j.1469-8137.2012.04202.x

Shen, X., Wan, S., Colin, C., Tada, R., Shi, X., Pei, W., Tan, Y., Jiang, X., & Li, A. (2018). Increased seasonality and aridity drove the C4 plant expansion in Central Asia since the Miocene–Pliocene boundary. *Earth and Planetary Science Letters*, *502*, 74–83. https://doi.org/10.1016/j.epsl.2018.08.056

Shi, N., Dupont, L. M., Beug, H.-J., & Schneider, R. (1998). Vegetation and climate changes during the last 21 000 years in S.W. Africa based on a marine pollen record. *Vegetation History and Archaeobotany*, *7*(3), 127–140. https://doi.org/10.1007/BF01374001

Singh, R. K., & Gupta, A. K. (2004). Late Oligocene–Miocene paleoceanographic evolution of the southeastern Indian Ocean: Evidence from deep-sea benthic foraminifera (ODP Site 757). *Marine Micropaleontology*, *51*(1), 153–170. https://doi.org/10.1016/j.marmicro.2003.10.003

Snitker, G. (2020). The Charcoal Quantification Tool (CharTool): A Suite of Open-source Tools for Quantifying Charcoal Fragments and Sediment Properties in Archaeological and Paleoecological Analysis. *Ethnobiology Letters*, *11*(1), 103–115.

Steinke, S., Groeneveld, J., Johnstone, H., & Rendle-Bühring, R. (2010). East Asian summer monsoon weakening after 7.5 Ma: Evidence from combined planktonic foraminifera Mg/Ca and δ18O (ODP Site 1146; northern South China Sea). *Palaeogeography,*

Palaeoclimatology, Palaeoecology, *289*(1), 33–43. https://doi.org/10.1016/j.palaeo.2010.02.007

Strömberg, C. A. E. (2011). Evolution of Grasses and Grassland Ecosystems. *Annual Review of Earth and Planetary Sciences*, *39*(Volume 39, 2011), 517–544. https://doi.org/10.1146/annurev-earth-040809-152402

Tipple, B. J., & Pagani, M. (2007). The Early Origins of Terrestrial C $_4$ Photosynthesis. *Annual Review of Earth and Planetary Sciences*, *35*(1), 435–461. https://doi.org/10.1146/annurev.earth.35.031306.140150

Tolonen, K. (1986). Charred particle analysis. *Handbook of Holocene Palaeoecology and Palaeolimonology, B.E. Berglund (Ed.)*, *1*, 485–496.

Umbanhowar, C. E., & Mcgrath, M. J. (1998). Experimental production and analysis of microscopic charcoal from wood, leaves and grasses. *The Holocene*, *8*(3), 341–346. https://doi.org/10.1191/095968398666496051

Vachula, R. S. (2019). A usage-based size classification scheme for sedimentary charcoal. *The Holocene*, *29*(3), 523–527. https://doi.org/10.1177/0959683618816520

Vachula, R. S., & Cheung, A. H. (2021). Late Neogene surge in sedimentary charcoal fluxes partly due to preservation biases, not fire activity. *Palaeogeography, Palaeoclimatology, Palaeoecology*, *567*, 110273. https://doi.org/10.1016/j.palaeo.2021.110273

Vachula, R. S., Karp, A. T., Denis, E. H., Balascio, N. L., Canuel, E. A., & Huang, Y. (2022). Spatially calibrating polycyclic aromatic hydrocarbons (PAHs) as proxies of area burned by vegetation fires: Insights from comparisons of historical data and sedimentary PAH fluxes. *Palaeogeography, Palaeoclimatology, Palaeoecology*, *596*, 110995. https://doi.org/10.1016/j.palaeo.2022.110995

Vachula, R. S., Sae-Lim, J., & Li, R. (2021). A critical appraisal of charcoal morphometry as a paleofire fuel type proxy. *Quaternary Science Reviews*, *262*(106979). https://doi.org/10.1016/j.quascirev.2021.106979

Vendramini, J. M. B., Silveira, M. L., & Moriel, P. (2023). Resilience of warm-season (C4) perennial grasses under challenging environmental and management conditions. *Animal Frontiers*, *13*(5), 16–22. https://doi.org/10.1093/af/vfad038

Weiguo, L., Xiahong, F., Youfeng, N., Qingle, Z., Yunning, C., & Zhisheng, A. N. (2005). δ13C variation of C3 and C4 plants across an Asian monsoon rainfall gradient in arid northwestern China. *Global Change Biology*, *11*(7), 1094–1100. https://doi.org/10.1111/j.1365-2486.2005.00969.x

Whitlock, C., & Larsen, C. (2001). Charcoal as a Fire Proxy. In J. P. Smol, H. J. B. Birks, W. M. Last, R. S. Bradley, & K. Alverson (Eds.), *Tracking Environmental Change Using Lake Sediments: Terrestrial, Algal, and Siliceous Indicators* (pp. 75–97). Springer Netherlands. https://doi.org/10.1007/0-306-47668-1_5

Wickham, H., Averick, M., Bryan, J., Chang, W., McGowan, L. D., François, R., Grolemund, G., Hayes, A., Henry, L., Hester, J., Kuhn, M., Pedersen, T. L., Miller, E., Bache, S. M., Müller, K., Ooms, J., Robinson, D., Seidel, D. P., Spinu, V., … Yutani, H. (2019). Welcome to the Tidyverse. *Journal of Open Source Software*, *4*(43), 1686. https://doi.org/10.21105/joss.01686

Wickham, H., Chang, W., Henry, L., Pedersen, T. L., Takahashi, K., Wilke, C., Woo, K., Yutani, H., Dunnington, D., Brand, T. van den, Posit, & PBC. (2025). *ggplot2: Create Elegant Data Visualisations Using the Grammar of Graphics* (Version 4.0.1) [Computer software]. https://cran.r-project.org/web/packages/ggplot2/index.html

Wilkinson, B. H., & Vachula, R. S. (2023). On the Sadler Effect and biases in Holocene paleofire records. *Palaeogeography, Palaeoclimatology, Palaeoecology*, *619*, 111548. https://doi.org/10.1016/j.palaeo.2023.111548

Yu, Z., Colin, C., Wan, S., Saraswat, R., Song, L., Xu, Z., Clift, P., Lu, H., Lyle, M., Kulhanek, D., Hahn, A., Tiwari, M., Mishra, R., Miska, S., & Kumar, A. (2019). Sea level-controlled sediment transport to the eastern Arabian Sea over the past 600 kyr: Clay minerals and SrNd isotopic evidence from IODP site U1457. *Quaternary Science Reviews*, *205*, 22–34. https://doi.org/10.1016/j.quascirev.2018.12.006

Zhang, Y., Gan, J., & Yang, Q. (2024). Spatiotemporal variability of streamflow in the Pearl River Basin: Controls of land surface processes and atmospheric impacts. *Hydrological Processes*, *38*(4), e15151. https://doi.org/10.1002/hyp.15151

Zhisheng, A., Kutzbach, J. E., Prell, W. L., & Porter, S. C. (2001). Evolution of Asian monsoons and phased uplift of the Himalaya–Tibetan plateau since Late Miocene times. *Nature*, *411*(6833), 62–66. https://doi.org/10.1038/35075035

Zhou, B., Bird, M., Zheng, H., Zhang, E., Wurster, C. M., Xie, L., & Taylor, D. (2017a). New sedimentary evidence reveals a unique history of C4 biomass in continental East Asia since the early Miocene. *Scientific Reports*, *7*(1), 170. https://doi.org/10.1038/s41598-017-00285-7

Zhou, B., Bird, M., Zheng, H., Zhang, E., Wurster, C. M., Xie, L., & Taylor, D. (2017b). New sedimentary evidence reveals a unique history of C4 biomass in continental East Asia since the early Miocene. *Scientific Reports*, *7*(1), 170. https://doi.org/10.1038/s41598-017-00285-7

Zhou, B., Rybski, D., & Kropp, J. P. (2017). The role of city size and urban form in the surface urban heat island. *Scientific Reports*, *7*(1), 4791. https://doi.org/10.1038/s41598-017-04242-2

Appendix 1

A multi-site examination of fuel type and fire activity in the late Miocene C_4 grass expansion through sedimentary charcoal from International Ocean Discovery Program Sites 1081, U1457, 717 and 1146

The target journal for this manuscript is *Paleoceanography and Paleoclimatology*.

Abstract

C_4 grasslands proliferated globally in the late Miocene and late Pliocene (8–3 Ma). Though initially thought to have occurred synchronously, more recent studies identified the expansion was asynchronous, suggesting that regional influences were the catalyst. The Fire Hypothesis proposed that frequent fire catalyzed the expansion by preferentially burning C_3 canopies and assisted in maintaining the grassland biomes, and this hypothesis has been supported in the literature. However, most of these studies are single site that used a variety of proxies for fire activity. This inhibits a direct comparison between the sites, creating a knowledge gap. A comparison is needed to resolve the true extent of fire's role in the C_4 grass expansion and of the validity of the Fire Hypothesis. This study offers a multi-site perspective on the role of fire in the C_4 grass expansion using sedimentary charcoal to observe fire activity and resolve fuel time throughout the C_4 grass expansion. We obtained ocean sediment from Ocean Drilling Program Sites 1146 (South China Sea), 717 (Bengal Fan), 1081 (Namibian Coast) and International Ocean Discovery Program Site U1457 (Indus Fan). Using sedimentary charcoal, we reconstructed fuel type and fire activity through L:W ratio, morphology type, and charcoal accumulation rate. We compared these data to previously published vegetation and fire data, and we found an increase in fire activity at all sites that coincided with the onset of the expansion. Additionally, we determined the primary fuel type was woody despite the expansion of grasses. We propose that fire assisted in the establishment of C_4 grass expansion all sites, but did not contribute to the fire-grass positive feedback loop per the Fire Hypothesis.

Key words

paleofire; charcoal morphometry and morphology; sedimentary charcoal; C_4 grass expansion

1. Introduction

Around 40% of Earth's land surface is covered by grassland and savanna biomes, which are primarily composed of either C_3 or C_4 grasses depending on latitude (Gibson, 2009; Strömberg, 2011). Most grass species utilize one of these two photosynthetic pathways, with C_4 plants having evolved a more efficient mechanism for carbon fixation (Sage, 2004; Strömberg, 2011). This adaptation allows C_4 grasses to thrive in environments characterized by high temperatures, intense sunlight, and low atmospheric CO_2 concentrations (Sage, 2004). As a result, C_4 grasslands tend to dominate tropical and subtropical regions, whereas C_3 grasslands are more prevalent at higher latitudes (Strömberg, 2011).

While C_4 grasses first evolved 30 Ma (Sage, 2004), their global domination did not occur until the late Miocene and early Pliocene (8–3 Ma), and the expansion was initially believed to have occurred synchronously (Edwards et al., 2010). Early explanations attributed this proliferation to declining atmospheric CO_2 during the Miocene, which promoted global cooling and aridification, conditions favorable for C_4 plant growth (Edwards et al., 2010; Herbert et al., 2016; Pagani et al., 1999). Yet, atmospheric CO_2 fell to levels advantageous to C_4 plants in the Oligocene (34–23 Ma) without triggering a C_4 grass expansion (Pagani et al., 2005). Subsequent research revealed the expansion occurred asynchronously, typically preceding an expansion of C_3 grasslands (Edwards et al., 2010). As a result, regional climate change, like aridification and monsoon seasonality, was the proposed catalyst (Cerling et al., 1993; Pagani et al., 1999).

The Fire Hypothesis, introduced by Keeley and Rundel (2005), proposed fire was the primary catalyst after observing an increase of sedimentary charcoal alongside the C_4 grass expansion. It posits that fire cleared forest canopies, which led to dry, sunny environments, and

more C_4 grasses to grow (Keeley & Rundel, 2005). C_4 grasses are more flammable than C_3 plants, and therefore increase the number of fires and create a positive feedback loop (Keeley & Rundel, 2005).

Today, fire is a pervasive ecological process in tropical and subtropical grasslands, which represent some of the most frequently burned ecosystems globally (Mouillot & Field, 2005). The dominance of C_4 grasses is strongly linked to fire regimes compared to their C_3 counterparts (Bond & Keeley, 2005; Lehmann et al., 2014). Recurrent fire, in combination with monsoon seasonality, plays a critical role in limiting the reestablishment of tall plants and canopies (Bond & Keeley, 2005). Frequent fires suppress the growth of saplings and constrain the development of closed-canopy vegetation to maintain open grass-dominated systems (Bond, 2008). C_4 grasses' efficiency to fixate carbon under warm and high-light conditions enables rapid biomass accumulation and post-fire recovery (Sage, 2004). Further, these grasses typically dry rapidly due to relatively low leaf moisture content, increasing their flammability (Bond, 2008). In addition, they have slower decomposition rates further increasing biomass accumulation over time (Bond, 2008). Monsoon seasonality reinforces this dynamic high primary productivity during the wet season leads to substantial biomass buildup, which subsequently desiccates during the dry season (Bond, 2008). Collectively, this maintains the C_4 grassland biomes throughout the world (Bond, 2008).

The Fire Hypothesis has been supported in previous studies with fire, vegetation, and climate reconstructions using ocean sediments from the International Ocean Discovery Program legacy sites, but a direct and thorough comparison between sites is still needed to assess the validity of the Fire Hypothesis. Because the expansions were asynchronous, it is crucial to be able to compare the sites to directly resolve what regional influences triggered the expansion.

Regional climate variations affect the relationships between vegetation and fire (Lehmann et al., 2014). Therefore, the catalyst of the C_4 grass expansion could be spatially dependent, and to assess the universality of the Fire Hypothesis a multi-site comparison is needed. Nevertheless, there are several factors that hinders our ability to compare the relationship between fire and vegetation across multiple locations.

First, while most of these studies use the same or similar vegetation proxies ($\delta^{13}C$ from plant wax and pollen), they use a diverse array of paleofire proxies and methodologies, such as the number of charred particles relative to the number of pollen grains (Hoetzel et al., 2013), numbers of charcoal per gram of sediment (Feakins et al., 2020), pyrogenic carbon content (Zhou et al., 2017), and sedimentary concentrations of total polycyclic aromatic hydrocarbons (PAHs; Karp et al., 2021) to estimate past fire changes. Without a standard proxy and methodology, there cannot be a direct comparison between different sites.

In addition to utilizing different paleofire proxies, most of these proxies do not account for possible influences of sedimentation rate. Many studies use fire proxies that do not factor in sedimentation rate, and the recorded increase in fire may be due to a change in sediment accumulation as opposed to fire activity (Feakins et al., 2020; Hoetzel et al., 2013; Karp et al., 2021; Zhou, 2017). Moreover, the increase in fire activity evident in marine sediments may be due to a more complete sedimentary record in more recent times (Sadler, 1981; Vachula & Cheung, 2021; Wilkinson & Vachula, 2023). Therefore, it can be problematic to assume there was increased fire activity of increased abundances of paleofire proxies without considering sedimentation rate.

Finally, there have only been a few studies that aimed to determine what fuel types burned through time (Karp et al., 2021; Zhou et al., 2017). Most studies tend to use proxies that

measure fire and vegetation separately, preventing a direct assessment of the potential preferential burning of C_3 plants (Shen et al., 2018; Tipple & Pagani, 2007). Consequently, a definitive assessment of the fire-C_4 relationship cannot be reached.

Sedimentary charcoal offers a unique perspective on the Fire Hypothesis as it can be used as a proxy for fuel type and fire activity simultaneously. Charcoal is generated through the incomplete combustion of organic material and preserves structural characteristics reflective of the original fuel source. Following production, these particles may be transported by fluvial or aeolian processes from the site of burning to depositional environments such as lakes or marine basins, where they can be preserved over geological timescales and serve as proxies for reconstructing past fire regimes (Patterson et al., 1987; Whitlock & Larsen, 2001; Daniau et al., 2019; Genet et al., 2021; Haliuc et al., 2023). These charcoal particles retain morphometric and morphological characteristics that provide insight into the fuel type (Crawford & Belcher, 2014; Enache & Cumming, 2006; Vachula et al., 2021). Furthermore, charcoal accumulation rate (CHAR) is an accurate proxy for fire activity, as it accounts for sedimentation rate.

In this study, we aim to examine how fire activity and fuel type changed throughout the late Miocene and early Pleistocene (our data range from 11.2 to 2.0 Ma) to critically examine the universality of the Fire Hypothesis in a multi-site investigation using sedimentary charcoal. To support the Fire Hypothesis through sedimentary charcoal across the sites, three key lines of evidence are needed: (1) an increase in fire activity concurrent with C_4 proliferation, (2) preferential burning of C_3 vegetation, and (3) a shift of fuel type from woody to grassy. Notably, few previous studies have undertaken proxy analyses which directly resolve both fire activity and fuel type. Furthermore, most studies have been single-site in focus using an array of different proxies. Therefore, our approach provides novel resolution of fire-fuel relationships across

multiple sites using uniform methods, enabling a uniquely informed synthesis of data with which to assess the Fire Hypothesis.

2. Methods

2.1. Study sites

For this study, we obtained 25–50 samples in 2 cm intervals of sediment from Ocean Drilling Project (ODP) Sites 1146 in the South China Sea (19°27.40′N, 116°16.37′E; Wang et al., 2000), 717 in the Bengal Fan (0°55.785'S, 81°23.408'E; Cochran et al., 1988), 1081 off the Namibian Coast (19°37.1818'S, 11°19.1598'E; Wefer et al., 1998), and Internation Ocean Discovery Program Site U1457 in the Indus Fan (17°9.95′N, 67°55.81′E; Pandey et al., 2016) via IODP repository requests (Figure 4).

These sites were chosen because of their unique locations, in addition to previous examination in the context of the C_4 grass proliferation (Feakins et al., 2020; Hoetzel et al., 2013, 2015; Karp et al., 2021; Polissar et al., 2021; Zhou et al., 2017). The regional climate change at Sites U1457, 717, and 1146 is largely controlled by monsoon system, with the South Asian Monsoons affecting Sites U1457 and 717 and the East Asian Monsoon affecting Site 1146 (Alam et al., 2023; Chauhan et al., 2025; Holbourn et al., 2021; Polissar et al., 2021; Quade et al., 1989; Steinke et al., 2010). Currently, the climate at these sites is defined by variable seasonality, where the summer monsoons transport warm and moist wind, and the winter monsoon transports cold and dry wind (Ding, 2007). The regional climate at Site 1081 is closely tied to the Benguela current and upwelling system (Mohanty et al., 2025). Currently, the biomes surrounding the South China Sea and the Bengal Fan consist of tropical forests with grasslands further inland (Dinerstein et al., 2017). Around the Indus Fan, the biomes are deserts and semi-arid grasslands

due to a weaker influence of the summer monsoons (Dinerstein et al., 2017; Quade et al., 1989). Along the Namibian coast (Site 1081), deserts and semi-deserts are the primary biome and are along the grassland-woodland transition (Dinerstein et al., 2017). The differences in climate controls and the availability of complementary proxy data allows for an interesting comparison to our charcoal data.

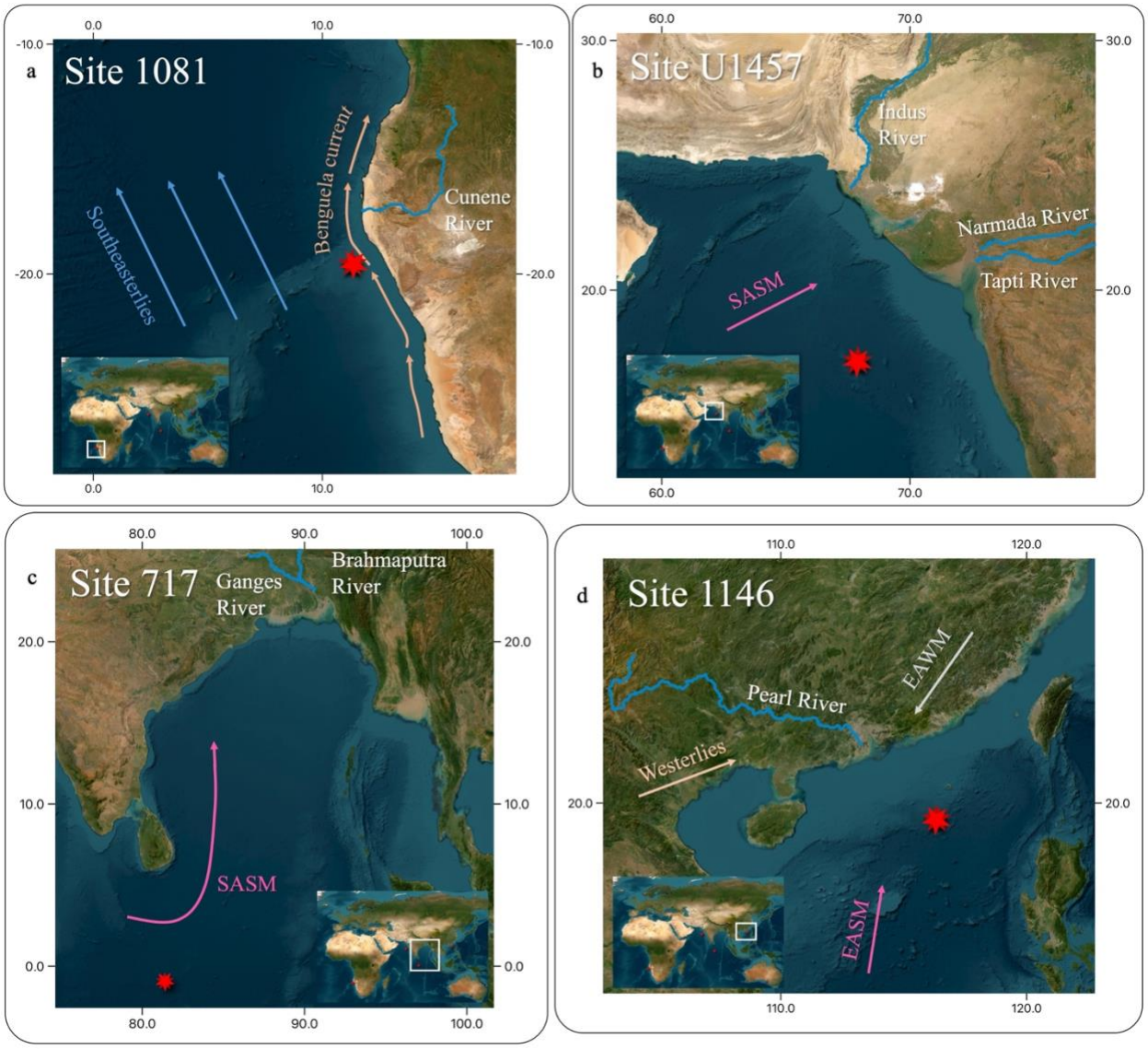

Figure 5. Map showing the four study sites: (a) Site 1081 off the Namibian Coast. Dark blue arrows indicate direction of the Southeasterlies. Orange arrows indicate the movement of the Benguela Current, (b) Site U1457 in the Indus Fan. Pink arrow indicates the direction of the

South Asian Summer Monsoon (SASM), (c) Site 717 in the Bengal Fan. Pink arrow indicates the direction of the South Asian Summer Monsoon System, and (d) Site 1146 in the South China Sea. Orange arrow indicates the direction of the westerlies. White arrow indicates the direction of the East Asian Winter Monsoon (EAWM). Pink arrow indicates the direction of the East Asian Summer Monsoon (EASM). Base map is from ESRI, river data is from HydroRIVERS Technical Documentation v1.0, and the projection is World Geodetic System 1984.

2.1.1. ODP Site 1081: Namibian Coast

ODP Site 1081 is ~160 km west of Namibia in the Atlantic Ocean (Wefer et al., 1998; Figure 5). The sediment composition was primarily clay and was strongly influenced by southeasterly winds, upwelling, and the Benguela Current (Dupont & Wyputta, 2003; Wefer et al., 1998). The Cunene River was redirected ~5 Ma and connected Lake Cunene with the Atlantic Ocean, which increased the fluvial discharge to Site 1081 (Hoetzel et al., 2015; Shi et al., 1998; Wefer et al., 1998). We analyzed 47 samples from hole 1081A with an age range from late Miocene (9.2 Ma) to late Pliocene (3.0 Ma).

Throughout the Miocene, the Namibian coast experienced a continuous trend toward aridification (Dupont et al., 2013). Starting around 12–10 Ma, sea surface temperatures cooled and Benguela Current upwelling intensified, which reducing continental moisture availability from the ocean (Diester-Haass et al., 1990; Rommerskirchen et al., 2011). Alongside these changes, there was a shift in vegetation cover. Prior to ~9 Ma, pollen and stable carbon isotopes from long-chain *n*-alkanes indicate the dominance of C_3 vegetation (Dupont et al., 2013; Hoetzel et al., 2015). Between 8 and 5 Ma, C_4 vegetation expanded with increasing arid conditions, and C_4 became the dominant vegetation type after 6 Ma (Hoetzel et al., 2015). The region continued

to dry from 5 to 2.7 mya, as shown by a reduction in grassy vegetation cover and an expansion of shrubland and desert vegetation (Dupont et al., 2005; Rubbelke et al., 2023).

2.1.2. IODP Site U1457: Indus Fan

IODP site U1457 is ~491 km from the western Indian coast in the Arabian Sea (Pandey et al., 2016; Figure 5). We analyzed 25 samples from hole U1457C with ages ranging from the late Miocene (11.2 Ma) to early Pliocene (5.5 Ma). Sediment deposition was episodic (Feakins et al., 2020; Pandey et al., 2016). Between 9.83 and 8 Ma, the sediment was hemipelagic with a sediment accumulation rate of ~2 cm ka^{-1}. Following this, there was an accumulation of turbiditic sediments with an average of ~34 cm ka^{-1} from ~8.1 to 7.6 Ma (Feakins et al, 2020). From 7.6 to 5.9 Ma, the sediment accumulation rate slowed back down to ~2–6 cm ka^{-1} with hemipelagic sediments. The sediment was transported fluvially from the Indus River (Alam et al., 2023; Pandey et al., 2016) with possible inputs from the western flowing rivers like the Narmada and Tapti Rivers (Yu et al., 2019; Figure 5).

The South Asian Summer Monsoon (SASM) was continuously weak since the late Miocene, with a pronounced weakening ~7.2 Ma, which reduced the moisture brought inland (Chauhan et al., 2025). This led to aridification, except for a humid period from 6.0 to 5.6 Ma, and increased upwelling at the location of this site (Alam et al., 2023; Feakins et al. 2020). C_4 vegetation has been present since 8.7 Ma but the main transition occurred between 7.4–7.2 Ma (Feakins et al., 2020). Unlike Site 1081, Site U1457 saw increased humidity and moisture throughout the Pliocene (Alam et al., 2023; Clift et al., 2020)

2.1.3. ODP Site 717: Bengal Fan

ODP Site 717 was drilled ~800 km south of Sri Lanka in the middle of the Indian Ocean on the edge of the Bengal Fan (Cochran et al., 1988; Figure 5). We analyzed 37 samples from hole 717C. The ages range from the late Miocene (9.6 Ma) to early Pleistocene (1.9 Ma). The turbiditic sediments recovered from Site 717 originated from Ganges-Brahaputra catchments and the Himalayan Mountains and were fluvially transported by the Ganges River (Polissar et al., 2021; Figure 5).

Site 717 saw significant hydrological changes throughout the Miocene and early Pliocene (Karp et al., 2021; Singh & Gupta, 2004). Around 7.2 Ma, there was a reduced and southward shift of the summer monsoon, creating a humid monsoonal environment, increased winter precipitation (Chauhan et al., 2025). Aridification intensified and created drier conditions as the Himalayas and Tibetan Plateau significantly rose (Chauhan et al., 2025; Polissar et al., 2021). C_4 taxa has been present since 9.5 Ma, but the C_4 grass expansion occurred 7.5–6.5 Ma, congruent with increased aridification (Karp et al., 2021; Polissar et al., 2021).

2.1.4. ODP Site 1146: South China Sea

ODP Site 1146 is located ~200 km south of Hong Kong in the South China Sea (Wang et al., 2000; Figure 5). We analyzed 50 samples from holes 1146A and 1146C, which comprise comparable stratigraphies (Wang et al., 2000). The sediment was largely transported from the Pearl River delta system and westerly winds, and the sediment was primarily composed of carbonates and clay (Wang et al., 2000; Clift et al., 2014; Jia et al., 2003). Our samples range from the late Miocene (8.0 Ma) to early Pliocene (5.0 Ma; Wang et al., 2000; Holbourn et al., 2021).

In the late Miocene, Eastern Asia experienced substantial regional climate change. The East Asian monsoon systems fluctuated from a stronger East Asian Summer Monsoon (EASM) to a stronger East Asian Winter Monsoon (EAWM) between ~7 and 5.5 Ma. This shift reduced moisture inland that was brought by the EASM and increased aridification from the dry air brought by the EAWM (Figure 5; Holbourn et al., 2021: Holbourn et al., 2018; Li et al., 2004; Steinke et al., 2010). The C_3/C_4 shift occurred in distinct stages around 20 Ma, 15 Ma, a gradual expansion from 7 to 4 Ma, 1 Ma, and 0.4 Ma (Li et al., 2023; Zhou et al., 2017).

For more in-depth information about this site, see Chapter 1.

2.2. Age-depth model determination

For each site, we relied on the most recently published age-depth models, which were created using a variety of techniques. The splice and chronology used for Site 1146 were from Holbourn et al. (2021). The splice was based on stratigraphic correlation from magnetic susceptibility, gamma-ray attenuation bulk density, and natural gamma radiation data (Wang et al., 2000) but was modified by removing duplications and inserting a 1.45 m segment to close a gap between 372.90 meters composite depth (mcd) and 374.35 mcd (Holbourn et al., 2021). The chronology of the Miocene sequence for Site 1146 was based on benthic foraminiferal isotopic records (Wang et al., 2000; Holbourn et al., 2021) and computed obliquity and eccentricity solutions (Laskar et al., 2004). The age model from Hoetzel et al. (2015) was used for Site 1081. The splice and chronology was based on biostratigraphy, magnetic reversals and magnetic susceptibility (Berger et al., 2002; Hoetzel et al., 2015; Wefer et al., 1998).The age model for U1457 was from Feakins et al. (2020), which utilizes nannofossils and foraminiferal, and paleomagnetism datums. Because some of the sediments are turbidites in the core, there are few

age control points available, leading to interpolation between the ages in the turbiditic sections (Feakins et al., 2020). There are notable gaps in the record due to the lack of availability of samples from the IODP repository. For Site 717C, we used the age-model from Polissar et al. (2021), which updated the shipboard data (Cochran et al., 1990) to include revised horizon ages for nannofossil and planktic foraminifera biostratigraphy.

2.3.Sedimentary charcoal analysis

Charcoal was isolated from the ocean sediment samples using an adapted methodology from Vachula et al. (2018). Sedimentary charcoal particles can be a broad range of sizes from microscopic scales (10–50 μm) to macroscopic scales (>125 μm; Umbanhowar & McGrath, 1998; Whitlock & Larsen, 2001; Vachula, 2019).

Around 100 milligrams (mg) of each sample were weighed from sites 717, U1457, and 1081 and ~150 mg for site 1146 due to limited sedimentary charcoal abundance from this site. To remove carbonates, HCl was gradually added until the sample no longer effervesced. Six milliliters (mL) of NaClO (2.25%) were added to bleach organic matter, and 6 mL $(NaPO_3)_6$ (6%) were added to disaggregate the sediment for ~24 hours before sieving (45 μm) to remove isolate the charcoal particles. Images were taken of the charcoal particulates using a Nikon SMZ745T microscope equipped with a DSFi3 camera.

CharTool (Snitker, 2020) was used to collect morphometric measurements of each charcoal particle. Quantitative morphometric parameters refine fuel-type interpretations (Crawford & Belcher, 2014; Inoue & Usuki, 2025; Vachula et al., 2021). In this study, we focus on length-to-width (L:W) ratio (major axis ÷ minor axis of the best fitting ellipse). A greater

length-to-width (L:W) ratio suggests grassy and non-woody fuel whereas a smaller L:W ratio suggests woody material (Crawford & Belcher, 2014; Vachula et al., 2021).

The morphology type was categorized using a flow chart adapted from Enache and Cumming (2006) and recorded using CharTool (Snitker, 2020). Morphological classification is based on particle shape, with elongated fragments associated with grass-derived fuels and more compact forms linked to leaves, bark, or woody tissues (Crawford & Belcher, 2014; Enache & Cumming, 2006; Feurdean, 2021; Pereboom et al., 2020). Further, following data collection, we consolidated several of the morphology types of Enache and Cumming (2006) by common characteristics to quantify the following groups: elongated (no ramifications; type F), elongated (ramifications; type D), geometric (types S/B and C), and irregular (types M and P). Finally, charcoal particle abundances were tallied, normalized by sample weight and count, and charcoal accumulation rates (CHAR) were calculated by the following equation:

$$CHAR = \left(\frac{charcoal\ count}{sample\ weight\ (mg)}\right) \times \frac{(bottom\ composite\ depth - top\ composite\ depth)}{(bottom\ age - top\ age)}$$

CHAR in marine sediments is used as a proxy for fire frequency and the extent of area burned (Genet et al., 2021; Haliuc et al., 2023).

Morphology type and L:W ratio are well established proxies for differentiating woody versus non-woody/grassy fuel types (Crawford & Belcher, 2014; Enache & Cumming, 2006; Feurdean, 2021; Frank-DePue et al., 2023; Li et al., 2019; Ogura, 2007; Zhang & Lu, 2005). The threshold for woody versus grassy fuel type L:W values is distinct based on region and vegetation and may greatly vary (Daniau et al., 2019; Vachula et al., 2021). In Southern Africa (applicable to Site 1081), the L:W ratio indicative for grassy fuel >2.1 in ocean sediments (Haliuc et al., 2023), though note that this value was not supported by experimental production

of charcoal. For the Tibetan Plateau (applicable to Site 717), L:W ratios >2.5 were observed in Quaternary sediment, but there are also no experimental charcoal production done for this location (Miao et al., 2019, 2020). For Site U1457, there is no record of L:W ratio for vegetation, and therefore, we utilize the grassy fuel threshold recorded in the Tibetan Plateau (Feakins et al., 2020; Miao et al., 2019). Finally, in southeastern China (Site 1146) experimental production of charcoal revealed variable L:W ratios of graminoids from 10.2 (Zhang and Lu, 2005) to an average of 2.1 (Li et al., 2019). Because Li et al. 2019 is more recent, L:W ratios >2.1 are interpreted to be grassy/non-woody fuel (Li et al., 2019). Regarding the morphology type, there is less site-specific knowledge about the interpretation of vegetation from the morphology type. However, we believe there is a plethora of research to support broad interpretations as we do here (Enache & Cumming, 2006). Elongated morphotypes, including both ramifications and no ramifications, is interpreted as grassy fuel. Geometric is interpreted as barky fuel, and irregular is interpreted as woody fuel. Despite no experimental charcoal production of three out of the four sites, the combination of L:W and morphology type offers a sound proxy for fuel type (Feurdean, 2021).

2.4.Statistical analysis

R version 4.4.3 was used to perform the statistical analysis (R Core Team, 2025). To quantify clusters of morphological type abundances over the time frames of our data, we utilized constrained incremental sum of squares cluster analysis (CONISS; Grimm, 1987). The CONISS is computed from a distance matrix, where Euclidean distance is used to quantify dissimilarity among samples. It is considered a hierarchical agglomerative technique because it progressively merges individual samples into larger clusters until all observations are combined into a single

grouping. The boundaries of the zones are determined by inspection of the stratigraphic diagrams. The analysis was conducted with package rioja (Juggins, 2024).

3. Results

3.1. Site 1081

We determined an average age resolution of 0.51 ka for our samples from Site 1081A (σ =0.051 ka). CHAR varied consistently from 0.4 to 23.2 (#·cm)/(mg·Ma) throughout the analysis period (9.3–3.0 Ma) and had an average of 11.1 (#·cm)/(mg·Ma) (σ = 6.8 (#·cm)/(mg·Ma)). L:W ratio remained low (μ = 1.8; σ = 0.66) and had two peaks around 8.7 Ma (5.1) and 4.5 Ma (3.7; Figure 6).

Irregular morphotype particles dominated the total charcoal particle morphological abundances at 73.8%, followed by geometric (20.4%), elongated (ramifications) (5.3%) and elongated (no ramifications) (0.5%). There was limited variation of morphotype presences with only two samples that did not contain irregular morphotype, supported by CONISS (refer to SI). There were three main stratigraphic morphological zones, with the separation around 7.1 and 5.1 Ma which had 100% geometric and 75% geometric and 25% elongated (no ramifications), respectively.

3.2. Site U1457

The average age resolution of each of our samples for Site U1457C was 0.71 ka (σ = 0.45 ka). We obtained a coarse resolution for this site due to limited availability in the repository, with some samples being close in age (for example 7.26, 7.27, 7.29 Ma) and with two large age gaps from 11.2 to 10.0 Ma and 9.0 to 7.7 Ma. CHAR remained low for most of the samples (μ = 27.7

(#·cm)/(mg·Ma); σ = 64.1(#·cm)/(mg·Ma)) from 11.2 Ma to 6.3 Ma until a spike ~5.5 Ma (312.1 (#·cm)/(mg·Ma); Figure 6). There is a smaller peak of CHAR (75.4 (#·cm)/(mg·Ma)) ~7.3 Ma. L:W ratio varied throughout time (1.9–9.1; μ = 3.9; σ = 2.0), remaining generally high until around 7.5 Ma (Figure 6).

The most abundant morphotype of total number of charcoal particles was irregular (48.1%) followed by elongated (no ramifications) (30.5%), geometric (18.2%), and elongated (ramifications) (3.2%; Figure 6). There was a shift in dominant morphotype around 7.3 Ma from primarily elongated (no ramifications) and irregular to geometric and irregular morphotype. This is supported by CONISS which found stratigraphic morphological zones from 11.2 to 9.5 Ma, 9.0 to 7.3 Ma, and 7.0 to 5.5 Ma. The first stratigraphic zone contains consistent internal subclusters, suggesting greater variability of the morphotypes within the cluster. This cluster was likely formed by the samples solely containing irregular, geometric, and elongated (no ramifications), whereas the sample next to this zone (9.5 Ma), contains ~28.6% elongated (ramifications). The second zone begins around 9.0 Ma and shows more variability within the morphotype abundance, where elongated (no ramifications) becoming the most prevalent morphotype. The last zone suggests relatively constant morphotype variation, comprising largely of irregular and/or geometric with a small percentage of elongated (ramifications and/or no ramifications).

3.3. Site 717

The average age resolution for each Site 717C samples was 7.4 ka (σ = 15.3 ka). CHAR generally varied from 0.02 to 61.1 (#·cm)/(mg·Ma) except for a peak of 152.8 (#·cm)/(mg·Ma) at 3.9 Ma (μ = 16.9 (#·cm)/(mg·Ma); σ = 27.0 (#·cm)/(mg·Ma); Figure 6). The second highest

peak of CHAR was 9.3 Ma with a value of 61.1 (#·cm)/(mg·Ma). L:W ratio also varied, ranging from 1.8 to 9.4 ($\mu = 4.0$; $\sigma = 2.0$). There are multiple peaks of high L:W from 8.7 to 8.1 Ma (9.4–8.7), 6.8 Ma (7.3) and 2.0 Ma (6.2; Figure 6).

The most prevalent morphotype of the charcoal particles in Site 717 sediments was irregular (46.4%) with peak abundance ~9.4 Ma at 85% (Figure 6). Elongated (ramifications) was 30.4% of the total morphotype abundance, followed by geometric at 19.2% and elongated (ramifications) at 3.9%. There was a shift from primarily irregular to geometric type abundance around 6.9 Ma. CONISS results showed 4 major stratigraphic morphological zones. The first zone is from 9.8 to 8.8 Ma where irregular morphotype was most abundant. The next zone is from 8.7 to 8.3 Ma in which the dominant morphotypes are elongated (no ramifications) and irregular. The third zone occurs from 8.2 to 6.6 Ma, and it encompasses a transitional period of the morphotypes, where the morphotypes are increasingly variable throughout time. In this stratigraphic group, the morphotypes transition from largely geometric to largely irregular. The final zone is from 6.6 to 2.0 Ma where the morphotypes are inconstant within containing a mix of geometric, elongated (no ramifications), elongated (ramifications), and irregular.

3.4. Site 1146

The 1146A samples we analyzed resolved an average age resolution of 0.66 ka each (standard deviation (σ) = 0.11 ka), and the 1146C samples averaged 26.68 ka ($\sigma = 2.45$ ka). CHAR varied (average (μ) = 1.4 (#·cm)/(mg·Ma), $\sigma = 1.0$ (#·cm)/(mg·Ma)), with the greatest values (maximum = 5.5 (#·cm)/(mg·Ma)) occurring between 7.3 Ma and 6.9 Ma (Figure 6). L:W ($\mu = 4.62$, $\sigma = 2.44$) varied throughout time with no notable long-term trends (Figure 6). Elongated (no ramifications) and irregular were the two most common morphotypes identified

(both with 45.12%), with both fluctuating through time, and geometric (8.94%) and elongated (ramifications) (0.91%) had much smaller assemblages (Figure 6).

For more in-depth Results, see Chapter 1.

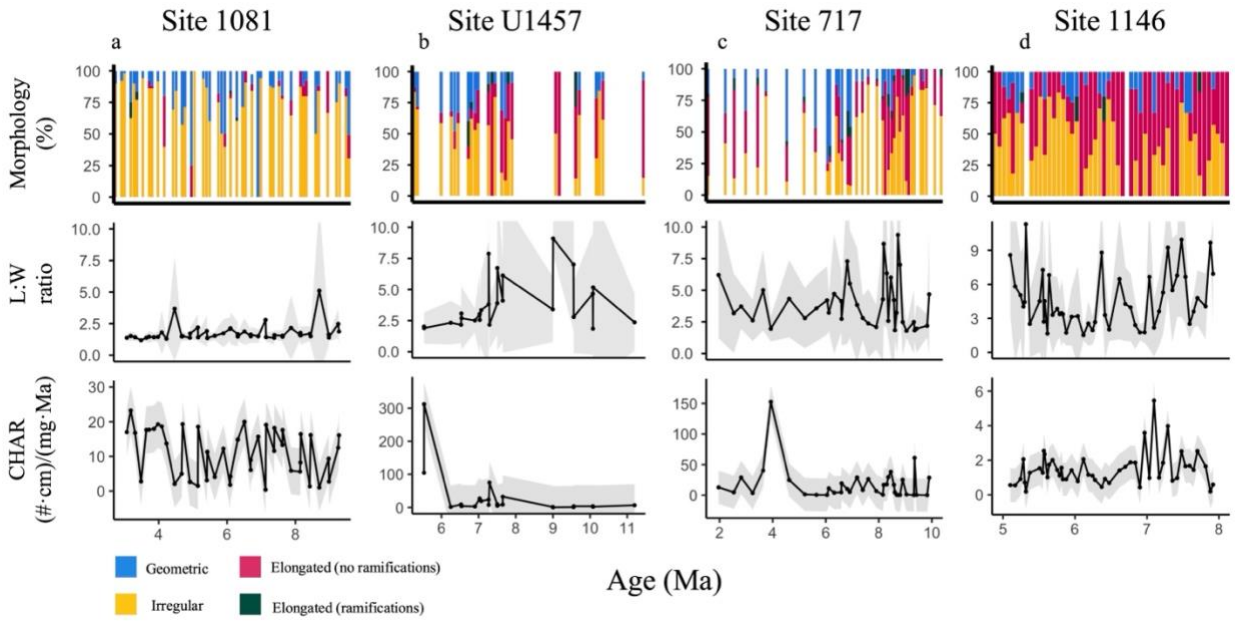

Figure 6. Morphology percentages, L:W ratio, and charcoal accumulation rates (CHAR) sedimentary charcoal from (a) Site 1081 off the Namibian Coast, (b) Site U1457 in the Indus Fan, (c) Site 717 in the Bengal Fan, and (d) Site 1146 in the South China Sea. Grey bar indicates standard deviation. Site 1081 charcoal count was capped at 50.

4. Discussion

Notably, the threshold for the differentiation of woody/non-woody or grassy L:W ratios are smaller for these locations than other studies. In a compilation of L:W ratios from previous studies, Vachula et al. (2021) reported L:W ratios greater than 3.5 to signify grass and non-woody fuels and values less than 2.5 to signify woody fuels. A possible explanation for the discrepancies is the absence of experimental charcoal production for ecosystems around Sites

1081, U1457, and 717. However, the experimental charcoal production for south China for Site 1146 (Li et al., 2019) still revealed L:W values for graminoids >2.1, suggesting that the lack of experimental burns does not explain the lower L:W ratios for grassy fuel. More likely, it is because the size of the charcoal particles may also influence the L:W values, given that smaller particles tend to yield lower ratios (Inoue & Usuki, 2025).

Altogether, charcoal morphology and morphometric parameters are one of the few proxies that simultaneously provide information on both fuel type and fire activity. Therefore, we believe that these data provide an informative approach for reconstructing fuel sources and fire activity during the late Miocene.

4.1. Fire activity and fuel type through charcoal

4.1.1. Site 1081

CHAR along the Namibian coast varies between 0.8 and 51.2 (#·cm)/(mg·Ma) across the studied interval (9.3–3.0 Ma; Figure 7), with no long-term directional trend through the late Miocene and early Pliocene. This pattern suggests oscillating periods of high and low fire activity (Genet et al., 2021; Haliuc et al., 2023). During the recorded C_4 transition between 8 and 7 Ma, fire activity starts low and then remains high from 7.6 to 7.1 Ma before falling again.

Charcoal morphology and L:W ratios indicate no substantial shift in dominant fuel type recorded in the Namibian coast between 9.3 and 1.9 Ma. Morphotypes are predominantly irregular and geometric, which indicate prolonged burning woody vegetation with little input from grass (Crawford & Belcher, 2014; Umbanhowar & Mcgrath, 1998). L:W ratios corroborate this interpretation. Most values in this study are <2.1, consistent with woody fuel dominance

(Haliuc et al., 2023). Overall pattern of CHAR, L:W ratio, and morphology type assemblages suggest that fire activity was highly variable, and the dominant fuel type remained woody.

Our CHAR data contrast with the charcoal data from Hoetzel et al. (2013) who reported an increase in fire activity between 7.1 and 5.8 Ma based on the ratio of charred particles to the sum of charred particles, pollen, and spores. CHAR incorporates sediment accumulation rates and therefore provides a flux-based metric of fire activity (see Methods; Whitlock & Larsen, 2001). Alternatively, Hoetzel et al. (2013) interprets fluxes in fire activity through charcoal concentration relative to pollen, assuming that pollen is deposited alongside charcoal rather than charcoal accumulation being independent of pollen throughout the sediment (Tolonen, 1986). Consequently, the reported increase in charred particle by Hoetzel et al. (2013) percentages between 7.1 and 5.8 Ma may reflect shifts in charcoal relative to pollen delivery, rather than increased fire activity (Vachula & Cheung, 2021). Overall, we believe that CHAR accumulation rate is a more accurate proxy for fire activity, and the combination of both CHAR and charcoal concentration assist in identifying the presence of wildfire throughout time.

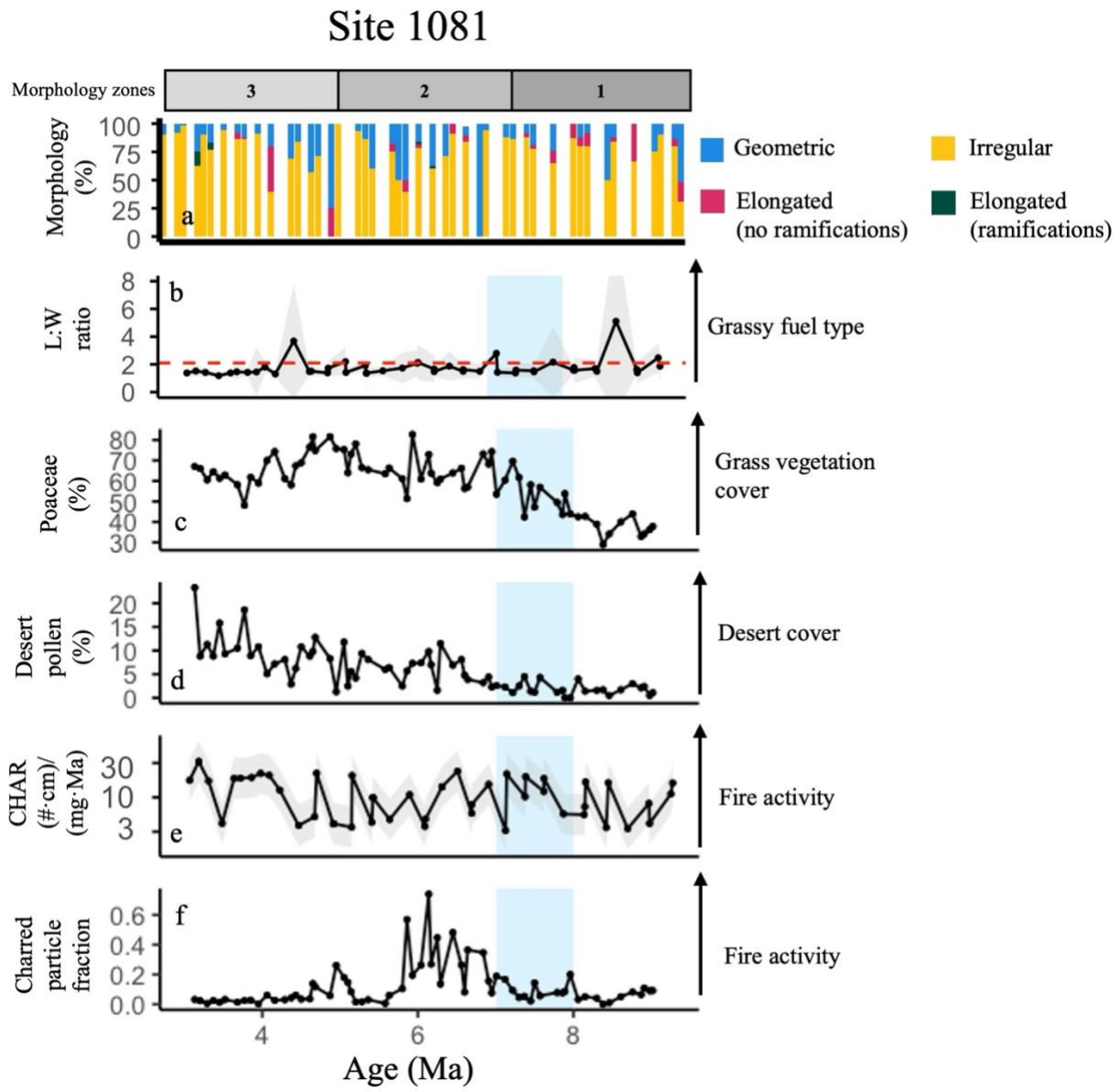

Figure 7. Comparison of charcoal data from Site 1081 with previously published vegetation, fire, and precipitation proxy data. (a) Morphology type percentages (%; this study), (b) L:W ratio (this study). Dashed red line indicates threshold of grassy fuel (Haliuc et al., 2023), (c) Poaceae percentage (%; Hoetzel et al., 2013), (d) desert pollen (%; Hoeztel et al., 2013), (e) CHAR ((#·cm)/(mg·Ma); this study), (f) charred particle ratio (charred particles/pollen + spores + charred particles; %; Hoetzel et al., 2013; 2015). Blue bar indicates the C_4 grass expansion from

8–7 Ma recorded by Hoetzel et al. 2013. Stratigraphic morphological zones from CONISS are shown with the gray bar.

4.1.2. Site U1457

In the Indus Fan, CHAR remained relatively low throughout the timespan of our data, indicating low fire activity, with a small increase (48.8 (#·cm)/(mg·Ma)) 7.3 Ma and a sharp increase 5.5 Ma (201.9 (#·cm)/(mg·Ma); Figure 8). For most of the timespan of the data, irregular morphotypes remain dominant throughout, indicating that woody vegetation constituted the principal fuel source from 11.2 to 5.5 Ma, which is supported by the L:W ratios (Crawford & Belcher, 2014; Enache & Cumming, 2006; Vachula et al., 2021). Within this range, there is a transition after 7.3 Ma from a dominance of elongated (without ramifications) and irregular morphotypes, consistent with mixed grassy and woody fuel inputs, to a dominance of geometric and irregular morphotypes, suggesting greater contributions from woody and bark fuels (Enache & Cumming, 2006; Umbanhowar & Mcgrath, 1998; Figure 8).

The trend in CHAR is different from previously published paleofire data, which shows more variability in sedimentary charcoal concentration (count per gram sediment) and a drastic increase in charcoal around 8.7 Ma (Feakins et al., 2020; Figure 8). This method for interpreting charcoal data as a representative for fire activity could be problematic, as it does not consider sedimentation rate. With this site, this is especially problematic because sedimentation rate varies so much with the turbiditic section. As a result, Feakins et al. (2020) interprets the presence of charcoal in their samples to reflect sustained fire activity, rather than interpreting how the presence of charcoal may show the trends of fire activity over time and the spike in total charcoal ~8.7 Ma is attributed to the turbiditic section of the core and high sedimentation rates.

Alternatively, CHAR likely provides a better record for fire activity because the methodology incorporates sediment accumulation rates.

Fuel type recorded by L:W ratio and morphology assemblages is divergent from vegetation proxies (Figure 8). $\delta^{13}C$ values of C_{31} n-alkanes and grass pollen percentages indicate expansion of C_4 grasslands beginning 7.4 Ma (Feakins et al. 2020). Despite this transition, charcoal morphologies and L:W ratios consistently indicate woody-dominated fuels. Furthermore, the decline in elongated morphotypes suggests that, although grasses may have burned preferentially at earlier intervals, woody vegetation became increasingly dominant as a fuel source. Regardless of the expansion of grasslands, the primary fuel type was woody vegetation.

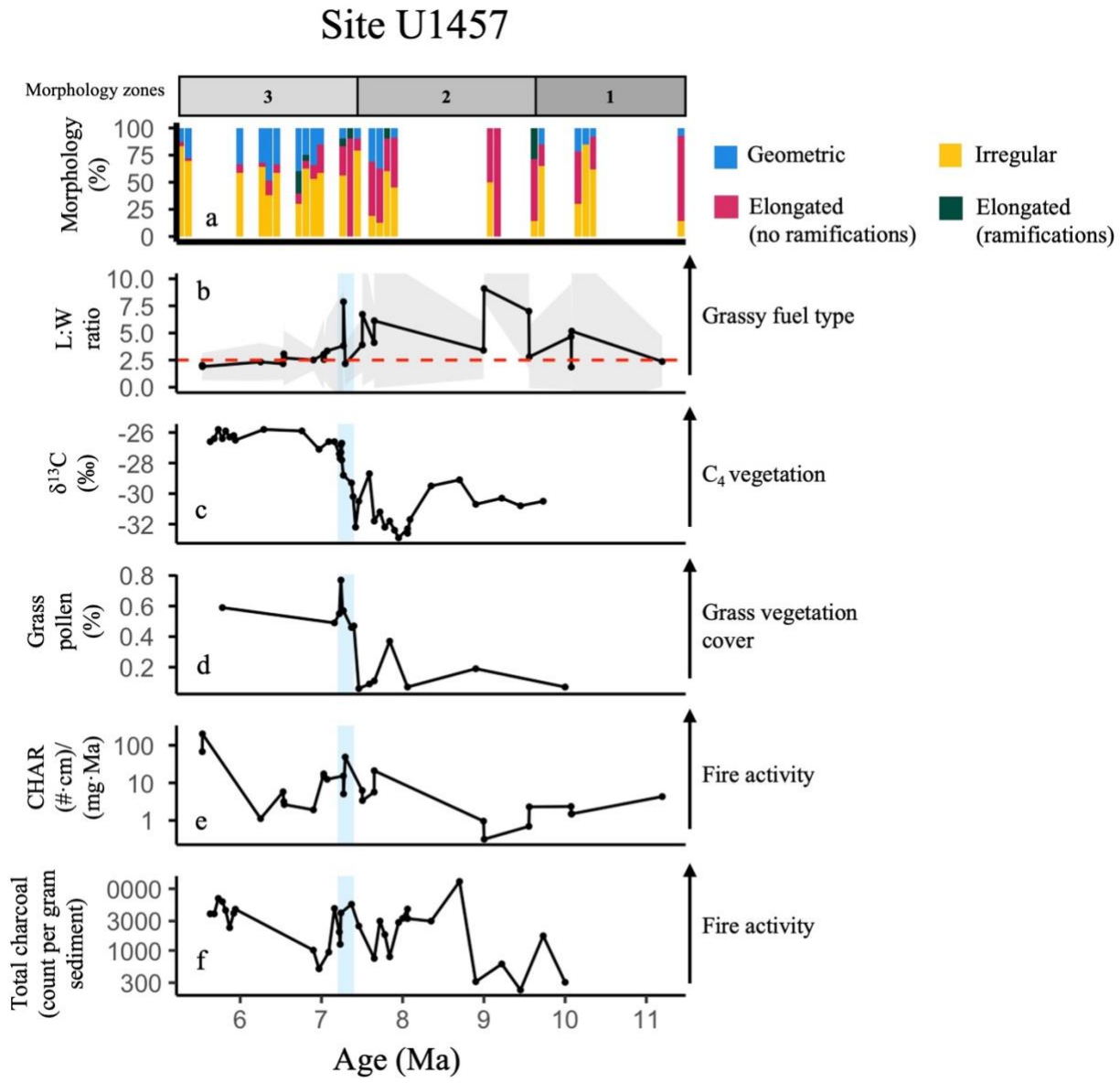

Figure 8. Comparison of charcoal data from Site U1457 with previously published vegetation, fire, and precipitation proxy data. (a) Morphology type percentages (%; this study), (b) L:W ratio (this study). Dashed red line indicates threshold of grassy fuel (Miao et al., 2019, 2020), (c) $\delta^{13}C$ of C_{31} *n*-alkanes (‰; Feakins et al., 2020), (d) grass pollen fraction of terrestrial pollen (fraction; Feakins et al., 2020), (e) CHAR ((#·cm)/(mg·Ma); this study), (f) total charcoal (count per gram; Feakins et al., 2020). Panels (e) and (f) are set to a logarithmic scale. Blue bar indicates C_4 grass

expansion recorded from 7.4–7.2 Ma by Feakins et al., 2020. Stratigraphic morphological zones from CONISS are shown with the gray bar.

4.1.3. Site 717

CHAR, L:W ratios, and morphology type assemblages in the Bengal Fan show variability in fire activity and fuel type between 9.8 and 2.0 Ma. There is a sustained period of high fire activity from 7.9 to 6.1 Ma and a pronounced increase at 3.9 Ma (Figure 9). From 8.8 to 8.1 Ma, fire activity dramatically rises and falls, which coincides with increased variability in L:W ratios, indicating fluctuating fuel types between grassy and woody fuels (Miao et al., 2019, 2020). However, the absence of long-term trends of L:W ratios suggest there was no preferential burning of woody nor grassy fuel types over the timespan of our data. The overall trend from 9.8 to 2.0 Ma in charcoal morphology assemblages reflects a shift from assemblages dominated by irregular and elongated (no ramification) morphotypes to elongated (no ramification) and geometric morphotypes (Figure 9). This pattern suggests a transition from mixed woody–grassy fuel sources to predominantly woody fuels, with woody fuels dominating throughout (Enache and Cumming, 2006). Overall, our data does not provide evidence for long-term changes in fire activity or fuel type.

Fire activity changes recorded by PAH concentrations (Karp et al., 2021) are at odds with CHAR (Figure 9). This discrepancy is likely the result of the two proxies recording different spatial scales of fire activity. CHAR is more representative of local fires, and PAHs may represent changes in more distal or regional burning (Crawford & Belcher, 2014; Vachula et al., 2022). Accordingly, from 9.7 to 5.2 Ma, CHAR and PAHs are relatively low reflecting low fire activity locally and regionally, and the rise in CHAR at 3.9 Ma is likely reflecting an increase in

local fire frequency or intensity, while the PAH increase at 5.2 Ma more likely reflects enhanced burning over a broader source area. Moreover, unlike CHAR, the PAHs data do not factor in accumulation rate, meaning the total PAH concentration could be more reflective of accumulation rate variations than fire activity (Daniau et al., 2019). The combination of the CHAR and PAHs datasets provides a unique view of fire activity, signaling localized and regional fire activity, respectively.

During recorded grassland expansion (6.9–6.0 Ma; Polissar et al., 2021), L:W ratios declined and there are no substantial changes in CHAR values. Therefore, despite the establishment of C_4 grasses as the dominant ecosystem, fire activity remained comparatively low and continued to preferentially burn woody vegetation.

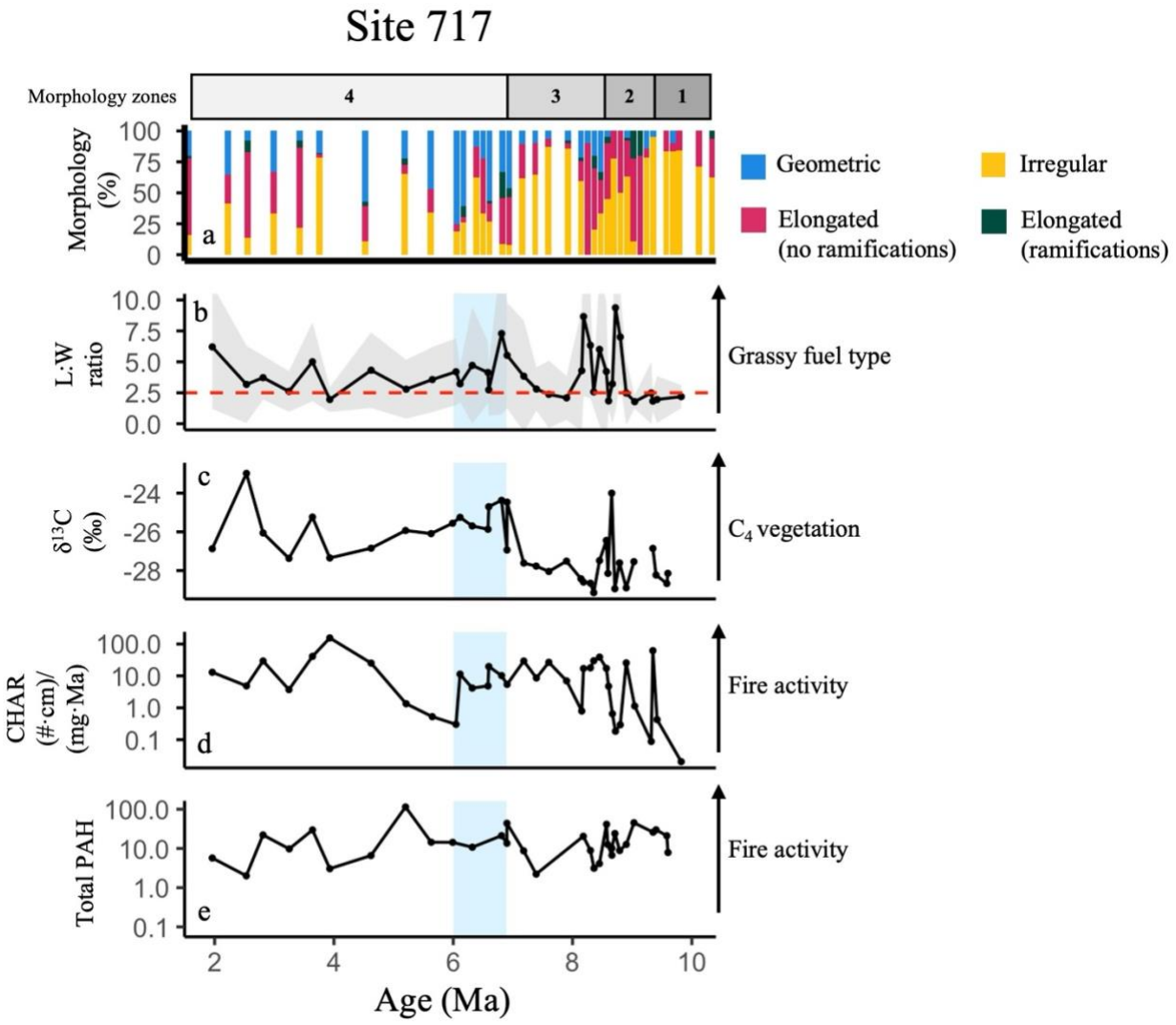

Figure 9. Comparison of charcoal data from Site 717 with previously published vegetation, fire, and precipitation proxy data. (a) Morphology type percentages (%; this study), (b) L:W ratio (this study). Dashed red line indicates threshold of grassy fuel (Miao et al., 2019, 2020), (c) $\delta^{13}C_{C29\text{-alkane}}$ from plant-wax (‰; Polissar et al., 2021), (d) CHAR ((#·cm)/(mg·Ma); this study), (e) total PAH (count per gram; Karp et al., 2021). Panels (d) and (e) are set to a logarithmic scale. Blue bar indicates C_4 grass expansion recorded from 6.9–6.0 Ma by Polissar et al., 2021. Stratigraphic morphological zones from CONISS are shown with the gray bar.

4.1.4. Site 1146

In the South China Sea, fire activity and fuel type as recorded by CHAR, L:W ratio, and morphology assemblages respectively, are variable throughout the timespan of our data (8–5 Ma). L:W ratios from 8 to 5 Ma fluctuate which is indicative of pendulating fuel types from woody to grassy (Li et al., 2019; Ogura, 2007; Zhang and Lu, 2005). The morphotype assemblages shift at 6.2 Ma from predominantly elongated (no ramifications) to irregular morphotypes (Figure 10), implying a transition of grassy fuel to woody fuel (Crawford & Belcher, 2014; Feurdean et al., 2021; Vachula et al., 2021).

From 7.3 to 6.9 Ma, there is a distinct increase in fire activity (Figure 10). During this interval, the morphology type assemblages do not indicate a corresponding shift in fuel type (Crawford & Belcher, 2014; Umbanhowar & Mcgrath, 1998; Figure 10).

The increase in fire activity recorded by CHAR (7.3–6.9) broadly coincides with modest increases in pyrogenic carbon percentages (PyC; 0.02–0.09%), which is also reflective of fire activity (Zhou et al., 2017). The variability among the long-term trends of these proxies likely stems from recording differences in spatial scales (Patterson et al., 1987; Preston & Schmidt, 2006). fire.

The vegetation changes recorded by $\delta^{13}C$ values from plant wax do not correspond with our fuel type data. Throughout the time of the study, the fuel type transitions from grassy to woody, despite $\delta^{13}C$ values of long chain alkanes indicating a gradual expansion of C_4 vegetation.

For an expanded Discussion for Site 1146, see Chapter 1.

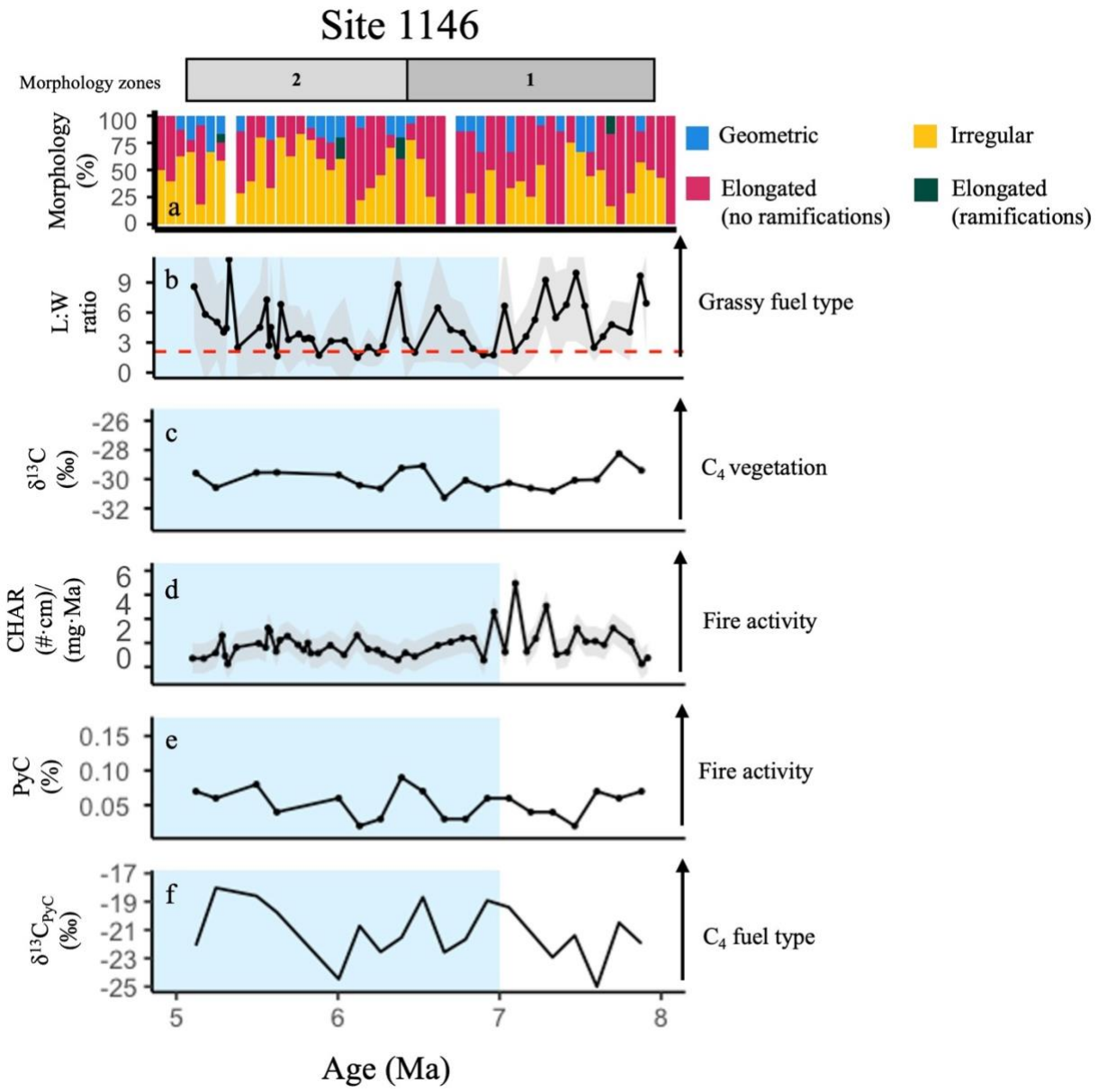

Figure 10. Comparison of charcoal data from Site 1146 with previously published vegetation, fire, and precipitation proxy data. (a) Morphology type percentages (%; this study), (b) L:W ratio (this study). Dashed red line indicates threshold of grassy fuel (Li et al., 2019), (c) $\delta^{13}C$ of long-chain *n*-alkanes (‰; Zhou et al., 2017), (d) CHAR ((#·cm)/(mg·Ma); this study), (e) PyC (%; Zhou et al., 2017), (f) $\delta^{13}C$ from PyC (‰; Zhou et al., 2017). Blue bar indicates gradual C_4 grass

expansion recorded from 7–4 Ma by Zhou et al., 2017. Stratigraphic morphological zones from CONISS are shown with the gray bar.

4.2. Validity of the Fire Hypothesis

4.2.1. Site 1081

The Fire Hypothesis is not supported at Site 1081 for two main reasons. First, the observed fuel type remains prominently woody throughout the time of the study despite terrestrial vegetation changes to grasslands. Poaceae pollen percentage is steadily increasing from 8 Ma and desert pollen percentage begins increasing around 4 Ma (Hoetzel et al., 2013, 2015). Yet, the morphology type and L:W ratio indicate a sustained preferential burning of woody vegetation. This is contradictory to the Fire Hypothesis which proposes that there was a transition from woody fuel to grassy fuel (Keeley & Rundel, 2005). Second, while CHAR shows an increase in fire activity just after the beginning of the expansion, it does not support an increase in fire activity after the C_4 grassland expansion. The Fire Hypothesis requires an increase in fire activity alongside the expansion in addition to prolonged high fire activity, sustained by the positive feedback loop of grasses being more flammable both promoting fire and inhibiting C_3 vegetation from reestablishing (Bond, 2008; Bond & Keeley, 2005; Keeley & Rundel, 2005; Scheiter et al., 2012). The desynchronization of CHAR and grassland expansion decouples fire activity and vegetation on land. Overall, the sedimentary charcoal data does not follow the patterns needed to support the Fire Hypothesis, suggesting outside mechanisms, like aridification and changes in regional hydroclimate (Dupont et al., 2013; Hoetzel et al., 2015), are more likely the cause of the C_4 grass expansion in Southwestern Africa.

4.2.2. Site U1457

Charcoal data during the recorded C_4 expansion from 7.4 to 7.2 Ma supports the Fire Hypothesis. Around 7.3 Ma, there is an increase in CHAR, L:W, and dominance of elongated morphotype, which is synchronous with the C_4 grass expansion shown by peaks in grass pollen percentage (Feakins et al., 2020). This suggests that as there was an increase in fire activity, C_4 grasses expanded and were the primary fuel type. This pattern is synonymous with the Fire Hypothesis (Feakins et al., 2020; Keeley & Rundel, 2005). However, the associated shift in charcoal morphology at 7.3 Ma indicates a transition from predominantly grassy to more woody fuel types, contrary to expectations under the Fire Hypothesis which hypothesizes a preferential burning of C_3 woody vegetation to C_4 grassy vegetation.

Charcoal across the entirety of the data does not support the Fire Hypothesis. The morphology type suggests a longer-term transition from mixed woody–grassy fuels toward predominantly woody fuel sources. This pattern implies preferential burning of woody vegetation rather than grasses, a trajectory inconsistent with the Fire Hypothesis. CHAR do not indicate sustained fire activity, as proposed by the Fire Hypothesis. In particular, there is no evidence for a prolonged increase in CHAR that would signal a positive feedback loop capable of maintaining open C_4-dominated grasslands (Keeley & Rundel, 2005).

4.2.3. Site 717

The Fire Hypothesis is partly supported in the Bengal Fan. The patterns of data we would expect to see per the Fire Hypothesis are evident (i.e. increased fire activity and a transition from woody to grassy fuel alongside the expansion of terrestrial grassy vegetation). It is supported because the initial pulse of C_4 vegetation cover at ~8.5 Ma corresponds with increased fire

activity and a greater contribution from grassy fuels, consistent with the hypothesis. However, across the broader time of the study, there is no sustained evidence for preferential grass burning or an increase in fire activity after the C_4 grass expansion. Additionally, at the beginning of the recorded C_4 grass expansion (6.9–6.0 Ma), L:W increases and fall dramatically, and a shift to increasingly variable morphological assemblages suggests no pattern or trend in fuel type. Fire activity declines after the C_4 grass expansion is complete. However, there is no corresponding drop in total PAHs after C_4 grass expansion, suggesting that regional fire activity was maintained and more localized fire activity declined, or alternatively sedimentation rates declined making total PAHs concentrations appear higher (Daniau et al., 2019; Vachula et al., 2022). Overall, this is the opposite of what we would expect to see per the Fire Hypothesis.

4.2.4. Site 1146

Fire activity and fuel type changes recorded by Site 1146 only partially support the Fire Hypothesis. Until 6.3 Ma, after the outset of the gradual C_4 grass expansion from 7 to 4 Ma, grassy fuel was the dominant biomass burning. However, the long-term shift toward more woody fuel from grassy fuel contradicts expectations of the Fire Hypothesis, which infers the opposite transition from woody to grassy fuel (Keeley & Rundel, 2005). Additionally, fire activity did not increase alongside expansion. Rather, fire activity increased between 7.3 and 6.9 Ma, just before the C_4 grass expansion and declined after C_4 grasses began expanding. During this period of increased fire activity, there is no evidence for preferential burning of C_3 vegetation or a transition toward grass-dominated fuels, which is also contradictory to the Fire Hypothesis. Therefore, fire alone was unlikely to have been the primary driver of vegetation change in this region.

4.3. Multi-site synthesis and conclusions

Across the broader timespan of all four sites, there is little evidence supporting the Fire Hypothesis. The L:W ratios and morphology type reveal continued dominance of woody fuel type, even following the documented C_4 grassland expansions, a pattern not consistent with preferential grass burning. Similarly, the fuel types from the four sites do not match vegetation changes on the adjacent landmasses. This may be due to grasses being less efficient when converting to charcoal and elongated morphology types, or the tendency for grass charcoal particles to be transported and deposited further from the origin (Feurdean, 2021).

Long-term CHAR trends do not demonstrate the sustained increase of fire activity or an establishment of a fire-grass positive feedback loop that would be expected per the Fire Hypothesis. Rather, our data show an increase in fire activity at the four sites that coincides with the beginning of the recorded C_4 grass expansions and a decrease in fire activity after or during the expansion. This suggests that increases in fire activity catalyzed the initial establishment of C_4 grasses, but that once the grasslands were established, fire activity decreased. To this end, our data suggest that fire was the agent for change rather than a component of the positive feedback loop. Other factors such as aridification, increases seasonality, monsoon variability, or atmospheric CO_2 decline, were more influential in sustaining the grasslands (Hoetzel et al., 2013; Huang et al., 2007; M. Li et al., 2023; Polissar et al., 2021; Schefuß & Dupont, 2020; Shen et al., 2018). We propose that the role of fire in the C_4 grass expansion was as an intermediary mechanism for change, rather than part of a self-sustaining fire-C_4 positive feedback loop.

This reinterpretation also has implications for predicting future vegetation changes due to climate change. If fire is not inherently self-reinforcing in these grassland ecosystems as

suggested by our charcoal data, then its role under future climate scenarios may be more limited than previously assumed. Rather than driving long-term biome stability, fire may primarily act as a disturbance that facilitates rapid shifts when climatic thresholds are crossed. Consequently, projections of grassland biome changes under ongoing climate change should place greater emphasis on regional climate controls such as hydroclimate variability and atmospheric CO_2 concentrations, with fire acting as a secondary control of ecosystem dynamics.

References

Alam, M., Muguli, T., Gurumurthy, G. P., Arif, M., Sohrin, Y., Singh, A. D., Radhakrishna, T., Pandey, D. K., & Verma, K. (2023). Hydroclimatic conditions and sediment provenance in the northeastern Arabian Sea since the late Miocene: Insights from geochemical and environmental magnetic records at IODP Site U1457 of the Laxmi Basin. *Geological Magazine*, *160*(4), 813–829. https://doi.org/10.1017/S0016756822001273

Berger, W. H., Lange, C. B., & Pérez, M. E. (2002). The early Matuyama Diatom Maximum off SW Africa: A conceptual model. *Marine Geology*, *180*(1), 105–116. https://doi.org/10.1016/S0025-3227(01)00208-0

Bird, M. I., Wynn, J. G., Saiz, G., Wurster, C. M., & McBeath, A. (2015). The Pyrogenic Carbon Cycle. *Annual Review of Earth and Planetary Sciences*, *43*(Volume 43, 2015), 273–298. https://doi.org/10.1146/annurev-earth-060614-105038

Bond, W. J. (2008). What Limits Trees in C_4 Grasslands and Savannas? *Annual Review of Ecology, Evolution, and Systematics*, *39*(1), 641–659. https://doi.org/10.1146/annurev.ecolsys.39.110707.173411

Bond, W. J., & Keeley, J. E. (2005). Fire as a global 'herbivore': The ecology and evolution of flammable ecosystems. *Trends in Ecology & Evolution*, *20*(7), 387–394. https://doi.org/10.1016/j.tree.2005.04.025

Cerling, T. E., Wang, Y., & Quade, J. (1993). Expansion of C4 ecosystems as an indicator of global ecological change in the late Miocene. *Nature*, *361*(6410), 344–345. https://doi.org/10.1038/361344a0

Chauhan, M. M., Ali, S., Khan, A. M., Kumar, P., Murari, M. K., Samal, P., Singh, B. P., Adlakha, V., Saikia, L., Phartiyal, B., & Sharma, A. (2025). Tracing South Asian monsoon variability through a late miocene record from the himalayan foreland basin. *Npj Climate and Atmospheric Science*, *9*(1), 21. https://doi.org/10.1038/s41612-025-01293-5

Clark, J. S., & Patterson, W. A. (1997). Background and Local Charcoal in Sediments: Scales of Fire Evidence in the Paleorecord. In J. S. Clark, H. Cachier, J. G. Goldammer, & B. Stocks (Eds.), *Sediment Records of Biomass Burning and Global Change* (pp. 23–48). Springer. https://doi.org/10.1007/978-3-642-59171-6_3

Clift, P. D., Kulhanek, D. K., Zhou, P., Bowen, M. G., Vincent, S. M., Lyle, M., & Hahn, A. (2020). Chemical weathering and erosion responses to changing monsoon climate in the Late Miocene of Southwest Asia. *Geological Magazine*, *157*(6), 939–955. https://doi.org/10.1017/S0016756819000608

Clift, P. D., Wan, S., & Blusztajn, J. (2014). Reconstructing chemical weathering, physical erosion and monsoon intensity since 25 Ma in the northern South China Sea: A review of competing proxies. *Earth-Science Reviews*, *130*, 86–102. https://doi.org/10.1016/j.earscirev.2014.01.002

Crawford, A. J., & Belcher, C. M. (2014). Charcoal morphometry for paleoecological analysis: The effects of fuel type and transportation on morphological parameters. *Applications in Plant Sciences*, *2*(8), 1400004. https://doi.org/10.3732/apps.1400004

Daniau, A.-L., Desprat, S., Aleman, J. C., Bremond, L., Davis, B., Fletcher, W., Marlon, J. R., Marquer, L., Montade, V., Morales-Molino, C., Naughton, F., Rius, D., & Urrego, D. H. (2019). Terrestrial plant microfossils in palaeoenvironmental studies, pollen, microcharcoal and phytolith. Towards a comprehensive understanding of vegetation, fire and climate changes over the past one million years. *Revue de Micropaléontologie*, *63*, 1–35. https://doi.org/10.1016/j.revmic.2019.02.001

Diester-Haass, L., Meyers, P. A., & Rothe, P. (1990). Miocene history of the Benguela Current and Antarctic ice volumes: Evidence from rhythmic sedimentation and current growth across the Walvis Ridge (Deep Sea Drilling Project Sites 362 and 532). *Paleoceanography*, *5*(5), 685–707. https://doi.org/10.1029/PA005i005p00685

Dinerstein, E., Olson, D., Joshi, A., Vynne, C., Burgess, N. D., Wikramanayake, E., Hahn, N., Palminteri, S., Hedao, P., Noss, R., Hansen, M., Locke, H., Ellis, E. C., Jones, B., Barber, C. V., Hayes, R., Kormos, C., Martin, V., Crist, E., … Saleem, M. (2017). An Ecoregion-Based Approach to Protecting Half the Terrestrial Realm. *BioScience*, *67*(6), 534–545. https://doi.org/10.1093/biosci/bix014

Du, S., Xiang, R., Liu, J., Liu, J. P., Islam, G. M. A., & Chen, M. (2020). The present-day atmospheric dust deposition process in the South China Sea. *Atmospheric Environment*, *223*, 117261. https://doi.org/10.1016/j.atmosenv.2020.117261

Dupont, L. M., Donner, B., Vidal, L., Pérez, E. M., & Wefer, G. (2005). Linking desert evolution and coastal upwelling: Pliocene climate change in Namibia. *Geology*, *33*(6), 461–464. https://doi.org/10.1130/G21401.1

Dupont, L. M., Rommerskirchen, F., Mollenhauer, G., & Schefuß, E. (2013). Miocene to Pliocene changes in South African hydrology and vegetation in relation to the expansion of C4 plants. *Earth and Planetary Science Letters*, *375*, 408–417. https://doi.org/10.1016/j.epsl.2013.06.005

Dupont, L. M., & Wyputta, U. (2003). Reconstructing pathways of aeolian pollen transport to the marine sediments along the coastline of SW Africa. *Quaternary Science Reviews*, *22*(2), 157–174. https://doi.org/10.1016/S0277-3791(02)00032-X

Edwards, E. J., Osborne, C. P., Strömberg, C. A. E., Smith, S. A., C Grasses Consortium, Bond, W. J., Christin, P.-A., Cousins, A. B., Duvall, M. R., Fox, D. L., Freckleton, R. P., Ghannoum, O., Hartwell, J., Huang, Y., Janis, C. M., Keeley, J. E., Kellogg, E. A., Knapp, A. K., Leakey, A. D. B., … Tipple, B. (2010). The Origins of C $_4$ Grasslands: Integrating Evolutionary and Ecosystem Science. *Science*, *328*(5978), 587–591. https://doi.org/10.1126/science.1177216

Edwards, E. J., Osborne, C. P., Strömberg, C. A. E., Smith, S. A., C4 Grasses Consortium, Bond, W. J., Christin, P.-A., Cousins, A. B., Duvall, M. R., Fox, D. L., Freckleton, R. P., Ghannoum, O., Hartwell, J., Huang, Y., Janis, C. M., Keeley, J. E., Kellogg, E. A., Knapp, A. K., Leakey, A. D. B., … Tipple, B. (2010). The Origins of C4 Grasslands: Integrating Evolutionary and Ecosystem Science. *Science*, *328*(5978), 587–591. https://doi.org/10.1126/science.1177216

Enache, M. D., & Cumming, B. F. (2006). Tracking recorded fires using charcoal morphology from the sedimentary sequence of Prosser Lake, British Columbia (Canada). *Quaternary Research*, *65*(02), 282–292. https://doi.org/10.1016/j.yqres.2005.09.003

Feakins, S. J., Liddy, H. M., Tauxe, L., Galy, V., Feng, X., Tierney, J. E., Miao, Y., & Warny, S. (2020). Miocene C4 Grassland Expansion as Recorded by the Indus Fan. *Paleoceanography and Paleoclimatology*, *35*(6), e2020PA003856. https://doi.org/10.1029/2020PA003856

Feurdean, A. (2021). Experimental production of charcoal morphologies to discriminate fuel source and fire type: An example from Siberian taiga. *Biogeosciences*, *18*(12), 3805–3821. https://doi.org/10.5194/bg-18-3805-2021

Feurdean, A., Vachula, R. S., Hanganu, D., Stobbe, A., & Gumnior, M. (2023). Charcoal morphologies and morphometrics of a Eurasian grass-dominated system for robust interpretation of past fuel and fire type. *Biogeosciences*, *20*(24), 5069–5085. https://doi.org/10.5194/bg-20-5069-2023

Frank-DePue, L., Vachula, R. S., Balascio, N. L., Cahoon, K., & Kaste, J. M. (2023). Trends in sedimentary charcoal shapes correspond with broad-scale land-use changes: Insights gained from a 300-year lake sediment record from eastern Virginia, USA. *Journal of Paleolimnology*, *69*(1), 21–36. https://doi.org/10.1007/s10933-022-00260-x

Galinger, M. R., Vachula, R. S., Goertzen, L. R., Hansen, C. J., & Cullen, T. M. (2025). A new approach to experimental charcoal analyses: Implications for the Cretaceous and other greenhouse climate intervals. *Global and Planetary Change*, *255*, 105079. https://doi.org/10.1016/j.gloplacha.2025.105079

Genet, M., Daniau, A.-L., Mouillot, F., Hanquiez, V., Schmidt, S., David, V., Georget, M., Abrantes, F., Anschutz, P., Bassinot, F., Bonnin, J., Dennielou, B., Eynaud, F., Hodell, D. A., Mulder, T., Naughton, F., Rossignol, L., Tzedakis, P., & Sánchez-Goñi, M. F. (2021a). Modern relationships between microscopic charcoal in marine sediments and fire regimes on adjacent landmasses to refine the interpretation of marine paleofire records: An Iberian case study. *Quaternary Science Reviews*, *270*, 107148. https://doi.org/10.1016/j.quascirev.2021.107148

Genet, M., Daniau, A.-L., Mouillot, F., Hanquiez, V., Schmidt, S., David, V., Georget, M., Abrantes, F., Anschutz, P., Bassinot, F., Bonnin, J., Dennielou, B., Eynaud, F., Hodell, D. A., Mulder, T., Naughton, F., Rossignol, L., Tzedakis, P., & Sánchez-Goñi, M. F. (2021b). Modern relationships between microscopic charcoal in marine sediments and fire regimes on adjacent landmasses to refine the interpretation of marine paleofire records: An Iberian case study. *Quaternary Science Reviews*, *270*, 107148. https://doi.org/10.1016/j.quascirev.2021.107148

Gibson, D. J. (2009). *Grasses and Grassland Ecology*. Oxford University Press.

Grimm, E. C. (1987). CONISS: A FORTRAN 77 program for stratigraphically constrained cluster analysis by the method of incremental sum of squares. *Computers & Geosciences*, *13*(1), 13–35. https://doi.org/10.1016/0098-3004(87)90022-7

Haliuc, A., Daniau, A.-L., Mouillot, F., Chen, W., Leys, B., David, V., Hanquiez, V., Dennielou, B., Schefuß, E., Bayon, G., & Crosta, X. (2023). Microscopic charcoals in ocean sediments off Africa track past fire intensity from the continent. *Communications Earth & Environment*, *4*(1), 1–11. https://doi.org/10.1038/s43247-023-00800-x

Herbert, T. D., Lawrence, K. T., Tzanova, A., Peterson, L. C., Caballero-Gill, R., & Kelly, C. S. (2016). Late Miocene global cooling and the rise of modern ecosystems. *Nature Geoscience*, *9*(11), 843–847. https://doi.org/10.1038/ngeo2813

Higuera, P. E., Peters, M. E., Brubaker, L. B., & Gavin, D. G. (2007). Understanding the origin and analysis of sediment-charcoal records with a simulation model. *Quaternary Science Reviews*, *26*(13), 1790–1809. https://doi.org/10.1016/j.quascirev.2007.03.010

Hoetzel, S., Dupont, L. M., & Wefer, G. (2015). Miocene–Pliocene vegetation change in south-western Africa (ODP Site 1081, offshore Namibia). *Palaeogeography, Palaeoclimatology, Palaeoecology*, *423*, 102–108. https://doi.org/10.1016/j.palaeo.2015.02.002

Hoetzel, S., Dupont, L., Schefuß, E., Rommerskirchen, F., & Wefer, G. (2013). The role of fire in Miocene to Pliocene C4 grassland and ecosystem evolution. *Nature Geoscience*, *6*(12), 1027–1030. https://doi.org/10.1038/ngeo1984

Holbourn, A. E., Kuhnt, W., Clemens, S. C., Kochhann, K. G. D., Jöhnck, J., Lübbers, J., & Andersen, N. (2018). Late Miocene climate cooling and intensification of southeast Asian winter monsoon. *Nature Communications*, *9*(1), 1584. https://doi.org/10.1038/s41467-018-03950-1

Holbourn, A., Kuhnt, W., Clemens, S. C., & Heslop, D. (2021). A ∼12 Myr Miocene Record of East Asian Monsoon Variability From the South China Sea. *Paleoceanography and Paleoclimatology*, *36*(7), e2021PA004267. https://doi.org/10.1029/2021PA004267

Huang, Y., Clemens, S. C., Liu, W., Wang, Y., & Prell, W. L. (2007). Large-scale hydrological change drove the late Miocene C4 plant expansion in the Himalayan foreland and Arabian Peninsula. *Geology*, *35*(6), 531–534. https://doi.org/10.1130/G23666A.1

Hui, Z., Gowan, E. J., Hou, Z., Zhou, X., Ma, Y., Guo, Z., & Zhang, J. (2021). Intensified fire activity induced by aridification facilitated Late Miocene C4 plant expansion in the northeastern Tibetan Plateau, China. *Palaeogeography, Palaeoclimatology, Palaeoecology*, *573*, 110437. https://doi.org/10.1016/j.palaeo.2021.110437

Inoue, J., & Usuki, T. (2025). Effects of particle size and pretreatment methods on the morphometry of grass charcoal particles: Implications for morphometric analysis of microcharcoal particles. *The Holocene*, *35*(4), 471–476. https://doi.org/10.1177/09596836241307296

Jia, G., Peng, P., Zhao, Q., & Jian, Z. (2003). Changes in terrestrial ecosystem since 30 Ma in East Asia: Stable isotope evidence from black carbon in the South China Sea. *Geology*, *31*(12), 1093–1096. https://doi.org/10.1130/G19992.1

Jin, H., Wan, S., Clift, P. D., Liu, C., Huang, J., Jiang, S., Li, M., Qin, L., Shi, X., & Li, A. (2022). Birth of the Pearl River at 30 Ma: Evidence from sedimentary records in the northern South China Sea. *Earth and Planetary Science Letters*, *600*, 117872. https://doi.org/10.1016/j.epsl.2022.117872

Karp, A. T., Behrensmeyer, A. K., & Freeman, K. H. (2018). Grassland fire ecology has roots in the late Miocene. *Proceedings of the National Academy of Sciences of the United States of America*, *115*(48), 12130–12135. https://doi.org/10.1073/pnas.1809758115

Karp, A. T., Uno, K. T., Polissar, P. J., & Freeman, K. H. (2021). Late Miocene C4 Grassland Fire Feedbacks on the Indian Subcontinent. *Paleoceanography and Paleoclimatology*, *36*(4), e2020PA004106. https://doi.org/10.1029/2020PA004106

Keeley, J. E., & Rundel, P. W. (2005). Fire and the Miocene expansion of C4 grasslands. *Ecology Letters*, *8*(7), 683–690. https://doi.org/10.1111/j.1461-0248.2005.00767.x

Laskar, J., Correia, A. C. M., Gastineau, M., Joutel, F., Levrard, B., & Robutel, P. (2004). Long term evolution and chaotic diffusion of the insolation quantities of Mars. *Icarus*, *170*(2), 343–364. https://doi.org/10.1016/j.icarus.2004.04.005

Lehmann, C. E. R., Anderson, T. M., Sankaran, M., Higgins, S. I., Archibald, S., Hoffmann, W. A., Hanan, N. P., Williams, R. J., Fensham, R. J., Felfili, J., Hutley, L. B., Ratnam, J., San Jose, J., Montes, R., Franklin, D., Russell-Smith, J., Ryan, C. M., Durigan, G., Hiernaux, P., … Bond, W. J. (2014). Savanna Vegetation-Fire-Climate Relationships Differ Among Continents. *Science*, *343*(6170), 548–552. https://doi.org/10.1126/science.1247355

Li, B., Wang, J., Huang, B., Li, Q., Jian, Z., Zhao, Q., Su, X., & Wang, P. (2004). South China Sea surface water evolution over the last 12 Myr: A south-north comparison from Ocean Drilling Program Sites 1143 and 1146. *Paleoceanography*, *19*(1). https://doi.org/10.1029/2003PA000906

Li, M., Wan, S., Colin, C., Jin, H., Zhao, D., Pei, W., Jiao, W., Tang, Y., Tan, Y., Shi, X., & Li, A. (2023). Expansion of C4 plants in South China and evolution of East Asian monsoon since 35 Ma: Black carbon records in the northern South China Sea. *Global and Planetary Change*, *223*, 104079. https://doi.org/10.1016/j.gloplacha.2023.104079

Liu, W., Huang, Y., An, Z., Clemens, S. C., Li, L., Prell, W. L., & Ning, Y. (2005). Summer monsoon intensity controls C4/C3 plant abundance during the last 35 ka in the Chinese Loess Plateau: Carbon isotope evidence from bulk organic matter and individual leaf waxes. *Palaeogeography, Palaeoclimatology, Palaeoecology*, *220*(3), 243–254. https://doi.org/10.1016/j.palaeo.2005.01.001

Miao, Y., Song, Y., Li, Y., Yang, S., Li, Y., Zhao, Y., & Zeng, M. (2020). Late Pleistocene fire in the Ili Basin, Central Asia, and its potential links to paleoclimate change and human

activities. *Palaeogeography, Palaeoclimatology, Palaeoecology*, *547*, 109700. https://doi.org/10.1016/j.palaeo.2020.109700

Miao, Y., Wu, F., Warny, S., Fang, X., Lu, H., Fu, B., Song, C., Yan, X., Escarguel, G., Yang, Y., Meng, Q., & Shi, P. (2019). Miocene fire intensification linked to continuous aridification on the Tibetan Plateau. *Geology*, *47*(4), 303–307. https://doi.org/10.1130/G45720.1

Mohanty, R. N., Gupta, A. K., & Clemens, S. (2025). Benguela upwelling system triggered and intensified southern African aridification in the Late Miocene. *Communications Earth & Environment*, *6*(1), 989. https://doi.org/10.1038/s43247-025-02948-0

Mouillot, F., & Field, C. B. (2005). *Fire history and the global carbon budget: A 1°× 1° fire history reconstruction for the 20th century*. *11*(3), 398–420. https://doi.org/10.1111/j.1365-2486.2005.00920

Nichols, G. J., Cripps, J. A., Collinson, M. E., & Scott, A. C. (2000). Experiments in waterlogging and sedimentology of charcoal: Results and implications. *Palaeogeography, Palaeoclimatology, Palaeoecology, Fire and the Palaeoenvironment*, *164*(1), 43–56. https://doi.org/10.1016/S0031-0182(00)00174-7

Pagani, M., Freeman, K. H., & Arthur, M. A. (1999). Late Miocene Atmospheric CO_2 Concentrations and the Expansion of C_4 Grasses. *Science*, *285*(5429), 876–879. https://doi.org/10.1126/science.285.5429.876

Pagani, M., Zachos, J. C., Freeman, K. H., Tipple, B., & Bohaty, S. (2005). Marked Decline in Atmospheric Carbon Dioxide Concentrations During the Paleogene. *Science*, *309*(5734), 600–603. https://doi.org/10.1126/science.1110063

Passey, B. H., Ayliffe, L. K., Kaakinen, A., Zhang, Z., Eronen, J. T., Zhu, Y., Zhou, L., Cerling, T. E., & Fortelius, M. (2009). Strengthened East Asian summer monsoons during a period of

high-latitude warmth? Isotopic evidence from Mio-Pliocene fossil mammals and soil carbonates from northern China. *Earth and Planetary Science Letters*, *277*(3), 443–452. https://doi.org/10.1016/j.epsl.2008.11.008

Patterson, W. A., Edwards, K. J., & Maguire, D. J. (1987). Microscopic charcoal as a fossil indicator of fire. *Quaternary Science Reviews*, *6*(1), 3–23. https://doi.org/10.1016/0277-3791(87)90012-6

Pausas, J. G., & Paula, S. (2020). Grasses and fire: The importance of hiding buds. *The New Phytologist*, *226*(4), 957–959.

Pereboom, E. M., Vachula, R. S., Huang, Y., & Russell, J. (2020). The morphology of experimentally produced charcoal distinguishes fuel types in the Arctic tundra. *The Holocene*, *30*(7), 1091–1096. https://doi.org/10.1177/0959683620908629

Polissar, P. J., Uno, K. T., Phelps, S. R., Karp, A. T., Freeman, K. H., & Pensky, J. L. (2021). Hydrologic Changes Drove the Late Miocene Expansion of C4 Grasslands on the Northern Indian Subcontinent. *Paleoceanography and Paleoclimatology*, *36*(4), e2020PA004108. https://doi.org/10.1029/2020PA004108

Preston, C. M., & Schmidt, M. W. I. (2006). Black (pyrogenic) carbon: A synthesis of current knowledge and uncertainties with special consideration of boreal regions. *Biogeosciences*, *3*(4), 397–420. https://doi.org/10.5194/bg-3-397-2006

Quade, J., Cerling, T. E., & Bowman, J. R. (1989). Development of Asian monsoon revealed by marked ecological shift during the latest Miocene in northern Pakistan. *Nature*, *342*(6246), 163–166. https://doi.org/10.1038/342163a0

Ripley, B., Venables, B., Bates, D. M., ca 1998), K. H. (partial port, ca 1998), A. G. (partial port, & polr), D. F. (support functions for. (2025). *MASS: Support Functions and Datasets for*

Venables and Ripley's MASS (Version 7.3-65) [Computer software]. https://cran.r-project.org/web/packages/MASS/index.html

Rommerskirchen, F., Condon, T., Mollenhauer, G., Dupont, L., & Schefuss, E. (2011). Miocene to Pliocene development of surface and subsurface temperatures in the Benguela Current system. *Paleoceanography*, *26*(3). https://doi.org/10.1029/2010PA002074

Rubbelke, C. B., Bhattacharya, T., Feng, R., Burls, N. J., Knapp, S., & McClymont, E. L. (2023). Plio-Pleistocene Southwest African Hydroclimate Modulated by Benguela and Indian Ocean Temperatures. *Geophysical Research Letters*, *50*(19), e2023GL103003. https://doi.org/10.1029/2023GL103003

S), A. C. (author of original code for, R, B. R. (conversion to, maintainer 1999--2022, support), author of parallel, & fixes), A. R. B. (minor bug. (2025). *boot: Bootstrap Functions* (Version 1.3-32) [Computer software]. https://cran.r-project.org/web/packages/boot/index.html

Sadler, P. M. (1981). Sediment Accumulation Rates and the Completeness of Stratigraphic Sections. *The Journal of Geology*, *89*(5), 569–584. https://doi.org/10.1086/628623

Sage, R. F. (2004). The evolution of C4 photosynthesis. *New Phytologist*, *161*(2), 341–370. https://doi.org/10.1111/j.1469-8137.2004.00974.x

Schefuß, E., & Dupont, L. M. (2020). Multiple drivers of Miocene C4 ecosystem expansions. *Nature Geoscience*, *13*(7), 463–464. https://doi.org/10.1038/s41561-020-0590-5

Scheiter, S., Higgins, S. I., Osborne, C. P., Bradshaw, C., Lunt, D., Ripley, B. S., Taylor, L. L., & Beerling, D. J. (2012). Fire and fire-adapted vegetation promoted C4 expansion in the late Miocene. *New Phytologist*, *195*(3), 653–666. https://doi.org/10.1111/j.1469-8137.2012.04202.x

Shen, X., Wan, S., Colin, C., Tada, R., Shi, X., Pei, W., Tan, Y., Jiang, X., & Li, A. (2018). Increased seasonality and aridity drove the C4 plant expansion in Central Asia since the Miocene–Pliocene boundary. *Earth and Planetary Science Letters*, *502*, 74–83. https://doi.org/10.1016/j.epsl.2018.08.056

Shi, N., Dupont, L. M., Beug, H.-J., & Schneider, R. (1998). Vegetation and climate changes during the last 21 000 years in S.W. Africa based on a marine pollen record. *Vegetation History and Archaeobotany*, *7*(3), 127–140. https://doi.org/10.1007/BF01374001

Singh, R. K., & Gupta, A. K. (2004). Late Oligocene–Miocene paleoceanographic evolution of the southeastern Indian Ocean: Evidence from deep-sea benthic foraminifera (ODP Site 757). *Marine Micropaleontology*, *51*(1), 153–170. https://doi.org/10.1016/j.marmicro.2003.10.003

Snitker, G. (2020). The Charcoal Quantification Tool (CharTool): A Suite of Open-source Tools for Quantifying Charcoal Fragments and Sediment Properties in Archaeological and Paleoecological Analysis. *Ethnobiology Letters*, *11*(1), 103–115.

Steinke, S., Groeneveld, J., Johnstone, H., & Rendle-Bühring, R. (2010). East Asian summer monsoon weakening after 7.5 Ma: Evidence from combined planktonic foraminifera Mg/Ca and δ18O (ODP Site 1146; northern South China Sea). *Palaeogeography, Palaeoclimatology, Palaeoecology*, *289*(1), 33–43. https://doi.org/10.1016/j.palaeo.2010.02.007

Strömberg, C. A. E. (2011). Evolution of Grasses and Grassland Ecosystems. *Annual Review of Earth and Planetary Sciences*, *39*(Volume 39, 2011), 517–544. https://doi.org/10.1146/annurev-earth-040809-152402

Tipple, B. J., & Pagani, M. (2007). The Early Origins of Terrestrial C 4 Photosynthesis. *Annual Review of Earth and Planetary Sciences*, *35*(1), 435–461. https://doi.org/10.1146/annurev.earth.35.031306.140150

Tolonen, K. (1986). Charred particle analysis. *Handbook of Holocene Palaeoecology and Palaeolimonology, B.E. Berglund (Ed.)*, *1*, 485–496.

Umbanhowar, C. E., & Mcgrath, M. J. (1998). Experimental production and analysis of microscopic charcoal from wood, leaves and grasses. *The Holocene*, *8*(3), 341–346. https://doi.org/10.1191/095968398666496051

Vachula, R. S. (2019). A usage-based size classification scheme for sedimentary charcoal. *The Holocene*, *29*(3), 523–527. https://doi.org/10.1177/0959683618816520

Vachula, R. S., & Cheung, A. H. (2021). Late Neogene surge in sedimentary charcoal fluxes partly due to preservation biases, not fire activity. *Palaeogeography, Palaeoclimatology, Palaeoecology*, *567*, 110273. https://doi.org/10.1016/j.palaeo.2021.110273

Vachula, R. S., Karp, A. T., Denis, E. H., Balascio, N. L., Canuel, E. A., & Huang, Y. (2022). Spatially calibrating polycyclic aromatic hydrocarbons (PAHs) as proxies of area burned by vegetation fires: Insights from comparisons of historical data and sedimentary PAH fluxes. *Palaeogeography, Palaeoclimatology, Palaeoecology*, *596*, 110995. https://doi.org/10.1016/j.palaeo.2022.110995

Vachula, R. S., Sae-Lim, J., & Li, R. (2021). A critical appraisal of charcoal morphometry as a paleofire fuel type proxy. *Quaternary Science Reviews*, *262*(106979). https://doi.org/10.1016/j.quascirev.2021.106979

Vendramini, J. M. B., Silveira, M. L., & Moriel, P. (2023). Resilience of warm-season (C4) perennial grasses under challenging environmental and management conditions. *Animal Frontiers*, *13*(5), 16–22. https://doi.org/10.1093/af/vfad038

Weiguo, L., Xiahong, F., Youfeng, N., Qingle, Z., Yunning, C., & Zhisheng, A. N. (2005). δ13C variation of C3 and C4 plants across an Asian monsoon rainfall gradient in arid northwestern China. *Global Change Biology*, *11*(7), 1094–1100. https://doi.org/10.1111/j.1365-2486.2005.00969.x

Whitlock, C., & Larsen, C. (2001). Charcoal as a Fire Proxy. In J. P. Smol, H. J. B. Birks, W. M. Last, R. S. Bradley, & K. Alverson (Eds.), *Tracking Environmental Change Using Lake Sediments: Terrestrial, Algal, and Siliceous Indicators* (pp. 75–97). Springer Netherlands. https://doi.org/10.1007/0-306-47668-1_5

Wickham, H., Averick, M., Bryan, J., Chang, W., McGowan, L. D., François, R., Grolemund, G., Hayes, A., Henry, L., Hester, J., Kuhn, M., Pedersen, T. L., Miller, E., Bache, S. M., Müller, K., Ooms, J., Robinson, D., Seidel, D. P., Spinu, V., … Yutani, H. (2019). Welcome to the Tidyverse. *Journal of Open Source Software*, *4*(43), 1686. https://doi.org/10.21105/joss.01686

Wickham, H., Chang, W., Henry, L., Pedersen, T. L., Takahashi, K., Wilke, C., Woo, K., Yutani, H., Dunnington, D., Brand, T. van den, Posit, & PBC. (2025). *ggplot2: Create Elegant Data Visualisations Using the Grammar of Graphics* (Version 4.0.1) [Computer software]. https://cran.r-project.org/web/packages/ggplot2/index.html

Wilkinson, B. H., & Vachula, R. S. (2023). On the Sadler Effect and biases in Holocene paleofire records. *Palaeogeography, Palaeoclimatology, Palaeoecology*, *619*, 111548. https://doi.org/10.1016/j.palaeo.2023.111548

Yu, Z., Colin, C., Wan, S., Saraswat, R., Song, L., Xu, Z., Clift, P., Lu, H., Lyle, M., Kulhanek, D., Hahn, A., Tiwari, M., Mishra, R., Miska, S., & Kumar, A. (2019). Sea level-controlled sediment transport to the eastern Arabian Sea over the past 600 kyr: Clay minerals and SrNd isotopic evidence from IODP site U1457. *Quaternary Science Reviews*, *205*, 22–34. https://doi.org/10.1016/j.quascirev.2018.12.006

Zhang, Y., Gan, J., & Yang, Q. (2024). Spatiotemporal variability of streamflow in the Pearl River Basin: Controls of land surface processes and atmospheric impacts. *Hydrological Processes*, *38*(4), e15151. https://doi.org/10.1002/hyp.15151

Zhisheng, A., Kutzbach, J. E., Prell, W. L., & Porter, S. C. (2001). Evolution of Asian monsoons and phased uplift of the Himalaya–Tibetan plateau since Late Miocene times. *Nature*, *411*(6833), 62–66. https://doi.org/10.1038/35075035

Zhou, B., Bird, M., Zheng, H., Zhang, E., Wurster, C. M., Xie, L., & Taylor, D. (2017a). New sedimentary evidence reveals a unique history of C4 biomass in continental East Asia since the early Miocene. *Scientific Reports*, *7*(1), 170. https://doi.org/10.1038/s41598-017-00285-7

Zhou, B., Bird, M., Zheng, H., Zhang, E., Wurster, C. M., Xie, L., & Taylor, D. (2017b). New sedimentary evidence reveals a unique history of C4 biomass in continental East Asia since the early Miocene. *Scientific Reports*, *7*(1), 170. https://doi.org/10.1038/s41598-017-00285-7

Zhou, B., Rybski, D., & Kropp, J. P. (2017). The role of city size and urban form in the surface urban heat island. *Scientific Reports*, *7*(1), 4791. https://doi.org/10.1038/s41598-017-04242-2

Appendix 2

Pearson's correlation analysis revealed several significant relationships among the measured charcoal morphometric characteristics (Table 1). Circularity was strongly positively correlated with solidity ($r = 0.92$, $p < 0.01$), and strongly negatively correlated with elongated (no ramifications) morphotype abundance ($r = –0.84$, $p < 0.01$). Feret diameter showed significant correlations with all parameters except rectangularity ($r = 0.13$, $p > 0.05$). L:W was negatively correlated with roundness ($r = –0.85$, $p < 0.01$), solidity ($r = –0.67$, $p < 0.01$), and irregular morphotypes ($r = –0.81$, $p < 0.01$), but positively correlated with elongated (no ramifications) ($r = 0.28$, $p < 0.01$). Roundness and solidity were positively correlated ($r = 0.86$, $p < 0.01$) and both were strongly negatively correlated with elongated (no ramifications) (roundness: $r = –0.85$ solidity: $r = –0.81$; $p < 0.01$) and positively correlated with irregular morphotypes (roundness: $r = 0.81$, solidity: $r = 0.70$; $p < 0.01$).

Table 1. Pearson correlations and significance levels among the different morphometric characteristics and elongated and irregular morphotypes from Sites 1081, U1457, 717, and 1146 (* denotes p < 0.01 and ** denotes p < 0.05).

	Circularity	Feret diameter	L:W	Roundness	Solidity	Rectangularity	Elongated (no ramifications)	Irregular
Circularity		−0.52*	−0.86*	0.90*	0.92*	−0.38*	−0.85*	0.80*
	Feret diameter		0.47*	0.51*	−0.50*	0.21*	0.41*	−0.40*
		L:W		−0.91*	−0.81*	0.06	0.28*	−0.78*
			Roundness		0.83*	0.05	−0.26*	0.86*
				Solidity		−0.21*	−0.86*	0.70*

Rectangularity		0.12	−0.08
	Elongated (no ramifications)		−0.78*
		Irregular	

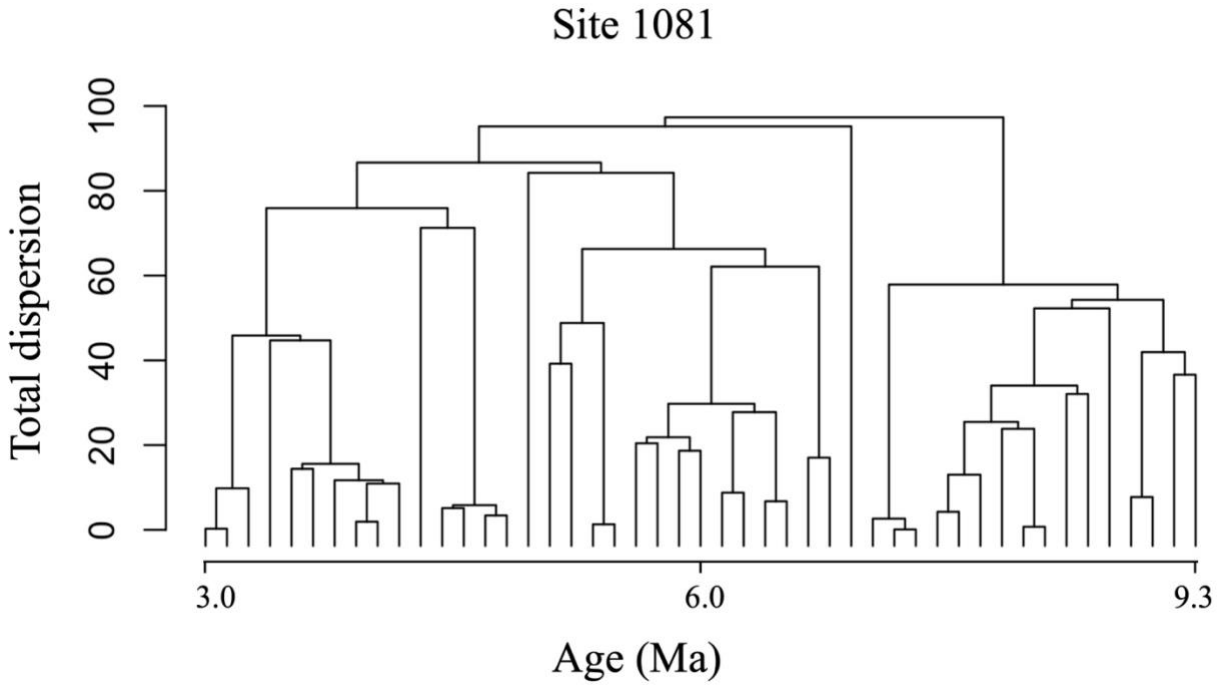

Figure 11. Dendrogram showing CONISS results for Site 1081 off the Namibian Coast.

Figure 12. Dendrogram showing CONISS results from Site U1457 in the Indus Fan.

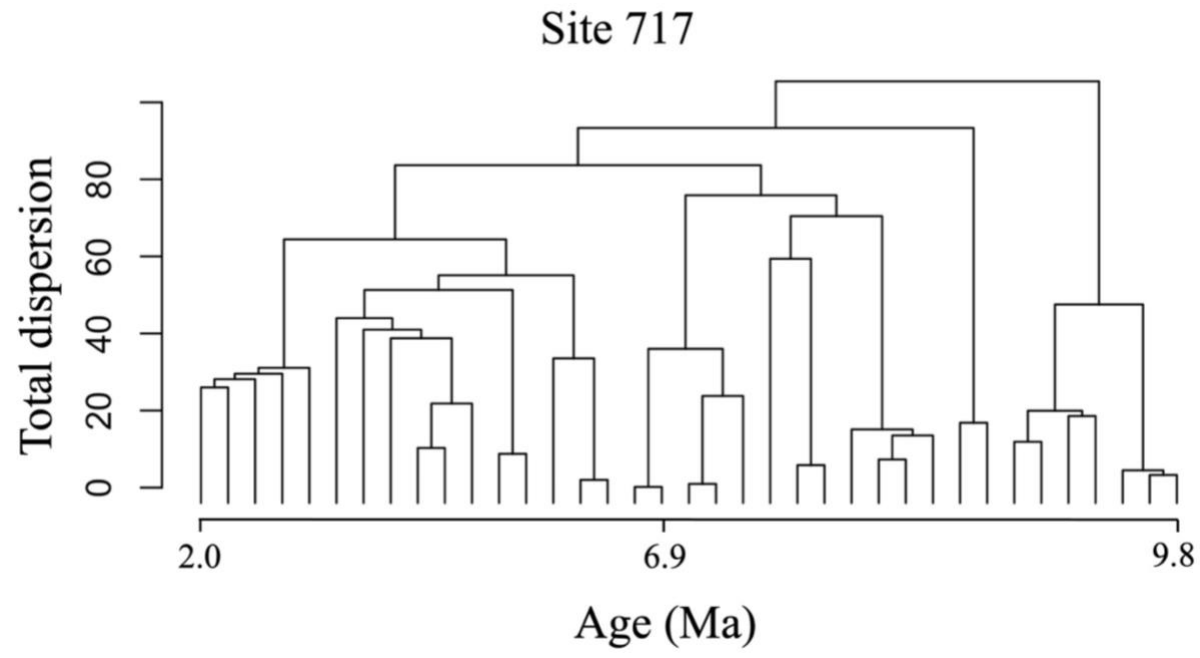

Figure 13. Dendrogram showing CONISS results from Site 717 in the Bengal Fan.

Appendix 3

Table 2. Sedimentary charcoal data for ODP Sites 1081, 717, and 1146 and IODP Site U1457. Abbreviations: cm, centimeters; mg, milligrams; MCD, meters composite depth; Ma, megaannum; CHAR, charcoal accumulation rate; circ, circularity; stdev, standard deviation; Fd, feret diameter; µm, micrometer; L:W, length to width ratio; R, roundness; S,solidity; Rect, rectangularity; d, elongated (ramifications); f, elongated (no ramificaitons); c/s.b, geometric; m/p, irregular. * indicates charcoal count capped at 50.

Site 1081																				
Sample label	Weight (mg)	MCD	Age (Ma)	SCC	Particle count	Circ mean	Circ stdev	Fd (µm) mean	Fd stdev	L:W mean	L:W stdev	R mean	R stdev	S mean	S stdev	Rect mean	Rect stdev	d	f	c/s.b	m/p
023X-4-W 64-66 cm	108	211.34	3.06	16.99	50*	0.64	0.13	98.77	40.55	1.38	0.25	0.75	0.13	0.89	0.05	0.91	0.07	0	0	10	90
024X-1-W 27-29 cm	57.3	215.63	3.18	23.23	37.00	0.60	0.10	83.25	20.92	1.52	0.39	0.69	0.14	0.88	0.04	0.92	0.06	0.00	0.00	8.11	91.89
024X-4-W 28-30 cm	105.7	230.65	3.31	16.77	50*	0.68	0.15	131.13	46.41	1.42	0.32	0.73	0.13	0.87	0.09	0.88	0.10	0.00	0.00	2.00	98.00
025X-1-W 136-138 cm	102.2	230.1	3.48	2.77	8.00	0.60	0.18	84.11	21.08	1.18	0.10	0.85	0.07	0.84	0.17	0.92	0.06	12.50	0.00	25.00	62.50
025X-5-W 94-96 cm	103.2	231.9	3.64	17.62	50*	0.63	0.14	92.38	45.90	1.38	0.31	0.75	0.14	0.89	0.04	0.93	0.10	0.00	0.00	10.00	90.00
026X-1-W 36-38 cm	100.9	235.92	3.72	17.68	48.00	0.43	0.10	138.97	29.15	1.46	0.50	0.73	0.15	0.88	0.05	1.10	0.11	6.25	0.00	16.67	77.08

026X-4-W 119-121cm	109	234.9	3.86	17.92	50*	0.68	0.09	79.64	25.83	1.42	0.30	0.73	0.14	0.90	0.02	0.88	0.05	0.00	0.00	6.00	94.00
027X-4-W 62-64cm	101.8	249.18	3.98	19.26	50*	0.64	0.13	161.07	79.76	1.45	0.44	0.74	0.17	0.89	0.05	0.91	0.08	0.00	2.00	12.00	86.00
027X-6-W 75-77cm	107.7	252.31	4.09	18.64	50*	0.69	0.16	179.17	133.89	1.81	1.72	0.69	0.19	0.89	0.05	0.85	0.05	0.00	6.00	8.00	86.00
028X-5-W 93-95cm	104.5	260.69	4.23	13.73	35.00	0.57	0.12	78.95	26.79	1.30	0.25	0.79	0.13	0.88	0.04	0.97	0.09	0.00	0.00	8.57	91.43
029X-1-W 134-136cm	102.1	264.7	4.47	2.05	5.00	0.44	0.25	137.46	103.47	3.68	4.14	0.54	0.35	0.76	0.17	0.95	0.13	0.00	40.00	20.00	40.00
030X-1-W 30-32cm	108.6	273.26	4.67	4.95	13.00	0.65	0.15	78.67	21.15	1.48	0.27	0.70	0.13	0.88	0.08	0.90	0.10	0.00	0.00	30.77	69.23
030X-2-W 132-134cm	106.3	275.78	4.70	19.32	50*	0.63	0.16	104.65	60.80	1.51	0.38	0.70	0.16	0.88	0.10	0.93	0.16	0.00	0.00	16.00	84.00
031X-1-W 38-40cm	107.6	283.04	4.91	2.59	7.00	0.56	0.08	63.45	9.21	1.39	0.21	0.74	0.11	0.90	0.03	0.96	0.05	0.00	0.00	42.86	57.14
031X-2-W 64-66cm	105.9	284.8	4.92	2.63	7.00	0.37	0.23	184.98	124.24	1.73	0.50	0.63	0.20	0.73	0.25	1.23	0.42	0.00	0.00	28.57	71.43
032X-2-W 12-14cm	105.3	293.88	5.15	1.48	4.00	0.50	0.14	130.79	68.67	2.20	1.04	0.55	0.27	0.89	0.05	0.93	0.13	0.00	25.00	75.00	0.00

032X-4-W 32-34cm	105.2	297.08	5.15	18.57	50*	0.69	0.16	121.77	42.52	1.42	0.30	0.73	0.13	0.87	0.10	0.89	0.13	0.00	0.00	0.00	100.00
033X-1-W 122-124 cm	108.4	303.06	5.42	11.26	31.00	0.65	0.15	88.29	28.82	1.36	0.36	0.77	0.15	0.89	0.05	0.92	0.12	0.00	0.00	6.45	93.55
033X-2-W 122-124 cm	104.6	304.56	5.46	11.29	30.00	0.62	0.17	113.34	56.71	1.37	0.32	0.76	0.15	0.89	0.05	0.94	0.12	0.00	0.00	13.33	86.67
033X-6-W 70-72 cm	102.0	310.04	5.60	3.18	8.00	0.66	0.25	148.77	106.75	1.92	1.24	0.68	0.29	0.87	0.07	0.90	0.10	0.00	25.00	0.00	75.00
034X-2-W 8-10cm	50.7	313.14	5.64	4.04	5.00	0.58	0.10	51.47	32.50	1.54	0.34	0.68	0.13	0.88	0.05	0.93	0.06	0.00	0.00	40.00	60.00
035X-2-W 118-120cm	100.3	323.84	5.89	12.24	28.00	0.50	0.17	132.72	59.43	1.73	1.12	0.69	0.21	0.85	0.07	1.00	0.10	0.00	7.14	17.86	75.00
036X-1-W 25-27cm	51.8	331.01	6.09	1.77	2.00	0.50	0.18	254.97	77.46	2.09	0.92	0.53	0.24	0.88	0.06	0.89	0.02	0.00	0.00	50.00	50.00
036X-5-W 67-69cm	109.3	337.43	6.10	4.28	10.00	0.49	0.13	104.88	37.17	2.14	1.26	0.58	0.24	0.82	0.08	0.94	0.10	0.00	10.00	50.00	40.00
037X-1-W 100-102cm	105	341.36	6.31	14.79	32.00	0.61	0.14	102.26	33.02	1.66	0.98	0.69	0.19	0.88	0.05	0.91	0.09	3.13	3.13	15.63	78.13

037X-5-W 100-102cm	104.5	347.36	6.31	14.87	32.00	0.59	0.12	139.97	101.72	1.48	0.35	0.71	0.14	0.89	0.06	0.94	0.07	0.00	3.13	9.38	87.50
038X-1-W 92-94cm	103.9	350.98	6.51	19.99	43.00	0.53	0.17	171.26	131.08	1.87	1.05	0.63	0.19	0.86	0.08	0.98	0.23	2.33	0.00	37.21	60.47
039X-2-W 16-18cm	52.7	361.32	6.69	6.08	7.00	0.60	0.13	129.64	13.28	1.50	0.51	0.72	0.19	0.90	0.05	0.94	0.06	0.00	0.00	28.57	71.43
039X-7-W 17-19cm	56.3	368.83	6.69	9.00	11.00	0.62	0.15	69.77	17.66	1.63	0.65	0.68	0.20	0.87	0.06	0.89	0.06	0.00	9.09	0.00	90.91
040X-1-W 46-48cm	106.1	369.82	6.91	15.67	38.00	0.52	0.15	238.43	239.12	1.50	0.54	0.72	0.16	0.85	0.05	1.00	0.14	0.00	5.26	7.89	84.21
041X-3-W 32-34cm	108.8	373.255	7.13	0.40	1.00	0.51	0.00	117.24	0.00	2.80	0.00	0.36	0.00	0.85	0.00	0.82	0.00	0.00	0.00	100.00	0.00
041X-4-W 90-92cm	108.8	382.28	7.14	19.11	50*	0.64	0.14	112.45	62.60	1.43	0.36	0.74	0.15	0.90	0.05	0.92	0.09	0.00	0.00	6.00	94.00
042X-5-W 100-102cm	107.4	384.36	7.38	19.00	50*	0.62	0.12	109.72	42.95	1.58	0.38	0.67	0.15	0.90	0.04	0.92	0.07	0.00	0.00	12.00	88.00
042X-2-W 126-128cm	101.6	391.32	7.39	11.53	30.00	0.63	0.20	100.74	45.17	1.38	0.55	0.78	0.16	0.88	0.06	0.94	0.16	0.00	0.00	13.33	86.67
043X-3-W 76-78 cm	106.7	401.92	7.70	0.12	50*	0.59	0.16	126.89	71.48	1.46	0.50	0.74	0.18	0.88	0.06	0.95	0.09	0	4	8	88

043X-5-W 67-69cm	101.5	404.83	7.78	0.04	36	0.63	0.14	144.56	66.78	1.54	0.45	0.70	0.17	0.86	0.05	0.89	0.09	0	2.777777778	19.44444444	77.77777778
044X-2-W 41-43cm	107.1	408.27	7.87	5.86	17.00	0.39	0.13	175.62	171.15	2.16	2.56	0.66	0.22	0.85	0.08	1.11	0.11	0.00	11.76	23.53	64.71
045X-1-W 29-31cm	50.7	417.75	8.14	5.60	8.00	0.64	0.09	77.70	19.06	1.59	0.32	0.65	0.12	0.88	0.03	0.91	0.06	0.00	12.50	0.00	87.50
045X-5-W 62-64cm	105.7	418.08	8.15	8.23	50*	0.52	0.18	139.78	93.10	1.57	0.73	0.72	0.20	0.86	0.13	1.02	0.20	0.00	8.00	12.00	80.00
045X-3-W 89.5-91.5cm	105.8	418.355	8.15	16.44	25.00	0.60	0.19	210.20	118.50	1.78	0.92	0.66	0.21	0.87	0.08	0.94	0.15	0.00	12.00	8.00	80.00
046X-3-W 45-47cm	101.6	427.61	8.42	1.35	4.00	0.36	0.08	85.84	33.21	1.70	0.58	0.63	0.18	0.85	0.04	1.16	0.08	0.00	0.00	50.00	50.00
046X-6-W 130-132cm	106.3	428.46	8.45	16.16	50*	0.62	0.15	140.37	76.32	1.50	0.68	0.75	0.20	0.90	0.04	0.93	0.09	0.00	4.00	12.00	84.00
047X-4-W 32-34cm	102.3	437.08	8.70	1.01	3.00	0.45	0.24	112.67	92.65	5.11	6.77	0.58	0.44	0.87	0.06	0.90	0.13	0.00	33.33	0.00	66.67
048X-1-W 37-39 cm	100.8	446.73	8.97	2.73	8.00	0.58	0.08	77.24	13.59	1.40	0.28	0.74	0.13	0.93	0.01	0.98	0.08	0.00	0.00	25.00	75.00

048X-7-W 11-13cm	110.2	455.47	9.23	9.36	30.00	0.45	0.16	208.31	185.77	1.63	0.81	0.68	0.16	0.87	0.11	1.09	0.20	0.00	0.00	10.00	90.00
049X-1-W 87-89cm	106.7	456.93	9.28	16.10	50*	0.53	0.16	192.48	130.28	1.87	1.02	0.64	0.22	0.87	0.07	0.96	0.11	0.00	6.00	14.00	80.00
049X-4-W 8-10 cm	107.4	460.64	9.38	12.48	39.00	0.44	0.15	471.96	313.84	2.47	1.16	0.48	0.18	0.87	0.05	0.99	0.14	0.00	17.95	51.28	30.77

Site U1457

Sample label	Weight (mg)	MCD	Age (Ma)	CHAR	Particle count	Circ mean	Circ stdev	Fd (µm) mean	Fd stdev	L:W mean	L:W stdev	R mean	R stdev	S mean	S stdev	Rect mean	Rect stdev	d	f	c/s.b	m/p
35R-6-W 5-7 cm	114.1	529.57	5.53	104.83	61.00	0.56	0.15	184.39	273.07	2.02	1.52	0.59	0.18	0.81	0.13	0.90	0.07	0.00	3.28	13.11	83.61
35R-6-W 38-40 cm	111.2	529.9	5.53	312.10	177.00	0.59	0.15	147.37	118.10	1.90	1.26	0.62	0.19	0.83	0.10	0.88	0.08	0.00	2.26	28.25	69.49
44R-5-W 65-67 cm	103.2	614.32	6.25	1.73	12.00	0.41	0.20	441.82	490.98	2.33	1.75	0.59	0.26	0.77	0.21	1.06	0.26	0.00	8.33	33.33	58.33
45R-2-W 10-12 cm	99	619.12	6.53	8.95	50.00	0.58	0.16	187.63	174.65	2.16	1.47	0.57	0.20	0.84	0.12	0.88	0.08	0.00	4.00	32.00	64.00
45R-2-W 25-27 cm	104.9	619.27	6.54	4.91	29.00	0.47	0.21	123.10	150.43	3.07	2.99	0.47	0.20	0.81	0.17	0.93	0.10	0.00	13.79	48.28	37.93
45R-2-W 35-37 cm	103.8	619.37	6.54	4.10	24.00	0.49	0.16	237.80	91.81	2.69	2.50	0.52	0.20	0.83	0.11	0.93	0.10	0.00	8.33	33.33	58.33
46R-1-W 66-68 cm	101.5	627.53	6.90	2.95	10.00	0.34	0.20	372.80	227.95	2.51	0.96	0.47	0.22	0.64	0.29	1.00	0.17	20.00	10.00	40.00	30.00
46R-4-W 41-43 cm	96.6	631.78	7.03	26.80	69.00	0.45	0.21	259.59	192.85	3.04	3.26	0.51	0.24	0.77	0.18	0.96	0.14	5.80	7.25	24.64	62.32

46R-4-W 51-53 cm	110.9	631.88	7.03	23.01	68.00	0.42	0.20	248.20	210.47	2.55	1.94	0.51	0.20	0.74	0.19	0.98	0.15	0.00	13.24	33.82	52.94
46R-5-W 50-52 cm	103.3	633.37	7.07	19.25	53.00	0.42	0.25	337.76	339.72	3.35	3.09	0.50	0.27	0.70	0.25	0.95	0.15	0.00	26.42	15.09	58.49
48R-1-W 11-13 cm	101.3	644.18	7.27	23.69	30.00	0.35	0.26	599.39	716.53	3.82	5.05	0.47	0.25	0.61	0.32	1.00	0.19	6.67	26.67	10.00	56.67
48R-1-W 26-28 cm	112.9	644.33	7.27	7.87	10.00	0.09	0.08	1148.80	1096.79	7.88	3.45	0.16	0.10	0.34	0.24	0.98	0.19	10.00	90.00	0.00	0.00
48R-2-W 62-64 cm	97.8	646.19	7.29	75.44	83.00	0.52	0.22	264.72	411.68	2.16	1.95	0.61	0.21	0.75	0.22	0.92	0.12	0.00	10.84	9.64	79.52
50R-1-W 45-47 cm	114.5	666.22	7.50	9.67	16.00	0.27	0.24	382.24	303.72	3.90	2.50	0.38	0.23	0.51	0.28	1.01	0.23	0.00	50.00	31.25	18.75
50R-1-W 58-60 cm	105.7	666.35	7.50	5.24	8.00	0.20	0.17	675.28	854.12	6.72	6.61	0.24	0.18	0.48	0.31	0.89	0.11	0.00	50.00	37.50	12.50
51R-2-W 76-78 cm	107.9	677.88	7.65	8.78	10.00	0.35	0.23	289.73	166.60	4.10	3.33	0.38	0.23	0.66	0.25	0.93	0.14	10.00	30.00	0.00	60.00
51R-2-W 95-97 cm	103.9	678.07	7.65	32.58	11.00	0.36	0.28	425.30	417.38	6.13	6.20	0.35	0.24	0.62	0.29	0.92	0.12	0.00	45.45	9.09	45.45
68R-6-W 13-15 cm	96.2	849.2	9.00	1.48	8.00	0.27	0.28	309.63	443.41	3.40	2.63	0.49	0.29	0.50	0.35	1.05	0.26	0.00	50.00	0.00	50.00
68R-6-W 26-28 cm	109.6	849.33	9.00	0.49	3.00	0.04	0.01	947.23	417.91	9.10	1.27	0.11	0.01	0.29	0.20	1.13	0.31	0.00	100.00	0.00	0.00
69R-6-W 30-32 cm	113.7	859.22	9.55	1.08	7.00	0.14	0.17	494.04	309.39	7.01	5.29	0.29	0.27	0.44	0.18	1.11	0.26	28.57	57.14	0.00	14.29
69R-6-W 38-40 cm	98.4	859.3	9.56	3.56	20.00	0.48	0.26	378.78	516.81	2.79	2.90	0.56	0.26	0.69	0.28	0.90	0.09	0.00	20.00	15.00	65.00

70R-6-W 24-26 cm	112.7	868.51	10.07	3.64	23.00	0.34	0.29	531.58	507.67	4.67	4.89	0.43	0.28	0.60	0.33	0.93	0.13	0.00	47.83	21.74	30.43
70R-6-W 29-31 cm	100.4	868.56	10.08	2.31	13.00	0.62	0.12	177.81	127.26	1.86	0.59	0.58	0.17	0.87	0.04	0.85	0.05	0.00	0.00	15.38	84.62
70R-6-W 37-39 cm	100.2	868.64	10.08	2.31	13.00	0.38	0.24	490.66	489.57	5.17	7.50	0.44	0.28	0.69	0.28	0.91	0.07	0.00	30.77	7.69	61.54
72R-6-W 28-30 cm	110.2	888.25	11.20	6.68	41.00	0.54	0.21	231.47	309.44	2.36	2.31	0.59	0.22	0.78	0.19	0.92	0.12	0.00	78.05	7.32	80.49

Site 717

Sample label	Weight (mg)	MCD	Age (Ma)	CHAR	Particle count	Circ mean	Circ stdev	Fd (µm) mean	Fd stdev	L:W mean	L:W stdev	R mean	R stdev	S mean	S stdev	Rect mean	Rect stdev	d	f	c/s.b	m/p
27X-6-W 53-55 cm	97.7	225.07	1.96	12.81	45.00	0.37	0.19	88.40	99.44	6.21	5.01	0.28	0.21	0.76	0.08	0.86	0.09	2.22	62.22	20.00	15.56
29X-4-W 48-50 cm	98.8	241	2.53	4.79	17.00	0.48	0.23	81.72	73.98	3.18	3.12	0.51	0.26	0.74	0.23	0.88	0.12	0.00	23.53	35.29	41.18
31X-2-W 98-100 cm	106.3	257.5	2.81	28.95	52.00	0.43	0.16	71.20	54.17	3.72	1.78	0.35	0.20	0.81	0.10	0.89	0.09	9.62	69.23	7.69	13.46
33X-7-W 18-20 cm	97.1	283.2	3.25	3.66	6.00	0.46	0.27	72.55	61.44	2.61	1.64	0.50	0.25	0.70	0.30	0.90	0.10	0.00	33.33	33.33	33.33
36X-3-W 77-79 cm	98.8	306.29	3.64	40.25	68.00	0.35	0.18	74.41	60.21	5.01	3.19	0.32	0.24	0.74	0.13	0.94	0.19	5.88	64.71	7.35	22.06
41X-1-W 27-29 cm	105.1	350.27	3.93	152.81	106.00	0.56	0.15	211.06	176.06	1.96	1.01	0.58	0.17	0.84	0.13	0.90	0.09	0.94	2.83	17.92	78.30
44X-3-W 13-15 cm	102.1	381.65	4.62	24.82	56.00	0.36	0.15	297.30	220.58	4.32	3.05	0.32	0.18	0.77	0.12	0.95	0.15	3.57	28.57	57.14	10.71

47X-2-W 78-80 cm	98.9	409.3	5.21	1.32	63.00	0.53	0.17	192.86	170.64	2.79	2.38	0.51	0.23	0.82	0.12	0.89	0.07	4.76	7.94	22.22	65.08
48X-5-W 40-42 cm	99.3	422.92	5.65	0.52	47.00	0.43	0.17	240.61	308.94	3.57	2.62	0.40	0.22	0.79	0.12	0.90	0.11	0.00	19.15	46.81	34.04
50X-4-W 73-75 cm	100.3	440.75	6.05	0.30	68.00	0.40	0.15	253.36	112.23	4.20	2.70	0.34	0.19	0.79	0.09	0.88	0.10	0.00	5.88	75.00	19.12
51X-2-W 45-47 cm	101.2	446.97	6.11	11.22	23.00	0.47	0.18	206.72	120.78	3.22	1.46	0.38	0.18	0.80	0.16	0.87	0.07	8.70	4.35	60.87	26.09
52X-2-W 102-104 cm	96.5	457.04	6.32	4.09	8.00	0.45	0.27	385.08	349.75	4.71	4.71	0.52	0.36	0.76	0.25	0.86	0.08	0.00	25.00	12.50	62.50
53X-5-X 10-12 cm	93.3	470.12	6.58	4.76	9.00	0.27	0.18	443.85	554.49	4.14	2.46	0.34	0.24	0.67	0.21	1.14	0.24	0.00	44.44	22.22	33.33
53X-5-X 75-77 cm	106.9	470.77	6.60	19.40	42.00	0.52	0.22	244.99	235.90	2.73	2.09	0.53	0.26	0.80	0.15	0.88	0.17	2.44	14.63	56.10	26.83
54X-6-W 37-39 cm	106.7	481.39	6.81	10.06	24.00	0.30	0.28	550.28	497.39	7.29	6.52	0.30	0.24	0.55	0.31	0.88	0.11	20.83	37.50	33.33	8.33
55X-2-W 100-102 cm	107.5	485.52	6.90	5.34	13.00	0.30	0.23	319.67	224.88	5.53	4.26	0.31	0.20	0.62	0.25	0.96	0.19	7.69	38.46	46.15	7.69
56X-4-W 84-86 cm	104.7	497.86	7.18	28.87	68.00	0.44	0.26	414.86	549.34	3.84	4.50	0.51	0.27	0.71	0.26	0.93	0.13	0.00	27.94	10.29	61.76
57X-4-W 50-52 cm	104.2	507.2	7.39	8.47	20.00	0.38	0.24	455.90	492.08	2.80	1.74	0.45	0.19	0.68	0.30	1.01	0.20	0.00	25.00	10.00	65.00
58X-4-W 38-40 cm	105.5	516.4	7.60	26.36	63.00	0.50	0.18	269.88	181.32	2.37	2.72	0.58	0.20	0.81	0.13	0.94	0.13	0.00	6.35	6.35	87.30

59X-6-W 95-97 cm	93.4	529.47	7.90	6.88	50.00	0.52	0.17	166.48	164.11	2.09	1.76	0.60	0.20	0.79	0.15	0.92	0.09	2.00	4.00	8.00	86.00
61X-1-W 17-19 cm	94.3	540.19	8.15	0.78	37.00	0.46	0.25	294.32	377.66	4.29	4.90	0.44	0.25	0.75	0.21	0.92	0.16	2.70	16.22	21.62	59.46
61X-2-W 55-57 cm	100.7	542.07	8.18	16.83	10.00	0.16	0.20	526.62	286.85	8.66	6.44	0.19	0.15	0.41	0.24	0.89	0.11	0.00	90.00	10.00	0.00
63X-3-W 10-12 cm	96	561.79	8.30	17.66	10.00	0.29	0.24	449.11	331.54	6.34	4.29	0.33	0.31	0.64	0.25	0.95	0.14	10.00	50.00	20.00	20.00
64X-3-W 100-102 cm	97.1	572.52	8.36	29.42	15.00	0.31	0.23	423.76	480.20	2.57	1.31	0.49	0.23	0.55	0.31	0.97	0.14	6.67	26.67	33.33	33.33
66X-3-W 50-52 cm	99.4	591.02	8.45	38.33	20.00	0.30	0.24	354.89	272.17	6.01	6.16	0.34	0.25	0.60	0.25	0.96	0.12	5.00	45.00	5.00	45.00
68X-5-W 35-37 cm	100.6	612.87	8.57	17.04	9.00	0.49	0.27	470.26	571.32	4.22	5.59	0.59	0.32	0.76	0.24	0.92	0.10	0.00	22.22	0.00	77.78
69X-2-W 50-52 cm	95.8	618.02	8.60	4.67	7.00	0.42	0.38	647.80	859.76	1.84	0.75	0.60	0.16	0.54	0.42	1.01	0.27	0.00	50.00	0.00	50.00
70X-4-W 08-10 cm	105.4	630.1	8.67	0.64	38.00	0.45	0.28	363.03	447.82	3.22	3.14	0.53	0.28	0.67	0.29	0.92	0.10	2.63	28.95	5.26	63.16
71X-4-W 56-58 cm	95.7	640.08	8.72	0.18	9.00	0.21	0.27	478.42	273.40	9.37	8.35	0.25	0.28	0.51	0.20	0.93	0.21	22.22	66.67	0.00	11.11
73X-1-W 100-102 cm	106.1	655.02	8.80	0.29	15.00	0.07	0.04	728.55	463.34	7.01	3.70	0.18	0.08	0.28	0.14	0.97	0.14	20.00	80.00	0.00	0.00
75X-3-W 50-52 cm	105.7	676.52	8.90	25.23	14.00	0.58	0.22	222.81	275.13	2.48	2.59	0.61	0.24	0.81	0.16	0.87	0.09	0.00	7.14	14.29	78.57

77X-7-W 20-22 cm	104.2	701.22	9.04	1.12	60.00	0.54	0.17	153.00	53.13	1.78	0.55	0.61	0.17	0.81	0.09	0.93	0.11	0.00	0.00	5.00	95.00
82X-1-W 54-56 cm	107.3	740.11	9.32	0.09	18.00	0.46	0.22	289.41	216.22	2.48	2.49	0.61	0.26	0.75	0.24	0.96	0.14	0.00	16.67	0.00	83.33
84X-3-W 42-44 cm	93.5	761.94	9.35	61.12	30.00	0.53	0.20	196.16	118.65	1.83	0.84	0.61	0.17	0.82	0.15	0.95	0.13	0.00	6.67	10.00	83.33
85X-3-W 100-102 cm	105.1	772.12	9.42	0.42	13.00	0.54	0.24	190.04	155.01	1.96	1.88	0.67	0.21	0.79	0.21	0.93	0.10	0.00	15.38	0.00	84.62
90X-1-W 68-70 cm	93.3	809.9	9.82	0.02	7.00	0.47	0.32	525.32	678.65	2.19	0.93	0.53	0.19	0.66	0.39	0.92	0.10	0.00	28.57	0.00	71.43
91X-4-W 21-23 cm	107.6	819.93	9.90	28.60	16.00	0.46	0.33	258.38	253.36	4.68	4.77	0.47	0.31	0.67	0.26	0.90	0.16	6.25	31.25	0.00	62.50

Site 1146

Sample label	Weight (mg)	MCD	Age (Ma)	CHAR	Particle count	Circ mean	Circ stdev	Fd (µm) mean	Fd stdev	L:W mean	L:W stdev	R mean	R stdev	S mean	S stdev	Rect mean	Rect stdev	d	f	c/s.b	m/p
1146A-32X-2-W 10-12 cm	148.6	310.67	5510.22	1.54	8.00	0.36	0.33	120.35	154.65	4.51	4.49	0.41	0.26	0.56	0.34	0.97	0.14	0.00	50.00	0.00	50.00
1146A-32X-2-W 140-142 cm	172.1	311.97	5553.33	1.27	5.00	0.09	0.08	231.18	192.29	7.27	8.10	0.25	0.16	0.32	0.21	1.01	0.21	0.00	60.00	0.00	40.00

1146A-32X-3-W 50-52 cm	155.8	312.57	5.57	2.26	8.00	0.41	0.27	42.93	39.59	4.52	6.62	0.62	0.35	0.72	0.15	1.00	0.28	0.00	25.00	12.50	62.50
1146A-32X-3-W 100-102 cm	149.6	313.07	5.58	2.64	9.00	0.57	0.23	75.86	96.93	2.70	2.59	0.55	0.26	0.76	0.23	0.85	0.04	0.00	11.11	22.22	66.67
1146A-32X-4-W 69-71 cm	144.5	314.26	5.62	1.86	11.00	0.22	0.22	127.59	186.77	6.82	5.46	0.32	0.30	0.49	0.23	0.98	0.13	0	72.72727273	9.090909091	18.18181818
1146A-32X-4-W 124-126 cm	153.7	314.81	5.64	0.95	6.00	0.52	0.08	85.97	78.64	1.66	0.53	0.66	0.21	0.80	0.04	0.92	0.07	0	0	33.33333333	66.66666667
1146A-32X-5-W 90.5-92.5 cm	145.1	315.98	5688.28	2.01	12.00	0.49	0.28	122.08	258.81	3.30	3.42	0.56	0.30	0.70	0.25	0.89	0.06	8.33	16.67	16.67	58.33
1146A-32X-6-W 141-143 cm	159.1	317.98	5753.36	1.44	7.00	0.35	0.36	157.60	174.39	3.85	2.83	0.43	0.31	0.52	0.37	0.96	0.16	0.00	57.14	14.29	28.57
1146A-33X-1-W 06-08 cm	147.5	319.13	5788.43	0.22	5.00	0.24	0.24	207.47	270.71	3.37	2.05	0.44	0.32	0.44	0.32	0.98	0.06	0.00	60.00	0.00	40.00

1146A-33X-1-W 80-82 cm	160.3	319.87	5.81	0.87	5.00	0.31	0.36	326.83	497.08	3.36	2.42	0.44	0.26	0.46	0.31	1.05	0.36	0.00	20.00	0.00	80.00
1146A-33X-1-W 130-132 cm	155.6	320.37	5.83	1.26	7.00	0.29	0.33	197.65	189.68	4.31	2.12	0.33	0.24	0.45	0.30	0.84	0.04	0.00	71.43	14.29	14.29
1146A-33X-2-W 109.5-111.5 cm	154.9	321.67	5878.31	1.08	5.00	0.47	0.30	30.42	20.07	1.73	1.10	0.72	0.29	0.74	0.16	1.11	0.40	0.00	20.00	0.00	80.00
1146A-33X-4-W 19.5-21.5	157.5	323.77	5953.43	1.42	8.00	0.47	0.35	429.43	950.18	3.14	2.53	0.52	0.31	0.64	0.35	0.90	0.11	0.00	37.50	0.00	62.50
1146A-33X-5-W 65.5-67.5 cm	160.2	325.73	6038.14	0.79	6.00	0.63	0.29	62.41	47.69	3.19	4.38	0.63	0.30	0.77	0.25	0.84	0.07	0.00	16.67	0.00	83.33
1146A-33X-6-W 119-121 cm	151.9	327.76	6118.27	2.06	9.00	0.51	0.28	81.12	162.21	1.52	0.48	0.70	0.16	0.74	0.27	1.01	0.22	0.00	11.11	11.11	77.78
1146A-34X-1-W 125-127 cm	150.3	330.12	6186.05	1.16	5.00	0.45	0.30	64.74	77.36	2.54	1.96	0.53	0.24	0.67	0.25	0.97	0.13	0.00	20.00	20.00	60.00

1146A-34X-3-W 26-28 cm	157.5	332.13	6.24	0.88	4.00	0.41	0.22	67.49	52.28	2.67	1.43	0.47	0.25	0.71	0.24	0.93	0.16	0.00	25.00	25.00	50.00
1146A-34X-3-W 144-146 cm	156.9	333.31	6.28	1.08	5.00	0.54	0.28	50.33	72.31	1.95	1.26	0.63	0.24	0.72	0.27	0.93	0.15	20.00	0.00	20.00	60.00
1146A-34X-6-W 08-10 cm	148.3	336.45	6371.14	0.46	2.00	0.10	0.07	133.72	98.02	8.81	4.03	0.13	0.06	0.47	0.26	1.07	0.27	0.00	100.00	0.00	0.00
1146A-35X-4-W 16-18 cm	157.4	343.88	6618.28	1.41	9.00	0.24	0.28	210.28	303.58	6.47	5.33	0.29	0.28	0.47	0.29	0.92	0.16	0.00	66.67	11.11	22.22
1146A-35X-5-W 70-72 cm	151.6	345.92	6698.40	1.62	9.00	0.27	0.29	256.37	500.70	4.27	3.28	0.37	0.23	0.46	0.28	0.98	0.13	0.00	66.67	0.00	33.33
1146A-35X-6-W 120-122 cm	160	347.92	6771.53	1.88	11.00	0.40	0.41	430.79	560.80	3.97	2.98	0.44	0.30	0.51	0.38	0.87	0.09	0.00	54.55	0.00	45.45
1146A-36X-2-W 106-108 cm	147.3	353.88	6965.77	3.59	17.00	0.62	0.25	98.40	189.54	1.76	0.93	0.66	0.19	0.76	0.25	0.86	0.08	0.00	11.76	17.65	70.59

1146A-36X-4-W 19-21 cm	159.2	356.01	7034.31	0.98	5.00	0.22	0.32	256.78	202.81	6.66	6.38	0.35	0.28	0.43	0.36	0.88	0.11	20.00	60.00	20.00	0.00
1146A-36X-5-W 65-67 cm	149.5	357.97	7097.88	5.46	27.00	0.59	0.26	138.47	285.70	2.18	2.56	0.69	0.25	0.78	0.21	0.91	0.12	0.00	14.81	7.41	77.78
1146A-36X-6-W 126-128 cm	152	360.08	7167.77	0.99	5.00	0.43	0.33	216.90	423.25	3.61	3.05	0.51	0.36	0.67	0.28	0.92	0.18	0.00	40.00	0.00	60.00
1146A-37X-3-W 100.5-102.5 cm	147.9	365.68	7353.07	0.82	4.00	0.21	0.29	116.34	109.33	5.48	4.58	0.36	0.29	0.42	0.32	0.92	0.13	0.00	75.00	0.00	25.00
1146A-37X-5-W 0-02 cm	156.1	367.67	7419.14	0.97	5.00	0.09	0.08	291.08	83.30	6.78	3.66	0.20	0.13	0.32	0.22	0.99	0.13	0.00	100.00	0.00	0.00
1146A-37X-6-W 55-57 cm	99.6	369.72	7479.86	2.51	7.00	0.08	0.07	261.24	200.10	9.95	6.83	0.17	0.15	0.37	0.21	1.04	0.20	0.00	85.71	14.29	0.00
1146A-38X-4-W 89-91 cm	99.2	377.66	7701.81	2.52	7.00	0.32	0.24	218.56	341.69	4.79	2.42	0.28	0.16	0.61	0.33	0.87	0.10	0.00	57.14	14.29	28.57

1146A-39X-2-W 129-131 cm	152.9	384.71	7916.79	0.59	3.00	0.22	0.23	341.28	444.13	6.93	4.75	0.27	0.27	0.51	0.28	0.99	0.15	0.00	66.67	33.33	0.00
1146A-39X-4-W 89-91 cm	153.7	387.31	8003.04	0.39	2.00	0.30	0.23	158.18	176.69	2.83	0.43	0.36	0.05	0.56	0.32	0.88	0.03	0.00	50.00	0.00	50.00
1146C-30X-1-W 30-32 cm	154.1	299.22	5100.35	0.56	3.00	0.08	0.03	492.44	190.48	8.58	5.39	0.15	0.07	0.38	0.14	1.03	0.20	0.00	100.00	0.00	0.00
1146C-30X-2-W 64-66 cm	148.6	301.06	5169.92	0.55	3.00	0.35	0.21	110.79	150.34	5.82	6.60	0.43	0.41	0.71	0.15	0.97	0.11	0.00	33.33	33.33	33.33
1146C-30X-3-W 114-116 cm	148.9	303.06	5243.54	0.91	5.00	0.26	0.22	69.69	62.29	5.05	3.74	0.36	0.30	0.53	0.25	0.89	0.08	0.00	60.00	0.00	40.00
1146C-30X-4-W 79-81 cm	151.9	304.21	5.28	0.75	4.00	0.26	0.42	128.77	92.35	4.43	3.02	0.37	0.32	0.37	0.37	0.93	0.08	0.00	75.00	0.00	25.00
1146C-30X-4-W 129-81 cm	159.8	304.71	5.30	1.97	11.00	0.41	0.28	174.17	369.98	4.04	5.34	0.52	0.30	0.63	0.28	0.95	0.15	0.00	36.36	9.09	54.55

1146C-30X-5-W 25-27 cm	151.9	305.17	5318.05	0.19	1.00	0.04	0.00	204.66	0.00	11.31	0.00	0.09	0.00	0.24	0.00	0.93	0.00	0.00	100.00	0.00	0.00
1146C-30X-6-W 30-32 cm	156.3	306.72	5372.21	1.28	7.00	0.62	0.23	51.61	27.60	2.51	2.94	0.65	0.28	0.81	0.13	0.88	0.07	0.00	85.71	14.29	0.00
1146C-34X-3-W 104-106 cm	146.7	338.01	6417.29	0.92	4.00	0.51	0.29	53.83	38.85	3.29	3.94	0.60	0.33	0.73	0.26	0.91	0.02	0.00	25.00	0.00	75.00
1146C-34X-5-W 0-02 cm	148.5	339.97	6475.28	0.68	3.00	0.61	0.30	28.62	17.74	2.02	1.02	0.57	0.24	0.81	0.11	0.87	0.08	0.00	0.00	33.33	66.67
1146C-35X-4-W 75-77 cm	150.2	349.87	6836.73	1.86	9.00	0.48	0.28	211.20	356.38	2.40	2.13	0.57	0.22	0.66	0.35	0.91	0.06	0.00	22.22	33.33	44.44
1146C-35X-5-W 128.5-130.5 cm	143.4	351.91	6902.21	0.43	2.00	0.27	0.32	147.96	99.35	1.76	0.71	0.62	0.25	0.49	0.41	1.17	0.35	0.00	50.00	0.00	50.00
1146C-36X-4-W 19-21 cm	97.9	361.76	7223.41	1.85	6.00	0.21	0.29	344.83	397.37	5.28	3.68	0.30	0.25	0.43	0.32	0.95	0.16	16.67	66.67	0.00	16.67

1146C-36X-5-W 69-71 cm	98.6	363.76	7289.65	3.98	13.00	0.10	0.09	274.52	269.89	9.24	4.46	0.14	0.08	0.38	0.18	0.96	0.22	0.00	100.00	0.00	0.00
1146C-37X-3-W 54-56 cm	151.2	371.66	7534.09	1.66	7.00	0.17	0.16	140.10	109.45	6.66	4.11	0.24	0.20	0.43	0.23	0.92	0.09	0.00	71.43	0.00	28.57
1146C-37X-4-W 109-111 cm	148.8	373.71	7591.39	1.68	7.00	0.34	0.36	138.03	138.61	2.51	1.38	0.50	0.23	0.50	0.36	0.95	0.13	0.00	28.57	14.29	57.14
1146C-37X-6-W 9-11 cm	99.2	375.71	7647.30	1.44	4.00	0.28	0.26	285.84	278.86	3.59	1.44	0.31	0.09	0.49	0.36	0.92	0.16	0.00	50.00	0.00	50.00
1146C-38X-2-W 134-136 cm	141	381.61	7813.95	1.65	7.00	0.35	0.32	93.29	44.70	4.06	2.90	0.43	0.32	0.57	0.29	0.89	0.07	0.00	57.14	0.00	42.86
1146C-38X-4-W 33-35 cm	153.2	383.60	7879.97	0.20	1.00	0.05	0.00	170.07	0.00	9.67	0.00	0.10	0.00	0.28	0.00	0.83	0.00	0.00	100.00	0.00	0.00